

2007

## Computer model of hybrid compensator of fast varying loads

Veronica Bohorquez

*Louisiana State University and Agricultural and Mechanical College*

Follow this and additional works at: [https://digitalcommons.lsu.edu/gradschool\\_dissertations](https://digitalcommons.lsu.edu/gradschool_dissertations)



Part of the [Electrical and Computer Engineering Commons](#)

---

### Recommended Citation

Bohorquez, Veronica, "Computer model of hybrid compensator of fast varying loads" (2007). *LSU Doctoral Dissertations*. 815.

[https://digitalcommons.lsu.edu/gradschool\\_dissertations/815](https://digitalcommons.lsu.edu/gradschool_dissertations/815)

This Dissertation is brought to you for free and open access by the Graduate School at LSU Digital Commons. It has been accepted for inclusion in LSU Doctoral Dissertations by an authorized graduate school editor of LSU Digital Commons. For more information, please contact [gradetd@lsu.edu](mailto:gradetd@lsu.edu).

# COMPUTER MODEL OF HYBRID COMPENSATOR OF FAST VARYING LOADS

A Dissertation  
Submitted to the Graduate Faculty of the  
Louisiana State University and  
Agricultural and Mechanical College  
in partial fulfillment of the  
requirements for the degree of  
Doctor of Philosophy

In

The Department of Electrical and Computer Engineering

by  
Veronica Bohorquez  
B.S., Universidad del Zulia, 1993  
M.S., Universidad Nacional Experimental Politecnica “Antonio Jose de Sucre”, 2000  
December 2007

## **Acknowledgments**

I would like to express my gratitude to my family, to my husband Freddy A. Simmonds, B.S in Electrical Engineering, and to my daughters Susana Paola and Lorena Beatriz for the extraordinary support and unconditional love during all these years.

I would like to express my gratitude to Dr. Leszek S. Czarnecki for his support, reviews and corrections of the dissertation. Dr. Czarnecki has been my anchor and role model during the course of my studies.

I would also express my gratitude to Dr. Ernest Mendrela, who devoted his expertise in Electrical Machinery and his time to review Chapter 5. I would also express my gratitude to all the members of my committee for their participation and accurate comments during all of my exams in the course of the Doctorate. I wish to dedicate a few lines also to express my gratitude to Dr. John Tyler, my minor professor, with whom I devoted a couple of years studying, working and enjoying High Performance Computing.

I would like to express my gratitude to Luke Hargus, M.S in Linguistics, who reviewed the writing of the dissertation.

I would like to acknowledge the extraordinary support I received from my mother Dr. Evangelina Garcia de Bohorquez and my father Guillermo Bohorquez, Vet.; both traveled long distances and for long period of times to support me and my family during all these years. I'd like to express my gratitude to my sisters Virginia Bohorquez, M.S. in Civil Engineering, Monica Bohorquez PhD candidate at LSU, and Natalia Bohorquez, M.S in Civil Engineering from LSU and my cousin Maria Hargus, B.S. in Industrial Engineering, for their unconditional love for me and my family.

I would like to express my gratitude and appreciation to Maria Murillo, M.S. in Civil Engineering, who proved to be the best friend ever.

## Table of Contents

ACKNOWLEDGMENTS .....	ii
LIST OF TABLES .....	v
LIST OF FIGURES .....	vi
ABSTRACT .....	ix
CHAPTER 1. INTRODUCTION .....	1
1.1 Dissertation Subject .....	2
1.2 Dissertation Objectives .....	2
1.3 Dissertation Thesis .....	2
1.4 Approaches to Objectives Fulfillment .....	2
1.5 Structure of Dissertation Chapters .....	3
CHAPTER 2. FAST VARYING LOADS .....	5
2.1 Introduction .....	5
2.2 Characteristics of Fast Varying Loads .....	5
2.2.1 Repetitive Fast Varying Load .....	6
2.2.2 Random Fast Varying Load .....	6
2.2.2 Burst Fast Varying Load .....	7
2.3 Common Fast Varying Loads .....	8
2.3.1 Crushers .....	8
2.3.2 Rolling Mills .....	9
2.3.3 Electrical Excavators .....	10
2.3.4 Arc Furnaces .....	11
2.3.5 Cycloconverter Fed Loads .....	12
2.3.6 Pulsing Loads .....	13
2.4 Effects of Fast Varying Loads in Distribution Systems .....	15
CHAPTER 3. POWER PROPERTIES OF FAST VARYING LOADS .....	18
3.1 Introduction .....	18
3.2 Approaches for Power Properties Identification of Non-periodic Signals .....	18
3.3 Application of CPC Theory of Semi-periodic Signals for Fast Varying Loads Power Properties Identification .....	19
3.4 Supply Current Decomposition for Fast Varying Loads .....	22
CHAPTER 4. COMPENSATION OF FAST VARYING LOADS .....	28
4.1 Introduction .....	28
4.2 Hybrid Compensator for Fast Varying Loads .....	30
4.3 Compensation Algorithm .....	31
4.3.1 Reference Signal for the Power Variation Compensator .....	31
4.3.2 Reference Signal for the Distortion Compensator .....	34

4.4 Integrated Operation of the Hybrid Compensator .....	35
CHAPTER 5. MATHEMATICAL MODEL OF THE HYBRID COMPENSATOR OF FAST VARYING LOADS .....	37
5.1 Introduction .....	37
5.2 Modeling of the Supply System .....	37
5.3 Modeling of the Fast Varying Load .....	39
5.4 Modeling of the Power Variation Compensator .....	45
5.5 Modeling of the Distortion Compensator .....	53
CHAPTER 6. COMPUTER SIMULATION OF THE HYBRID COMPENSATOR OF FAST VARYING LOADS .....	56
6.1 Introduction .....	56
6.2 Block 1: Variables Definition and Initialization .....	57
6.3 Block 2: C Class Object Definition .....	59
6.4 Block 3: Integration .....	61
6.5 Block 4: FVL Supply Current Calculation .....	62
6.6 Block 5: Sample Supply Voltage and Current .....	63
6.7 Block 6: Generate Reference Signals .....	64
6.8 Block 7: Generate PWM Switching Sequences .....	67
6.9 Block 8: Hybrid Compensator Current Calculation .....	67
6.10 Block 9: Compensated Supply Current Calculation .....	68
6.11 Block 10: Results.....	69
CHAPTER 7. VERIFICATION OF THE PERFORMANCE OF MODEL OF THE HYBRID COMPENSATOR .....	70
7.1 Introduction .....	70
7.2 Simulation of the Test Loads Supply Current .....	71
7.3 Simulation of CPC Decomposition of the Supply Current .....	71
7.4 Simulation of the Reference Signals for the Hybrid Compensator .....	74
7.5 Simulation of the Compensator Current .....	78
CHAPTER 8. CONCLUSIONS .....	85
REFERENCES .....	87
APPENDIX A. USER INTERFACE SCREENS OF THE COMPUTER MODEL .....	92
APPENDIX B. PARAMETERS FOR VERIFICATION OF THE COMPUTER MODEL .....	106
VITA .....	107

## **List of Tables**

2.1 General Properties and Power Variation for Some Common Fast Varying Loads .....	16
5.1 Converter Modes and Equivalent Voltages .....	41
5.2 Converter Commutation .....	44

## List of Figures

2.1 Example of power variation of a FVL .....	6
2.2 Power variation of a repetitive-FVL .....	7
2.3 Power variation of a random-FVL .....	7
2.4 Power variation in a repetitive burst-FVL .....	8
2.5 Example of a random FVL (a) supply voltage. (b) supply current .....	15
3.1 Example of FVL supply current .....	18
3.2 Variation of the active power and median power of a FVL .....	21
3.3 Rms value of the supply current .....	23
3.4 Current decomposition for the supply current of the FVL. (a) Fundamental active current. (b) Fundamental reactive current. (c) Distorted current .....	26
4.1 Structure of the hybrid compensator of FVLs .....	30
4.2 Identification of the modes of operation of the power variation compensator .....	31
4.3 Reference signal and modes of operation for the power variation compensator .....	34
4.4 Reference current for the distortion compensator .....	35
4.5 Difference between the distorted component of the supply current and the reference current of the distortion compensator .....	35
5.1. Structure of the supply system for the hybrid compensator .....	37
5.2. Structure of the FVL .....	39
5.3. Types of loads investigated .....	39
5.4. Structure of the AC/DC converter and FVL .....	40
5.5. Equivalent circuit of the AC/DC converter and FVL .....	40
5.6. Structure of the AC/DC converter and FVL during commutation .....	43
5.7. Equivalent circuit of the AC/DC converter and FVL during commutation .....	43
5.8. Structure of the power variation compensator .....	46

5.9. PV compensator with equivalent circuit of PMSM .....	48
5.10. abc and dq axis representation of PMSM .....	49
5.11. Equivalent circuit of the stator winding of the PMSM in dq mode .....	49
5.12. Mechanical system representation for the FESS .....	52
5.13. Structure of the distortion compensator .....	54
6.1 General flow diagram of the model .....	57
6.2 Example of the definition of values in FlywheelDoc.h .....	58
6.3 Example of the structures related to the FVL specification in FlywheelDoc.h .....	59
6.4 Example of dynamic memory allocation for the pointer of a two dimensional array and initialization of the supply system structure variables FlywheelDoc.h .....	60
6.5 Main view screen selections from the menu .....	60
6.6 MFC ClassWizard for CParameter class .....	61
6.7 CParameter class definition as structure variables .....	61
6.8 Integration subroutine .....	62
6.9 Processes within block 4 .....	62
6.10 FVL setting in parameters dialog box .....	63
6.11 First two approximations of the Runge-Kutta Fehlberg 4 <sup>th</sup> /5 <sup>th</sup> order subroutine .....	64
6.12 Processes within block 4 .....	65
6.13 CPC current decomposition subroutine .....	65
6.14 Prediction of current components subroutine .....	66
6.15 Reference PV current subroutine .....	66
6.16 Processes within block 7 for PV compensator .....	67
6.17 Processes within block 7 for DC compensator .....	68
6.18 Set of differential equations for inverter A and supply side of the PV compensator subroutine .....	68

6.19 Set of differential equations for inverter B and FESS of the PV compensator subroutine ...	69
6.20 Differential equation for DC compensator subroutine .....	69
6.21 Compensated supply current subroutine .....	69
7.1 Running active and median power of FVL1 .....	70
7.2 Running active and median power of FVL2 .....	70
7.3 Running active and median power of FVL3 .....	71
7.4 Supply current of test loads. (a) FVL1, (b) FVL2, (c) FVL3 .....	72
7.5 Running rms value of the fundamental active current. (a) FVL1, (b) FVL2, (c) FVL3 .....	73
7.6 Running rms value of the fundamental reactive current. (a) FVL1, (b) FVL2, (c) FVL3 .....	74
7.7 Distorted component of the supply current. (a) FVL1, (b) FVL2, (c) FVL3 .....	75
7.8 Difference between the actual and the predicted running rms value of the distorted component of the supply current. (a) FVL1, (b) FVL2, (c) FVL3 .....	76
7.9 Power variation compensator reference current, $\tilde{j}_{p_{REF}}$ . (a) FVL1, (b) FVL2, (c) FVL3 .....	77
7.10 Distortion compensator current, $\tilde{j}_{D_{REF}}$ . (a) FVL1, (b) FVL2, (c) FVL3 .....	78
7.11 Power variation compensator current, $\tilde{j}_p$ . (a) FVL1, (b) FVL2, (c) FVL3 .....	79
7.12 Distortion compensator current, $\tilde{j}_D$ . (a) FVL1, (b) FVL2, (c) FVL3 .....	80
7.13 Supply current of FVL1. (a) non-compensated, (b) compensated .....	81
7.14 Supply current of FVL2. (a) non-compensated, (b) compensated .....	82
7.15 Supply current of FVL3. (a) non-compensated, (b) compensated .....	82
7.16 Running active power of compensated load. (a) FVL1, (b) FVL2, (c) FVL3 .....	83
7.17 Harmonic spectrum of compensated supply current. (a) FVL1, (b) FVL2, (c) FVL3 .....	84

## **Abstract**

A computer model of the hybrid compensator of fast varying loads was developed in this dissertation. The computer model was implemented in MFC Visual C++ compiler version 6.0.

The classification of fast varying loads and effects of their operation in distribution systems were described in this dissertation.

The power properties of fast varying loads were expressed in terms of the Currents' Physical Components Theory. Therefore, the Currents' Physical Components Theory was applied to systems with non-periodic voltages and currents.

The supply current of the fast varying loads was decomposed into the useful and the useless components using an algorithm based in the Currents' Physical Components Theory. The current components resulting from this decomposition were used to generate the reference signals for compensator control.

The systems of equations that modeled the integrated operation of the distribution system, the fast varying load and the hybrid compensator were developed in detail.

The computer model was developed with sequential subroutines that allowed both the analytical solution of the compensation of fast varying loads and the incorporation of the hybrid compensator in the compensation of fast varying loads.

The performance of the computer model was verified by comparison between the analytical results with the results obtained with the effect of the hybrid compensator.

Finally, the computer model provided reduction of the active and reactive power variation and reduction of the distorted component of the supply current of the fast varying loads tested.

## **Chapter 1**

### **Introduction**

The supply capability of a distribution system is best utilized if the load is resistive, balanced and has a constant active power. This capability declines with the power variation, reactive current and distortion increase in the distribution system. A load can be defined as fast varying when a substantial change of the load power can be observed in part of a second or part of a minute. This variation could cause undesirable disturbances or an increase in energy losses. In addition, if the fast varying load (FVL) is energized by power electronics equipment, there are bursts of distortion. Therefore, high variation of the energy consumption and distortion are the two major features of systems with such loads. These effects can be reduced by compensators.

Compensators of FVLs should reduce the variation of the active power in the system and should reduce the burst of waveform distortion. Power variation compensation requires that a compensator be capable of storing and releasing back to the distribution system a sufficient amount of energy. Bursts of distortion compensation require that a compensator is capable of generating the fast varying current capable of compensating the distorting component of the load current. These two requirements are substantially different. Therefore, a compensator of FVLs should be built of two separate compensators; one for the power variation and the other one for distortion component. It should have a hybrid structure.

Compensators to reduce the distorted component of the supply current are referred as switching compensators, also known as active filters, active power or harmonic filters. In many applications generation of the reference signals for the switching compensator control is based in the Instantaneous reactive p-q Theory. In recent years, the Currents' Physical Components (CPC) Theory is the approach used to generate the reference signals for the distortion compensator control. CPC Theory enables the direct decomposition of the load current into the useful and the

useless component. CPC theory also can be extended for the case of the non-periodic signals of fast varying loads.

Compensation of the power variation of fast varying loads has not been attempted yet. Therefore, the importance of the computer model of the hybrid compensator is emphasized as the first step in the development and implementation of a hybrid compensator of fast varying loads.

### **1.1 Dissertation Subject**

A computer model of the hybrid compensator of fast varying loads is the subject of this dissertation.

### **1.2 Dissertation Objectives**

1. Classification of fast varying loads.
2. Identification of power properties of fast varying loads in terms of Currents' Physical Components Theory.
3. Development of a Currents' Physical Components Theory based algorithm of generation of reference signals for compensator control.
4. Development of a computer model of a compensator of fast varying loads.
5. Model verification

### **1.3 Dissertation Thesis**

Currents' Physical Components Theory provides an effective theoretical foundation for compensation of fast varying loads.

### **1.4 Approaches to Objectives Fulfillment**

Approaches to the objectives fulfillment:

1. To achieve objective 1, power properties of fast varying loads have to be investigated.

Analysis of the power variation of common fast varying loads is required. Study of

recorded data of currents and voltages waveforms, as well as the time variation of the active and reactive power is necessary for their classification.

2. To achieve objective 2, power properties of fast varying loads have to be expressed in terms of the Currents' Physical Components Theory. It means that the CPC power theory has to be applied to systems with non-periodic voltages and currents.
3. To achieve objective 3, the FVL supply current has to be decomposed using CPC theory into the useful and useless components. An algorithm to obtain the reference signals using the results of the current decomposition obtained after achieving objective 2 is needed. The computer model implements this algorithm in a subroutine programmed in Visual C++. As a result, the reference signals for the compensation control can be generated.
4. To achieve objective 4, a system of equations that model the integrated operation of the distribution system, the fast varying load and the compensator has to be developed.
5. To achieve objective 5, the effects of compensation by the computer model have to be compared with the analytical results. Verification of the model can be done by repeating this comparison for a variety of types of FVL, classified in objective 1. The data of the supply voltage and current of the FVLs obtained from the system analysis can be stored in memory and used as base cases for verification of the model and analysis of compensator performance. The power variation of the compensated load and its harmonic spectrum can be used to verify the ability of the compensator to reduce the power variation and distortion of the test loads.

## **1.5 Structure of Dissertation**

The dissertation is structured as follows:

Chapter 2 describes the classification of the fast varying loads in terms of the power pulses occurrence. This Chapter is also devoted to compiling features of common FVL in distribution

system. The effects of FVL operation on distribution system complete the classification of these loads.

Chapter 3 is devoted to the power properties identification of FVL. The application of the CPC theory for identification of power properties of FVL and calculation and modeling of the current decomposition of a FVL supply current is presented in this Chapter.

Chapter 4 explains the concept of hybrid compensation of FVLs and the structure of the hybrid compensator. An algorithm of the reference signal generation and integrated operation of the hybrid compensator are presented in Chapter 4.

Chapter 5 presents the complete development of the system of equations used to model the FVL operation and the compensator of FVL. It includes the model for each element of the system into consideration: distribution system, FVL load and the hybrid compensator.

Chapter 6 presents the flow diagram of the hybrid compensator computer model. It describes the structure of the program and windows, and solutions of the systems of equations developed in Chapter 5.

Chapter 7 presents the results of the computer modeling of the compensator in the form of plots. Several types of FVL and the results of its compensation are modeled and results are plotted.

Two appendixes are included in the dissertation. Appendix A contains a description of the user interface of the program developed in Visual C++ for this dissertation. Appendix B contains the values of the hybrid compensator parameters used for verification of the computer model.

## **Chapter 2**

### **Fast Varying Loads**

#### **2.1 Introduction**

The energy demanded in a distribution system varies in time. Depending on the type of loads, residential, commercial or industrial, the time varying characteristic of the load differs [1, 2]. The load profile, meaning a plot of the variation of the electric active power versus time is used to describe it. Distribution systems are designed to account for the power variation due to the time varying characteristic of the load. However, the load active power variation over a single period or a 24 hour period or a week is not the subject of this dissertation.

The meaning of “Fast Varying Load” is not well defined, but a load can be considered as fast varying when substantial change of the load power can be observed in part of a second or part of a minute. This variation can cause undesirable disturbances or an increase in power losses. Moreover, if the FVL is energized by power electronics equipment then bursts of distortion can occur. To conclude, high variation of the power consumption and distortion are the two major features of systems with such loads. This Chapter classifies FVLs in terms of these two properties. It also discusses the effects of FVLs operation on the quality of the supply.

Traditionally, system reconfiguration and reactive power compensation are some of the techniques used to reduce the effects of time varying loads operation in distribution systems [3-5]. A discussion of the compensation requirements and techniques to reduce the effects of FVLs operation is presented in Chapter 4.

#### **2.2 Characteristics of Fast Varying Loads**

The power variation associated with FVL operation, should not be confused with the change in the power associated to a transient or a momentary disturbance caused by a load faults such as short circuits. A load is regarded as FVL if a substantial variation in power takes place during

steady state operation.

A load that can have a short random increase of energy consumption is the simplest FVL. An example of the power variation of such load, its short term average and the median power,  $P_m$ , is shown in Figure 2.1.

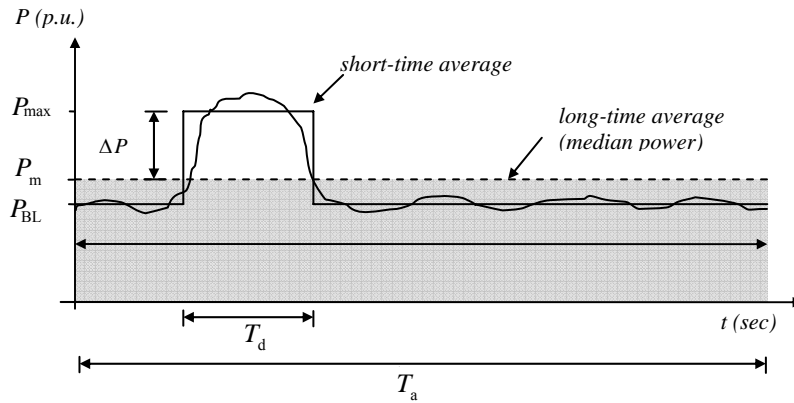


Figure 2.1. Example of power variation of a FVL

In the example presented in Figure 2.1, the active power in interval  $T_d$  increases over the median by  $\Delta P$ . As a consequence, there is an increment in the value of the  $P_m$  for that particular distribution system.

In terms of the rate of occurrence, FVLs can be classified as: repetitive, random and burst FVL

### 2.2.1 Repetitive Fast Varying Load

An example of a FVL with a sequence of power pulses is shown in Figure 2.2. The repetition interval,  $T_r$ , could be constant or variable. The duration of the individual pulses is much smaller than  $T_r$ . The median power calculated in Figure 2 is done considering the averaging interval,  $T_a$ , equal to  $T_r$ .

### 2.2.2 Random Fast Varying Load

A random fast varying load is characterized by random power pulses. The pulses may

vary one to the other in amplitude or in the repetition interval.

An example of a random FVL is shown in Figure 2.3.

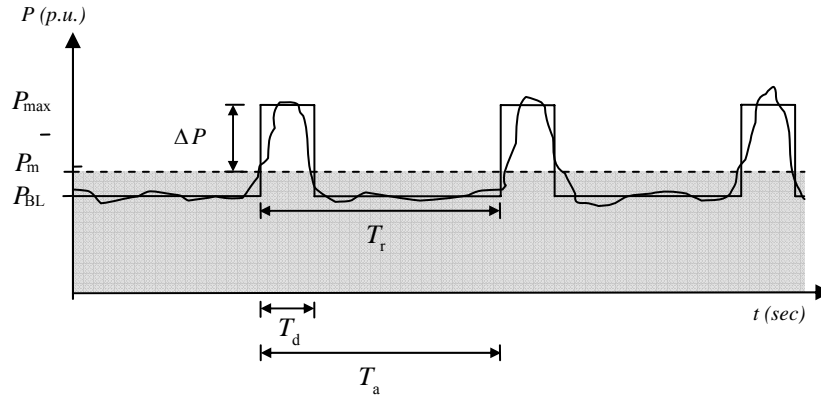


Figure 2.2. Power variation of a repetitive FVL

The averaging interval and the short-term average of the power variation are shown in the plot.

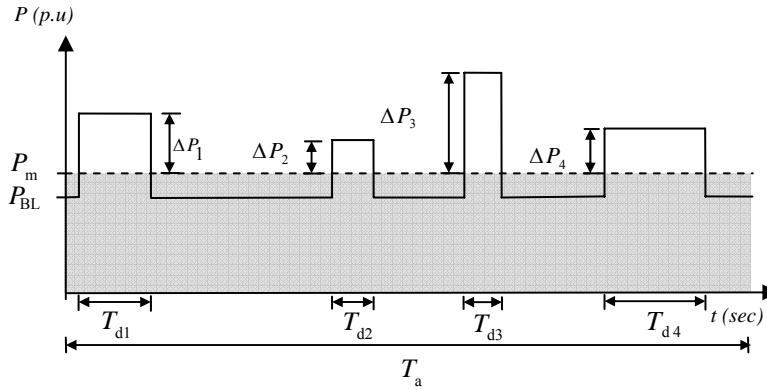


Figure 2.3. Power variation of a random FVL

### 2.2.3 Burst Fast Varying Load

A burst fast varying load is characterized by groups of power pulses that can be periodic or random.

If the burst FVL is periodic, the next interval of operation of the load requires another identical set of power pulses as shown in Figure 2.4. Again, only the short-term average of the power variation is plotted and calculated considering  $T_a$  equal to  $T_r$ .

## 2.3 Common Fast Varying Loads

Electric loads that behave as the FVLs described in Section 2.2 can be found in industrial,

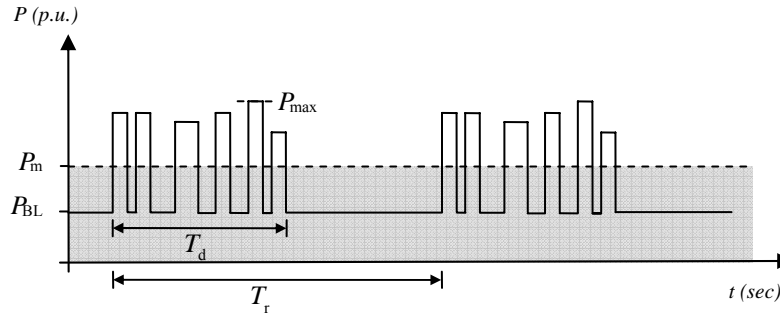


Figure 2.4. Power variation in a repetitive burst FVL

mining, medicine, physic and military areas. Crushers, rolling mills, arc furnaces and spot welders are examples of industrial FVLs. Electrical excavators are common fast varying loads in mining. Lasers and particle accelerators are typical representations of these loads in physics and medicine. Electric guns represent a particular case of FVL; pulsing loads. The characteristics of some of these loads are developed below.

### 2.3.1 Crushers

Crushers are in most cases heavy equipment used in variety of processes to decompose or break a material into smaller pieces. Crushers are widely use also in mining, food processing, paper industry and mills. Depending on the application, the operation of a crusher can be random, repetitive or burst.

The random operation of a crusher demands a distribution system capable to supply the high torque peak to crush the material. Also, it should resume to normal operation within a short period of time. Not all the rocks/materials are the same size, therefore, the demand of torque from the drive changes, as well as the size of the material to be crushed changes. When the material passes thorough the crusher, the different streams are accelerated and compressed by the

force produced by the motor. Different factors act to produce the final crushing of the material until it is discharged.

The repetitive burst operation conditions of five 2000 HP crusher-conveyors with a variable frequency drive were studied in [6] to analyze the transient temperature response of the cables used to energize them. The current profile characteristic, meaning the current versus time, for these crushers were drawn for up to 8 hours in [7]. The analysis of the BP-PL characterizing the crushers from the measurements in [6, 7] and the “design current profile” plotted in [7] showed that start-up pulse has a  $T_d = 30\text{sec}$  during the first initial load. After the first repetition cycle in the operation of the crusher each pulse of the following bursts of pulses have  $T_d = 20\text{sec}$ . The repetition interval for this burst FVL is  $T_r = 2\text{hrs}$ .

The operation conditions of a motor used to drive a crusher are severe. For example, the recommendation based on the torque requirements for such motors in the cement industry take into account a 250% overload at least for 10 to 15 sec, for up to 10 times per hour [8] as well as other constraints. The load profile, power consumption, technical specifications and other electrical variables during the operation of crushers have been successfully investigated before [6-11]. Some authors have shown field recorded data during the operation of crushers [6, 7, 12], others have plotted the actual load profile for a particular crusher [7, 13].

In all the papers investigated the operation of crushers is repetitive, random or burst

### **2.3.2 Rolling Mills**

Rolling mills are used to change the width of material, for example steel. The load characteristics faced by the drive are variable [14]. Depending on the reduction required, the gear ratios and speed of the motors vary. In a typical metal production [15] the main idea is to maintain a continuous operation regardless the wide range of dimensions and finished products required. A rolling process for a single bar may last for several minutes, and the interval

between each bar might be a few seconds.

In steel rolling mills this process can be repetitive; for example, every minute a new steel bar needs to be compressed. The process can be non-repetitive; for example, several passes of the material within a period of time. In both cases it is characterized by high energy consumption. A study for a cold rolling mill in [16] located in the U.S. Midwest showed that the load fluctuation caused as much as 1.5% fluctuation in the voltage, as measured in the 12.47kV line feeders. As a consequence the adjacent loads were disturbed by flickers. An analysis of the current profile for that cold rolling milling application showed also a random variation of the maximum peak demands within that one minute. The measurements taken for the load profile at the secondary winding of the transformer energizing the 500 HP DC drive for the same mill showed emanating pulses. The load pulses occurred 3-5 times per second and had a 1-2 cycle duration.

The type of load for the rolling mills in cement and steel industries investigated are either repetitive-FVL or random-FVL.

### **2.3.3 Electrical Excavators**

An Electrical Excavator, also known as a Power Shovel, has been used in the open cast mining industry for years. In most mining facilities there is more than one Power Shovel in use at a time. The energy demand for these machines is rapidly variable.

A study done in an open-cast lignite mine in Turkey in [17] showed the actual active power and reactive power consumption for three power shovels and a dragline. The power shovels A and B at the Turkey mine were driven by a DC motor supplied from a four quadrant 6-pulse thyristor converter. The power shovel C has a Ward Leonard Drive with an induction motor and the dragline is driven by another Ward Leonard Drive with synchronous motors in the supply side. Regardless of the diverse range of devices used as drives in this particular application, the active and reactive power plots showed a random, fast and highly variable behavior. For

example, the power shovel A registered multiple variations of the consumed active power that comes from -220 kW up to 1000kW for the 200 sec observation window recorded. As for the Reactive Power recorded, the same highly variable consumption profile is observed. In this case it could vary from -400 kVAr (Capacitive) to 600 kVAr (Inductive). Similar results are shown for the power shovel B, the power shovel C and the dragline, the range of variation in the active and reactive power registered is similar, although the profile of each electrical excavator is different. In all cases, the active power and the reactive power profile are typical for fast varying loads. The power consumption rises and falls randomly depending on the use of the machine. The highly variable torque demanded by the electrical excavator load implies a similar response from the driving system.

A similar response in terms of the active power and reactive power consumption is presented in [18] for the case of a power shovel used in an open-tip mine. In this paper, the researchers presented the shovel active power consumption for a complete load truck cycle. The authors specified the stages in the movement of the shovel. Each of the seven loading actions for the shovel including regenerative operation recorded distinct and highly variable values for the active power consumption. In a single truck load cycle, the active power of the shovel registered varied from -1.2 MW to 2.51 MW in less than 1 min. Regeneration accounts for 15% of the power absorbed from the supply, as investigated in [18]. The study investigates the different drives used for power shovels and describes some operation problems encountered and its solutions.

#### **2.3.4 Arc Furnaces**

Electric arc furnaces are used in the steel or aluminum industry. Their main function is to melt and to refine metals, in many cases from scratch. The system consists of electrodes that are moved into the material to be melted. The material is melted due to the high power surge coming

from the electrodes [19]. An electro-thermal energy conversion process takes place. The proximity of the energized electrodes to the material develops an electric arc while the electrodes are lowered and raised. The energy of the arc is converted into heat, melting the material, in this case steel or aluminum. The melting process is not linear, it is dynamic, and it varies depending on the material response to the electric arc and the heat. In fact, the nature of this load can be described as a highly non-linear, randomly time varying load. Each phase of the melting process affects the dynamic of the electric arc [20]. As it is developed in [20] the three basic periods of the arc are: first, the arc reignites from zero; second, the arc is established; third the arc begins to extinguish. The dynamic, duration and energy required in each stage depend on the dynamic behavior of the material during the melting process. The dynamic nature of the arc makes the process absolutely stochastic. Moreover, this process can be described as batch type operation [21]. Each heating process is followed by another heating process with almost no interruptions until the desired material is obtained. In addition, as stated in [21] it is also common to experience furnace power in and out. All this leads to the random behavior of the electric arc that is reflected as random variation of the supply current and voltage waveform. As a consequence, operation of an arc furnace in a network results in major disturbances in the supply. These disturbances are characterized mainly by voltage flicker and harmonic injection to the system.

### **2.3.5 Cycloconverter Fed Loads**

A Cycloconverter is a power electronics device used to change an AC signal at a fixed frequency to an AC signal at a different magnitude and frequency.

It can be designed as a single phase or a three phase unit. Cycloconverters are also known as dual converters. The design technology for cycloconverter varies, having the flexibility to be found as three-pulse, six-pulse or twelve-pulse configurations for three phase units. A three-pulse

cycloconverter is designed using three AC/DC converter units. A six-pulse cycloconverter is designed using three AC/DC converter units and three DC/AC inverters units. And a twelve-pulse cycloconverter is designed using six AC/DC converter units and six DC/AC inverter units.

The speed control of high power synchronous and induction AC motors is done using cycloconverters. Some of the industrial loads driven by cycloconverter fed motors are large mills, grinding mills, pumps, compressors, induction heaters, aircraft and marine industry, for example.

The steady state operation of a cycloconverter itself produces a distorted signal. In a cycloconverter fed FVL both strong distortion and power variation are combined. The impact of the operation of cycloconverters in power systems is much more harmful due to the combination of these two phenomena.

### **2.3.6 Pulsing Loads**

Pulsing loads, PLs, are electric loads that consume energy in short intervals of time separated by much longer intervals of low energy consumption. The pulse duration and the separation time depend on the application.

Representative cases of FVLs that behave as PLs are found in industrial, medicine, physic and military applications. Some of these examples are spot welders, lasers, particle accelerators and electric guns. Two typical PLs are:

- Spot welders

This is a typical PL for the power system. In all cases, during the operation of the welder a high pulsed energy is required. The power consumed by a welder during its operation is mainly reactive, after using it no power is required. Resistance Spot welders can be found in several applications such as automobile industry, marine/ship industry, aircraft industry, oil industry, steel manufacturing, pipe welding and cutting and construction. A typical operation for welders

requires large amount of power for short periods several times within their operation period. The average size of electric welders is in the order of several hundred kVA with short circuit currents in the order of 1 kA to 250 kA depending on the application. Another characteristic of the signals drawn by spot welders are its short time duration. It could be from 2 to 120 cycles of 60 Hz [22]. Since the main energy drawn by welders is reactive one of the problems associated with its operation is the poor power factor. The use of Spot Welders may also affect the quality supply standards of a Power System due to the system flicker they produce [23]. One of the cases studied in [22] is a 1200 kVA spot welding machine. The recorded current during its operation was 2 kA with an approximate duration of less than a half second in average, recorded for as long as 8 seconds. On the other hand, the results of the welding current measurements taken in [22] showed pulses of more than 8.1 kA with a duration of 5 cycles or 15 cycles in average for a three-phase current spot welding machine at 20, 40 and 60% of its nominal 50% duty cycle of 96KVA capacity. Real time measurement of the operation of resistance welders in an automotive plant [24], showed a pulse in the order of 1 kA during approximately 7 ms. A spot welder represents a Random-FVL for the distribution system.

- Electric guns

Electric guns used in the military field require a controlled pulse-power supply capable to generate the substantial energy to accelerate the projectile [25]. Depending on the type of electric gun, electromagnetic or electrothermal, the requirements for the particular pulse supply changes [26]. In some electromagnetic guns a high voltage, low current pulse is required. In some electrothermal guns a low voltage, high current pulse is required. In other cases a burst of pulses is required. On the other hand, portability of electric guns in the battle field is a case of research nowadays [26, 27]. In this case, the pulse-power supply needs to be capable of storing energy. The control of electric guns is done using solid-state switches [28, 29]. Therefore, electric guns not

only contribute to the power variation but also contribute to distortion in the supply.

Table 2.1 compiles general characteristics for some common FVLs. It also presents the plots of the variation of the active power and its median for typical examples.

Additional harmful effects of FVLs can be caused by the power electronics equipment used for supplying such loads. There are usually bursts of distortion.

The supply current for the crusher in Table 2.1 is shown in Figure 2.5 (b). In this example the FVL is energized from an AC/DC Converter with a symmetrical supply voltage as illustrated in Figure 2.5 (a). The analysis in this dissertation is done for per unit parameters. The two most distinct properties of FVL are illustrated in this example. Table 2.1 shows the profile of the power variation and Figure 2.5 illustrates the strongly distorted supply current and the sinusoidal supply voltage.

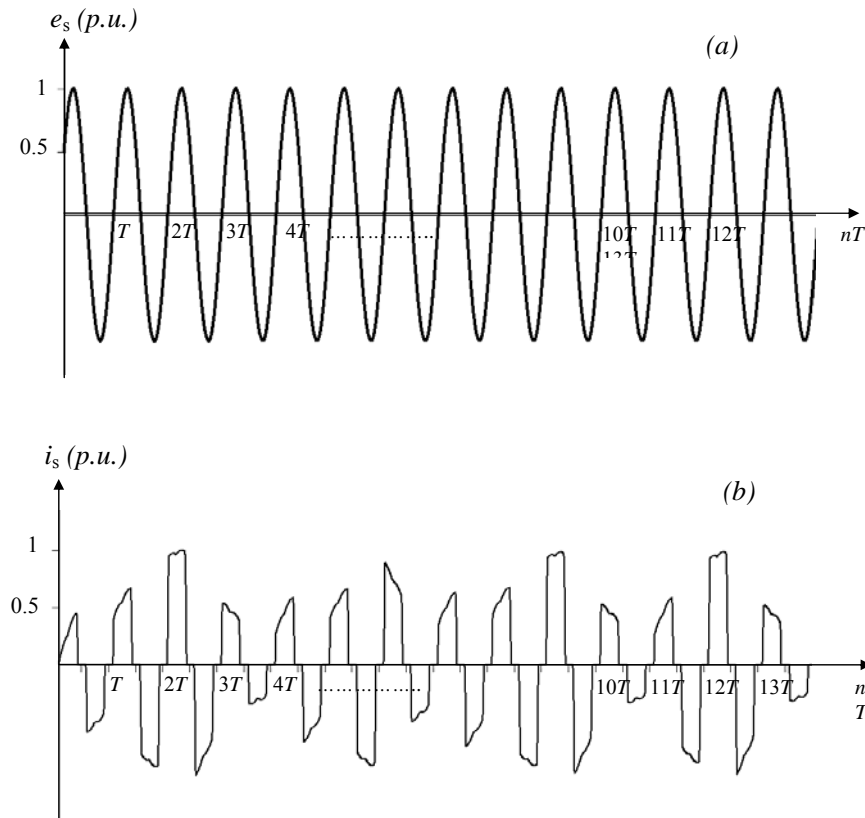
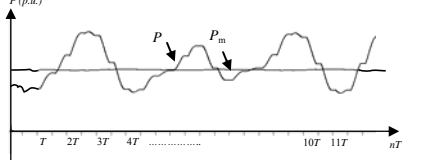
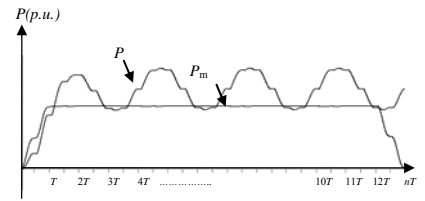
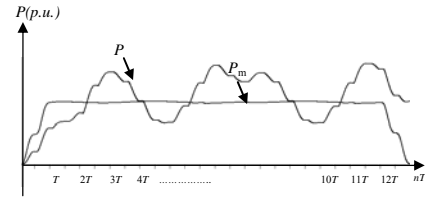
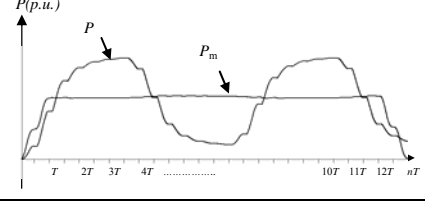
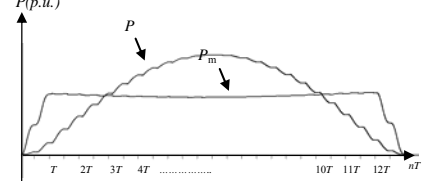


Figure 2.5. Example of a random FVL (a) supply voltage. (b) supply current

## 2.4 Effects of Fast Varying Loads in Distribution Systems

The supply capability of a distribution system is best utilized when it is loaded with a constant active power. In such case, the rms value of the supply current is constant. The power

Table 2.1 General Properties and Power Variation for Some Common Fast Varying Loads

Load	Properties of the load			
	Operation characteristics	Motor/ Drive/Supply	Type	Active and median Power
Crusher	High torque peaks to crush the volume of material. Also, it should resume to normal operation within a short period of time	DC motor driven by an AC/DC Converter. AC drives are used too.	Random, Repetitive	-Random variation of up to 200% of the load torque 
Rolling Mill	Cyclic or acyclic pulsing or highly increasing and decreasing torque peaks to compress the volume of material. Also, it last several cycles	AC and DC drives	Single, Repetitive	-Repetitive variation of the load torque every 3 cycles 
Electrical Excavator	Rapidly variable. It could be totally random, fast and highly variable too	DC drive system, four quadrant operation	Random, Burst	-Random variation of up to $\pm 100\%$ of the load torque 
Welder	Pulses. A spot welder represents a fluctuating load with a random operation for the Power System	AC or DC supply	Random	-Two consecutive operations 
Electric Gun	Pulsing load. Its operation could last several cycles	Pulsed power supply	Single, Random	-Pulse load 

losses and voltage drop are constant and predictable. In such scenario, the limits in the steady-state voltage supply are kept within the  $\pm 10\%$  limit established by ANSI C84.1-1989 for the United States, for example. A load demanding an active power variation as the one illustrated in Table 1, causes a variation in the rms value of the current and a variation in the losses. As a

consequence, the +10% tolerance limit might be exceeded. Also, such variation in the rms value of the current could cause an increase in the voltage drop above the limits established by the National Electrical Code® (NEC®) (NFPA 70), of 3% for a feeder and 3% for a branch circuit, but the total drop cannot exceed 5%, of the utilization voltage.

Large-scale FVLs, as the ones described in section 2.3, are capable of causing severe voltage sags or “dips” beyond the tolerance established by ANSI C84.1-1989. The duration of the voltage sag is determined by the characteristics of the load (from a few to several cycles).

Voltage sags affect surrounding loads. Shunt surge-protective devices (SPDs), commonly used to limit or divert disturbances in power systems, could be non-responsive to these sags if they contained only nonlinear components. A combination of both shunt and series linear components might be needed.

Another major disturbance caused by the operation of FVLs is its contribution to the distortion in the supply voltage and current waveform. As a reference, the limit in the distortion established by IEEE Std 519-1992 for an individual load 69KV and below is 3% and 5% for the total voltage distortion. The amount of distortion caused by the operation of FVLs energized by power electronic equipment needs to be evaluated. In the instance that these limits are exceeded then compensation might be needed.

The severe operation conditions imposed by FVLs might affect the ability of the supply to fulfill the energy demand, affect the operation of other loads and circuits surrounding them and might need to be compensated. Traditional compensation techniques might not be suitable for FVLs. This dissertation discusses the compensation requirements for FVLs.

## Chapter 3

### Power Properties of Fast Varying Loads

#### 3.1 Introduction

The compensator control requires that the power properties of the load are identified. This identification has to be performed in situation where currents are non-periodic, for example as demonstrated in Figure 3.1.

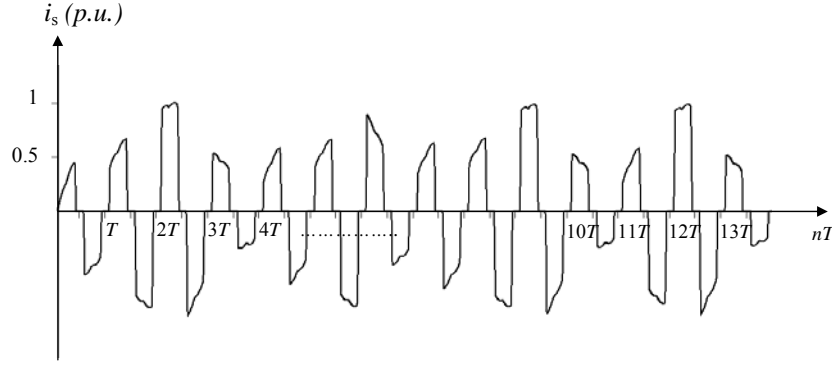


Figure 3.1. Example of FVL supply current

The non-periodicity and high distortion of the supply current can be observed in Figure 3.1.

When these voltages and currents are periodic, then Fourier series is the mathematical tool for identification of power properties. This is not possible when these quantities are non-periodic.

#### 3.2 Approaches for Power Properties Identification of Non-periodic Signals

There are two main approaches in Power Theory to identification of power properties and compensation. The first approach is given by the Instantaneous Reactive p-q Theory [30, 31]. The second one is provided by the Currents' Physical Components Theory [32, 33].

The identification of power properties of a load requires that the instantaneous values of the load current and terminal voltage are measured. These values are used next for detection of useless components of the supply current which should be compensated.

The Instantaneous Reactive p-q theory requires that two instantaneous powers active  $p$  and

reactive  $q$  are calculated with Clarke's transform. The compensator's control signal is obtained from the inverse Clarke transform of the reactive power  $q$  and the alternating component of the active power  $\tilde{p}$  [34].

CPC theory enables a direct decomposition of the load current into the useful and the useless component [35, 36]. It enables the combination of time-domain and the frequency-domain approach for the compensator control.

### **3.3 Application of CPC Theory of Semi-periodic Signals for Fast Varying Loads Power Properties Identification**

The current decomposition for a pulsing load using CPC theory is presented in [37]. That approach provides fundamentals for generating the reference signals for the compensator in this dissertation.

Currents in electrical power systems, although non-periodic, have some particular properties that distinguish them from other non-periodic quantities. Energy to such systems is delivered exclusively at the frequency of the sinusoidal voltage generated by power generators. Moreover, currents of FVLs could be considered as quantities with only temporally or permanently "disturbed periodicity". Because of these two properties, the period  $T$  of the generated voltage can be detected and used as the main time-frame for analysis of power properties for such loads.

The supply current in Figure 3.1, although non-periodic, can be considered as semi-periodic. Definitions and consideration for characterization of semi-periodic signals are presented in [38].

Accordingly to the CPC theory, a balanced load supplied with a sinusoidal voltage can be described in terms of three physical current components. These currents are: the active current,  $i_{1a}$ , the reactive current,  $i_{1r}$ , the distorted current,  $i_d$ , the unbalanced current,  $i_u$  and the scattered current,  $i_s$ . On the other hand, performing the current decomposition and power properties identification of semi-periodic currents requires the use of the common functionals as in [39]

described below.

Let supply voltages and currents of a load be observed at the instant  $t$ . The energy delivered to the load, per phase, in the time-window of duration  $T$  that proceeds the instant  $t$ , is equal to

$$W(t) = \int_{t-T}^t u(\tau) i(\tau) d\tau \quad (3.1)$$

The average value of this energy over the window  $T$ , calculated at the end of this window, meaning at instant  $t$ , has properties of the active power, with the exception that it could not be constant, but changes with the observation instant  $t$ , namely

$$\tilde{P}(t) = \tilde{P} = \frac{1}{T} \int_{t-T}^t u(\tau) i(\tau) d\tau \quad (3.2)$$

The power in (3.2) will be referred to as the running active power. It is not a common active power. Therefore, to avoid confusion, it will be denoted by  $P$  with the mark  $\sim$ . When voltages and currents are periodic with period  $T$ , these two powers are identical. When they are not periodic however, then the common active power  $P$  is not defined.

The voltage and current of the load can be specified in the observation window by a sequence of  $N$  equidistant samples, taken at intervals  $\Delta\tau = T/N$ , namely,  $u_n = u(n\Delta\tau)$  and  $i_n = i(n\Delta\tau)$ . At a sufficiently high sampling rate and satisfying the Niquist criterion, the running active power at the end of the observation window  $t_k = k\Delta\tau$  has the value

$$\tilde{P}(t_k) = \tilde{P}_k = \frac{1}{N} \sum_{n=k-N+1}^{n=k} u_n i_n \quad (3.3)$$

This running active power for the FVL calculated as in (3.3) is presented in Figure 3.2. This example represents the crusher load in Table 2.1. The computational algorithms implemented in this dissertation are done in Visual C++.

The analysis and results plotted are done for per-unit parameters.

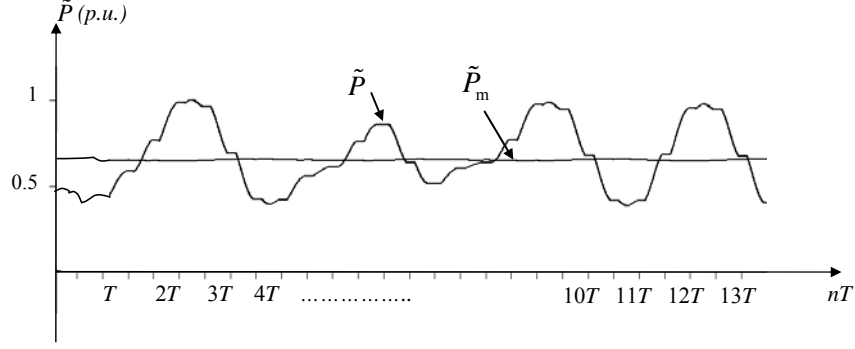


Figure 3.2. Variation of the active power and median power of a FVL

The median power,  $\tilde{P}_m$ , shown in Figure 3.2 is calculated considering 14 cycles as the averaging interval,  $T_a$ .

For the voltages and currents segments, interpreted as the sequence N of equidistant samples, a *running scalar product* can be defined. If  $x$  and  $y$  denote segments of semi-periodic quantities of  $T$  duration, then their running scalar product can be defined as

$$\left(\tilde{x}, \tilde{y}\right)_t = \frac{1}{T} \int_{t-T}^t x(\tau) y(\tau) d\tau \quad (3.4)$$

The scalar product can be calculated after the last samples,  $x_k$  and  $y_k$ , in the observation window are delivered, namely

$$\left(\tilde{x}, \tilde{y}\right)_k = \frac{1}{N} \sum_{n=k-N+1}^{n=k} x_n y_n \quad (3.5)$$

Moreover, a *running rms value* can be allocated to such segment

$$\|\tilde{x}\|_k = \sqrt{\left(\tilde{x}, \tilde{x}\right)_k} = \sqrt{\frac{1}{N} \sum_{n=k-N+1}^{n=k} x_n^2} \quad (3.6)$$

Segments  $x$  and  $y$  are orthogonal when their running scalar product is equal to zero. Then their running rms values satisfy the relationship

$$\|x \tilde{\mp} y\|_k = \sqrt{\|\tilde{x}\|^2 + \|\tilde{y}\|^2} \quad (3.7)$$

### 3.4 Supply Current Decomposition for Fast Varying Loads

A summary of implementation of the CPC theory for decomposition of the semi-periodic supply current into the useful and the useless components for the FVL considered are presented below. The computational algorithms implemented in this dissertation are done in Visual C++. The analysis is done in for per unit parameters.

The segment observed in the window of duration  $T$  can be interpreted as one period of a *hypothetical periodic extension*. It can be described in terms of the Fourier series. In particular, the segment of the load supply current,  $i(t)$ , in the observation window can be decomposed into the fundamental harmonic and the distorted current, denoted as  $i_1(t)$  and  $i_d(t)$  respectively. The fundamental component corresponds to one of the current component of main interest. It corresponds to the component for the main energy carrier. The distorted current is composed of all the quasi-harmonics of the current. Next, the fundamental  $i_1(t)$  can be decomposed into the active and the reactive fundamental currents,  $i_{1a}(t)$  and  $i_{1r}(t)$  respectively as shown in (10).

$$i(t) = i_1(t) + i_d(t) = i_{1a}(t) + i_{1r}(t) + i_d(t) \quad (3.8)$$

These three currents  $i_{1a}(t)$ ,  $i_{1r}(t)$  and  $i_d(t)$ , have a distinct physical meaning and can be considered as physical components of the load supply current. This decomposition into physical components can be performed after the last samples,  $i_k = i(k\Delta\tau)$  and  $u_k = u(k\Delta\tau)$ , in the window are provided by a data acquisition system.

Decomposition of the current into the fundamental and distorted components can be obtained by calculating the crms value of the fundamental quasi-harmonic with the Discrete Fourier Transform, DFT, applied to semi-periodic signals.

In general, at the end of the observation window, the crms value of the running quasi-

harmonic components of the supply current are calculated as,

$$\tilde{I}_{nk} = \frac{\sqrt{2}}{N} \sum_{n=k-N+1}^{n=k} i_n e^{-j\frac{2\pi}{N}nk} = \tilde{I}_{nk} e^{j\tilde{\beta}_{nk}} \quad (3.9)$$

The crms value of a running quasi-harmonic specified in (3.9) changes with the instant of the current observation, thus, it is not an instantaneous value of a sinusoidal current, but a current that can be referred to as a quasi-harmonic component. An example of the rms value of the running fundamental quasi-harmonic of the FVL supply current in Figure 3.1 is shown in Figure 3.3.

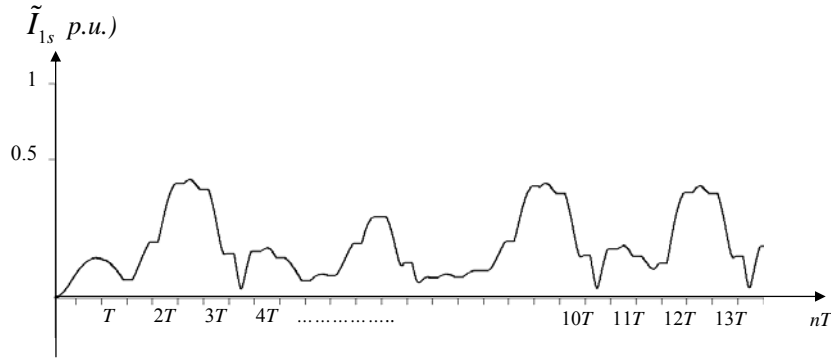


Figure 3.3. Rms value of the supply current fundamental quasi-harmonic component

There is a variation of the rms value of the fundamental quasi-harmonic component of the FVL shown in Figure 3.3. If the load under consideration were periodic, these values were constant. Since the FVL supply current is semi-periodic there can be an estimation of as many quasi-harmonic components as allowed by the Nyquist criterion. Since the quasi-harmonic component of interest for compensation purposes is the fundamental, the expression for this particular component is

$$\tilde{I}_{1k} = \frac{\sqrt{2}}{N} \sum_{n=k-N+1}^{n=k} i_n e^{-j\frac{2\pi}{N}n} = \tilde{I}_{1k} e^{j\tilde{\beta}_{1k}} \quad (3.10)$$

Thus, the instantaneous value of the supply fundamental current at instant of time  $t_k$  is obtained

$$i_{1k} = \sqrt{2} \operatorname{Re} \{ \tilde{I}_{1k} e^{j\omega_1 k \Delta \tau} \} \quad (3.11)$$

The distorted component of this current at instant  $t_k$  is equal to

$$i_{dk} = i_k - i_{1k} \quad (3.12)$$

The fundamental quasi-harmonic of the load voltage can be determined in the same way, namely at the instant  $t_k$

$$\tilde{U}_{1k} = \frac{\sqrt{2}}{N} \sum_{n=k-N+1}^{n=k} u_n e^{-j2\left(\frac{\pi}{N}\right)n} = \tilde{U}_{1k} e^{j\tilde{\alpha}_{1k}} \quad (3.13)$$

$$u_{1k} = \sqrt{2} \operatorname{Re} \{ \tilde{U}_{1k} e^{j\omega_1 k \Delta \tau} \} = \sqrt{2} \tilde{U}_{1k} \cos(\omega_1 k \Delta \tau + \tilde{\alpha}_{1k}) \quad (3.14)$$

Formula (3.13) presents the crms value of the fundamental quasi-harmonic of the load voltage periodic extension of what is observed in the window. Voltage in (3.14) is the fundamental quasi-harmonic of the load voltage. If the phase difference of the voltage and the current fundamental quasi-harmonics is

$$\tilde{\alpha}_{1k} - \tilde{\beta}_{1k} = \tilde{\varphi}_{1k} \quad (3.15)$$

The instantaneous value of  $i_{1k}$  can be decomposed in two components, the instantaneous value of the active current  $i_{1ak}$  and the instantaneous value of the reactive current  $i_{1rk}$  as follows

$$i_{1k} = \sqrt{2} \operatorname{Re} \{ \tilde{I}_{1k} e^{j\omega_1 k \Delta \tau} \} = \sqrt{2} \tilde{I}_{1k} \cos(\omega_1 k \Delta \tau - \tilde{\varphi}_{1k}) \quad (3.16)$$

$$i_{1k} = \underbrace{\sqrt{2} \tilde{I}_{1k} \cos \tilde{\varphi}_{1k} \cos(\omega_1 k \Delta \tau)}_{i_{1ak}} + \underbrace{\sqrt{2} \tilde{I}_{1k} \sin \tilde{\varphi}_{1k} \sin(\omega_1 k \Delta \tau)}_{i_{1rk}} \quad (3.17)$$

$$i_{1ak} = \sqrt{2} \tilde{I}_{1k} \cos \tilde{\varphi}_{1k} \cos(\omega_1 k \Delta \tau) \quad (3.18)$$

$$i_{1rk} = \sqrt{2} \tilde{I}_{1k} \sin \tilde{\varphi}_{1k} \sin(\omega_1 k \Delta \tau) \quad (3.19)$$

The instantaneous value of the active and reactive components of the quasi-harmonic fundamental supply current can also be expressed in terms of the equivalent running admittance.

$$\tilde{\mathbf{Y}}_{1k} = \frac{\tilde{\mathbf{I}}_{1k}}{\tilde{\mathbf{U}}_{1k}} = \frac{\tilde{\mathbf{S}}_{1k}^*}{\|\tilde{\mathbf{u}}_{1k}\|^2} = \tilde{G}_{1k} + j\tilde{B}_{1k} \quad (3.20)$$

Using (3.20), currents  $i_{1ak}$  and  $i_{1rk}$  can be expressed also as

$$i_{1ak} = \tilde{G}_{1k} u_{1k} \quad (3.21)$$

$$i_{1rk} = \sqrt{2} \operatorname{Re} \{ j\tilde{B}_{1k} \tilde{\mathbf{U}}_{1k} e^{j\omega_1 t_k} \} \quad (3.22)$$

The current components in (3.21) and (3.22) allow the calculation of the running fundamental active and reactive power by the following expressions

$$\tilde{P}_{1k} = \tilde{G}_{1k} \tilde{U}_{1k}^2 \quad (3.23)$$

$$\tilde{Q}_{1k} = -\tilde{B}_{1k} \tilde{U}_{1k}^2 \quad (3.24)$$

Since both the supply current and the *running fundamental current* can be estimated at any instant of time  $t_k$ , the distorted component is then

$$i_d(t) = i(t) - i_1(t) \quad (3.25)$$

Equations (3.21), (3.22) and (3.25) are the expressions used to generate the three needed components for compensation. These are: two components of the fundamental quasi-harmonic current, the fundamental active and fundamental reactive and the distorted component of the supply current.

These three components for the considered FVL supply current in Figure 3.1 are presented in the plot below.

Currents in Figure 3.4 are the basis to generate the reference current needed for control of the hybrid compensator. The fundamental active quasi-harmonic component shown in Figure 3.4(a) is the main energy carrier component of the supply current.

The current in Figure 3.4(a) is characterized by the similar variation of the magnitude at any

instant of time observed in the Figure 3.1 for the running active power for the FVL under consideration.

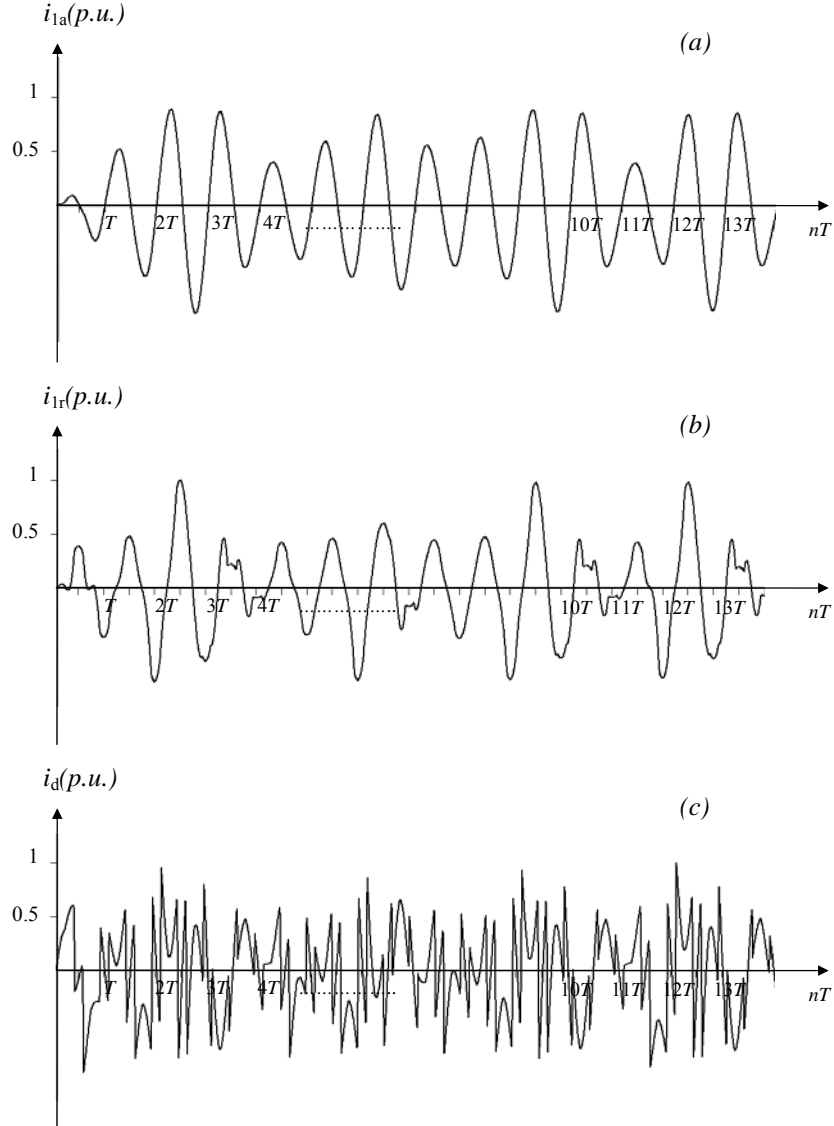


Figure 3.4. Current decomposition for the supply current of the FVL. (a) fundamental active current. (b) fundamental reactive current. (c) distorted current.

This is the useful component for energy delivery. The fundamental reactive quasi-harmonic component Figure 3.4(b) is the component responsible for the phase shift between the supply current and voltage of the FVL into consideration. The distorted component Figure 3.4(c) is the component responsible for the deviation of the FVL supply current from its fundamental. These last two components are useless in energy delivery but cause phase shift and increment in the

rms value of the supply current.

The application of the CPC theory enables the decomposition of the semi-periodic supply current of the FVL into the useful and useless components necessary to identify the reference signals for the compensator.

## **Chapter 4**

### **Hybrid Compensation of Fast Varying Loads**

#### **4.1 Introduction**

Compensation can have various objectives. In the case of compensation of FVLs, compensation of the power variation requires that a compensator is capable of storing and releasing back to the distribution system a sufficient amount of energy; compensation of burst of distortion requires that a compensator is capable of generating the fast varying current to compensate the distorting component of the load current.

These two requirements are substantially different. Compensators that provide the capability of energy storage do not have to be very fast. The amount of energy such compensators are capable of storing instead is crucial for such compensators. Compensators that have the capability of generating a distorting component of the current do not essentially need energy storage capability. Therefore, compensator of FVLs should be built of two separate compensators; one for reduction of the power variation and the other one for reduction of the waveform distortion. Therefore the compensator of FVL should have a hybrid structure.

The required energy storage capability for reduction of the power variation in distribution systems can be provided by Energy Storage Systems (ESSs). These systems could use batteries, (BESS), flywheels (FESS), super capacitors (SCESS), or superconducting magnetic energy storage systems (SMES) as the means for energy storage. The criteria in the selection of a suitable ESS for compensation of the variation on the active power in FVLs is a combination of the amount of energy that can be stored in the ESS and the rate of energy transfer from or to the load, meaning their power. Among these criteria also technical features and the benefit/cost ratios must also be taken into account. BESS have been widely used in power systems applications. It is a proven technology that has fulfilled the purpose of an alternate supply

successfully. Other emerging technologies tend to replace the use of batteries in recent years.

However, a comprehensive analysis of the advantages of using flywheels instead of batteries for Uninterruptible Power Supply, UPS, applications was conducted by the U.S. Department of Energy, Energy Efficiency and Renewable Energy, and by the Pacific Northwest National Laboratory [40]. In this document, many advantages of using flywheels exceeded batteries in terms of life cycle, maintenance, safety, environmental concerns, power density, space, reliability and costs. Ribeiro et al. [41] presented the advantage of applying ESSs to compensators in utility applications. In [41] the relationship between power (W/Kg) and Energy (Wh/Kg) was plotted showing the range of application for the different ESSs. In this paper the low cost/benefit ratio for the application of BESS in large storage capability is also pointed out. In this same paper, the advantage of the application of SCESS for high-peak low-energy loads is shown. For this type of loads, SCESS has an advantage with respect to the energy density, life and cost. However due to the nature of the FVLs considered in this dissertation, existing SCESS could not meet the criteria of the high energy required during its operation. Another plot of the range of applications for SCESS is found in [42]. The application of SMESS and FESS is widespread in power systems. Both technologies are comparable in terms of high efficiency, life-cycle, fast response and energy density [43, 44]. The major disadvantage for SMESS is its cost with respect to FESS in very large power applications [41, 44]. Two widespread applications for FESSs are as UPS and as voltage sag compensator [40, 45,46]. To some extent any ESS could fulfill the requirements for the compensation of the variation of the active power. In this dissertation the compensator of the active power variation is equipped with a Flywheel Energy Storage System.

The required fast response for reduction of the distorted component of the FVL current can be provided by a switching compensator. These devices, also known as active filters, have been

successfully used before for this purpose. Implementation of the CPC theory to generate the reference signals for the control of switching compensator is an innovation introduced in this dissertation.

#### 4.2 Hybrid Compensator for Fast Varying Loads

A hybrid compensator structure is shown in Figure 4.1. It is built of a compensator for reducing power variation and a compensator for reducing the distorting component of the supply current. The compensator for PV uses a Flywheel Energy Storage System in combination with PWM-based inverters with a DC bus capacitor to drive the electrical machine and the flywheel coupled to it. Permanent-Magnet Synchronous Motors, Synchronous Reluctance Motors or Homopolar Induction Motors can be used as a driving machine. A permanent-magnet synchronous motor is used as the driving machine in this dissertation. The compensator for the distorted current is built as a PWM-based switching compensator, also known as active filter or harmonic filter. The hybrid compensator is connected in shunt at node CN at the terminals of the load.

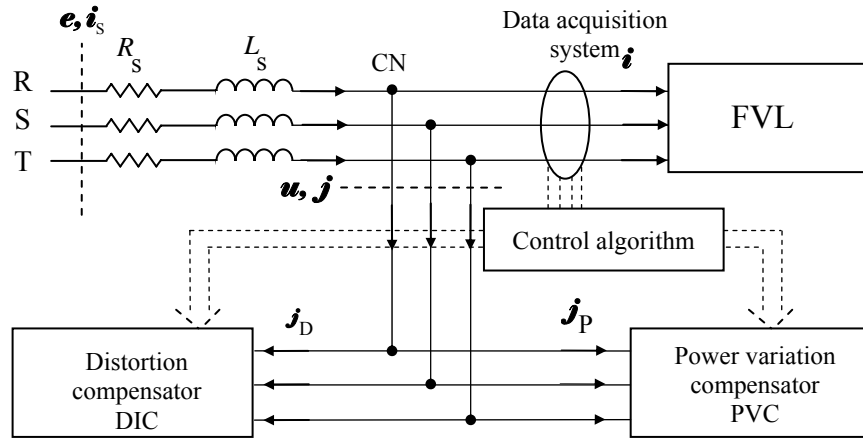


Figure 4.1. Structure of the hybrid compensator of FVLs

The power variation compensator (PVC) operates in two distinct modes, namely, energy storing (charging) mode and energy releasing mode. The active power variation of the FVL is

compared to the median power,  $\tilde{P}_m$ . If  $\tilde{P}_m > \tilde{P}$  then the PVC operates in charging mode. If  $P_m \leq \tilde{P}$  then the PVC operates in energy releasing mode. These modes of operation are shown in Figure 4.2.

The distortion compensator (DIC) is designed to inject the distorted component of the supply current to the distribution system.

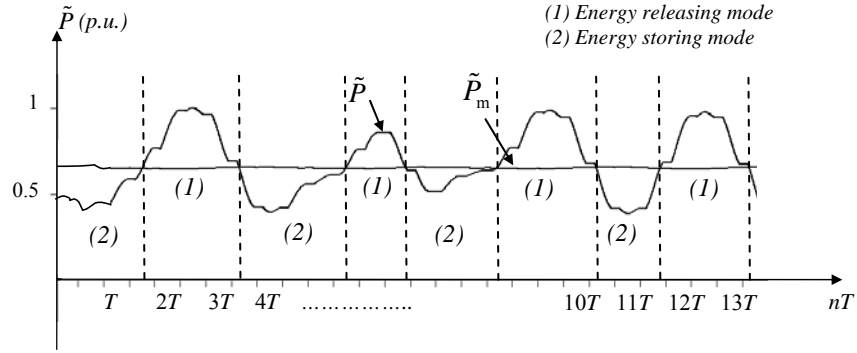


Figure 4.2. Identification of the modes of operation of the power variation compensator

### 4.3 Compensation Algorithm

To fulfill compensation objectives, two distinct reference signals need to be generated. These are the reference signal for the power variation compensator and the reference signal for the distortion compensator.

#### 4.3.1 Reference Signal for the Power Variation Compensator

The difference between the load active power and its median value provides the reference signal for the PVC control.

To reduce the difference between the actual active current and active current median, the PVC current,  $j_p$ , represented in Figure 4.1, needs to be injected into the system. This current is calculated as follows:

$$j_{Pa} = i_{1a} - i_m \quad (4.1)$$

The current in (4.1) is the reference signal for compensation of the active power variation.

To compensate the reactive power the fundamental reactive current,  $i_{lr}$ , has to be added to the reference signal. This consideration makes the reference signal for the PVC equal to:

$$j_p = i_{la} - i_m + i_{lr} \quad (4.2)$$

Power properties of a load can be identified for the instant of time when the last set of voltage and current samples are provided. The control signal when applied to the compensator would be delayed, based on these properties. The effective operation of the compensator is improved considering the calculation of the reference current with the predicted values of the fundamental active and reactive currents in the next sample. The prediction is done at the instant  $t_{k+1} = t_k + T_s$ . In other words, if the reference for calculation is the original observation window, then the prediction is done as in [10] with all the quantities shifted back by  $T_s$ , as follows:

$$\tilde{x}'(t) = \tilde{x}(t + T_s) \quad (4.3)$$

Therefore applying the shifting property, the crms values of such quantity is equal to

$$\tilde{X}_1' = \tilde{X}_1 e^{j\omega T_s} \quad (4.4)$$

In such a case, each quantity can be predicted by adding the linear difference between the current sampled value and its predecessor as follows:

Predicted equivalent conductance and susceptance

$$\tilde{G}_{1k+1} = \tilde{G}_{1k} + (\tilde{G}_{1k} - \tilde{G}_{1k-1}) = 2\tilde{G}_{1k} - \tilde{G}_{1k-1} \quad (4.5)$$

$$\tilde{B}_{1k+1} = 2\tilde{B}_{1k} - \tilde{B}_{1k-1} \quad (4.6)$$

Predicted crms value of the voltage fundamental quasi-harmonic

$$\tilde{U}_{1k+1} = 2\tilde{U}_{1k} - \tilde{U}_{1k-1} \quad (4.7)$$

The crms value of the fundamental quasi-harmonic of the load voltage in (4.7) is calculated from the latest set of samples as follows:

$$\tilde{U}_{1k} = \frac{\sqrt{2}}{N} \sum_{n=k-N+1}^{n=k} u_n e^{-j\frac{2\pi}{N}n} = \tilde{U}_{1k} e^{j\alpha_{1k}} \quad (4.8)$$

Therefore, the predicted active and reactive current

$$\tilde{i}_{1ak+1} = \tilde{G}_{1k+1} \sqrt{2} \tilde{U}_{1k+1} \cos[\omega_1(k\Delta\tau) + \alpha_{1k}] \quad (4.9)$$

$$\tilde{i}_{1rk+1} = -\sqrt{2} \tilde{B}_{1k+1} \tilde{U}_{1k+1} \sin[\omega_1(k\Delta\tau) + \alpha_{1k}] \quad (4.10)$$

Thus, the reference signal for the PVC is equal to:

$$\tilde{j}_p = \tilde{i}_{1ak+1} - \tilde{i}_{mk} + \tilde{i}_{1rk+1} \quad (4.11)$$

The median current,  $\tilde{i}_{mk}$ , is calculated with the conductance in (3.20) averaged over the interval  $T_a$ . Considering  $N_m$  the number of samples to account in the averaging interval, the running median conductance at sample k is calculated as follows:

$$\tilde{G}_{mk} = \frac{1}{N_m} \sum_{n=1}^m \tilde{G}_{1k} \quad (4.12)$$

Therefore, the median current is

$$\tilde{i}_{mk} = \tilde{G}_{mk} \sqrt{2} \tilde{U}_{1k} \cos[\omega_1(k\Delta\tau) + \alpha_{1k}] \quad (4.13)$$

The reference signal for PVC calculated as in (4.11) is shown in Figure 4.3.

Calculation of the predicted values for the conductance allows also the identification of the mode of operation for the PVC for the next sample as follows

Charging mode:

$$\tilde{G}_m > \tilde{G}_{1k+1} \quad (4.14)$$

Energy releasing mode:

$$\tilde{G}_m < \tilde{G}_{1k+1} \quad (4.15)$$

The reference current shown in Figure 4.3, represents the current that is necessary to inject

to the system in order to reduce power variation and reactive power caused by the FVL operation.

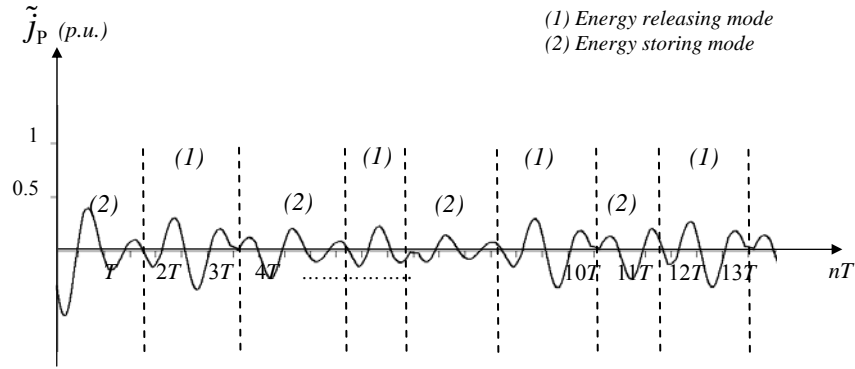


Figure 4.3. Reference signal and modes of operation for the power variation compensator

The reference current shown in Figure 4.3, represents the current that is necessary to inject to system in order to reduce power variation and reactive power caused by the FVL operation.

#### 4.3.2 Reference Signal for the Distortion Compensator

On the other hand, to reduce the distortion the distorted component of the supply current needs to be compensated for as well. The prediction of the distorted component of the supply current at sample  $k + 1$  can be performed as follows:

$$\tilde{j}_{Dk+1} = i_{k+1} - \tilde{i}_{1ak+1} - \tilde{i}_{1rk+1} \quad (4.16)$$

The predicted supply current,  $i_{k+1}$ , in (4.16) is not a slowly varying signal. Any switching operation performed in the load is reflected as a rapid change in the value of the supply current. Commutation of the AC/DC Converter energizing the FVL causes a change in the supply current that is not easy to predict. The supply current is predicted as follows

$$i_{k+1} = 2i_k - i_{k-1} \quad (4.17)$$

The reference current for the distortion compensator calculated as in (4.16) is illustrated in Figure 4.4.

The difference between the predicted distortion compensator reference current in Figure 4.4

and the distorted component of the supply current in Figure 3.4(c) is plotted in Figure 4.5.

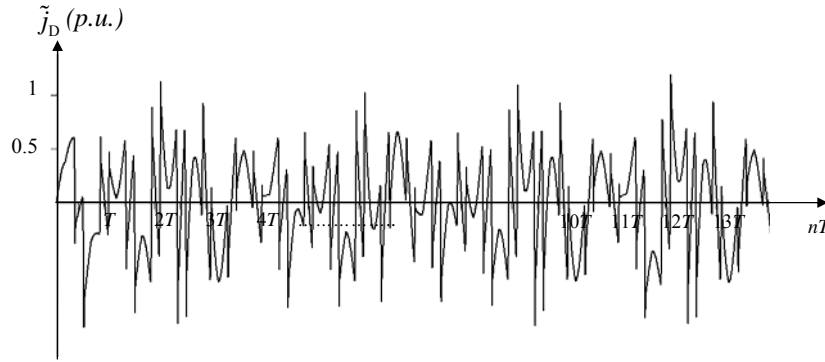


Figure 4.4. Reference current for the distortion compensator

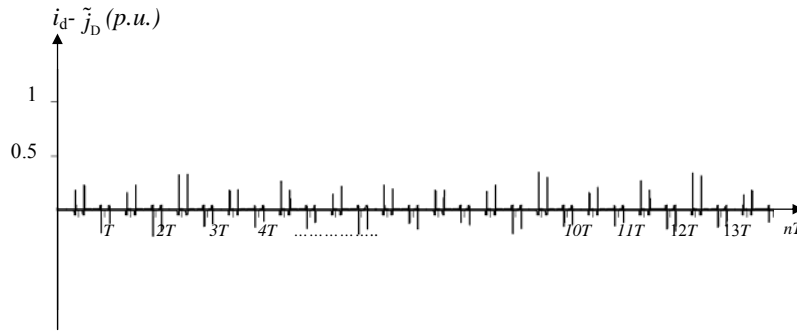


Figure 4.5. Difference between the distorted component of the supply current and the reference current of the distortion compensator

The difference between the currents shown in Figure 4.5 is not zero at the instants of time in which commutation in the AC/DC converter energizing the FVL takes place.

This result is anticipated since the sudden change in the value of the supply current during commutation is difficult to predict.

The supply current drops to zero or increases to a certain value rapidly when commutation takes place.

#### 4.4 Integrated Operation of the Hybrid Compensator

The integrated operation of the hybrid compensator requires that the supply voltages and supply current of phases R and S are sampled at instant  $k$ . The sampled values are then stored in memory. The number of samples stored in the look up tables correspond to one sampling period

( $N= 256$  samples per period, for example). An observation window of length  $N$  is created in each calculation. This look up table is updated at every sample; the new sampled point displaces the first sample. These sampled values are used to perform the current decomposition according to CPC theory as presented before. Calculation of the predicted value of the median and actual running equivalent conductances takes place. These two values are compared to determine the mode of operation for the hybrid compensator. The reference currents are obtained as per (4.11) and (4.16). Then the reference values for the operation of the PWM-based inverters of the compensator are generated and the switching sequence is established accordingly. The switching sequence is applied in the following sample and compensation takes place.

## Chapter 5

### Mathematical Model of the Hybrid Compensator of Fast Varying Loads

#### 5.1 Introduction

The system of equations to be solved to model the compensator's operation presented in Chapter 4 is developed in this Chapter. The hybrid compensator for reduction of power variation and reduction of distortion is modeled as an open loop system. The principle of superposition is going to be used to develop the systems of equations for each element of the system.

#### 5.2 Modeling of the supply system

The supply system is modeled as a three-phase sinusoidal symmetrical supply as shown in Figure 5.1.

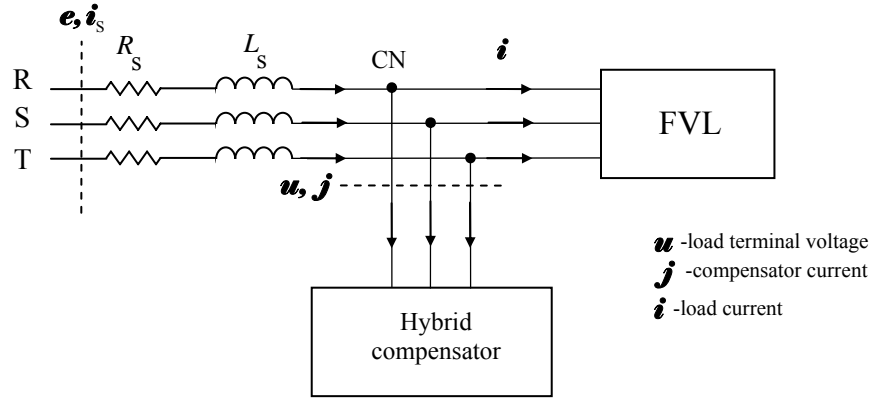


Figure 5.1. Structure of the supply system for the hybrid compensator

Currents and voltages symbols shown in 5.1 are used to develop the system of equations that represent the compensator model. The supply voltage is of the form

$$\begin{aligned}
 e_R &= \sqrt{2}E \sin(\omega t - \phi) \\
 e_S &= \sqrt{2}E \sin(\omega t - \phi - \pi/3) \\
 e_T &= \sqrt{2}E \sin(\omega t - \phi - 2\pi/3)
 \end{aligned} \tag{5.1}$$

Due to the symmetry the rms value of the supply voltage in each phase satisfies  $\|e_R\| = \|e_S\| = \|e_T\| = \|e_s\|$ . This assumption simplifies the representation of the supply. The vector

representing supply voltages and currents for all three phases is denoted by  $\mathbf{e} = [e_R \ e_S \ e_T]^T$  and  $\mathbf{i}_s = [i_R \ i_S \ i_T]^T$  respectively. Therefore, the sub-index differentiating the phase in all the currents, (R, S or T) is going to be omitted in all the equations. Also, it is assumed for the instantaneous value of the currents and voltages that  $e(t) = e$  and  $i_s(t) = i_s$  respectively.

Circuit analysis of Figure 5.1 shows that the system of equations for the supply voltage is equal to

$$\mathbf{e}_s = R_s \mathbf{i}_s + L_s \frac{d\mathbf{i}_s}{dt} + \mathbf{u} \quad (5.2)$$

The unknown terms in (5.2) represent the following:

$R_s \mathbf{i}_s$  -voltage drop across the supply resistance

$L_s \frac{d\mathbf{i}_s}{dt}$  -voltage drop across the supply inductance

$\mathbf{u}$  -load terminal voltage

Load terminal voltage is calculated from (5.2) as follows

$$\mathbf{u} = \mathbf{e} - R_s \mathbf{i}_s - L_s \frac{d\mathbf{i}_s}{dt} \quad (5.3)$$

On the other hand, the system of equations for the supply current at common node CN is equal to

$$\mathbf{i}_s = \mathbf{i} + \mathbf{j} \quad (5.4)$$

The unknown terms in (5.4) represent the following:

$\mathbf{i}$  -FVL current

$\mathbf{j}$  -hybrid compensator current

Current  $\mathbf{j}$  is the result of

$$\mathbf{j} = \mathbf{j}_p + \mathbf{j}_D \quad (5.5)$$

The unknown terms in (5.5) represent the following:

$\mathbf{j}_p$  -PVC current

$\mathbf{j}_D$  -DIC current

### 5.3 Modeling of the Fast Varying Load

The fast varying load is modeled as an AC/DC converter-fed three-phase symmetrical load with operation characteristics as the one described in Chapter 2, as shown in Figure 5.2.

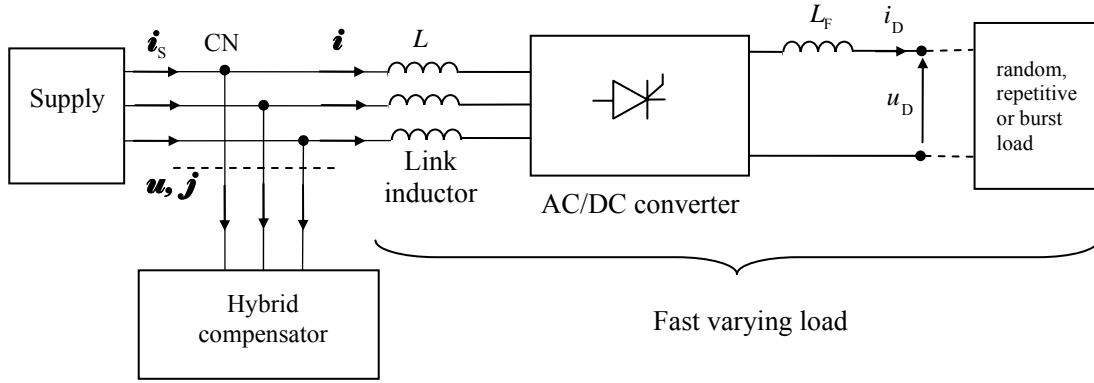


Figure 5.2. Structure of the FVL

The types of loads investigated and modeled at the output of the filtered AC/DC converter are: resistive-inductive, DC motor load and capacitive-inductive (pulsing) as shown in Figure 5.3.

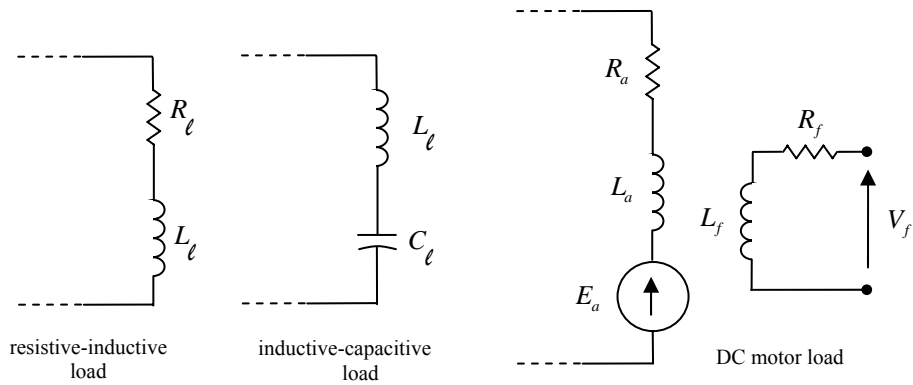


Figure 5.3. Types of loads investigated

Modeling of the load needs to take into account the systems of equation for the converter operation. The structure of the AC/DC converter and the load is presented in Figure 5.4.

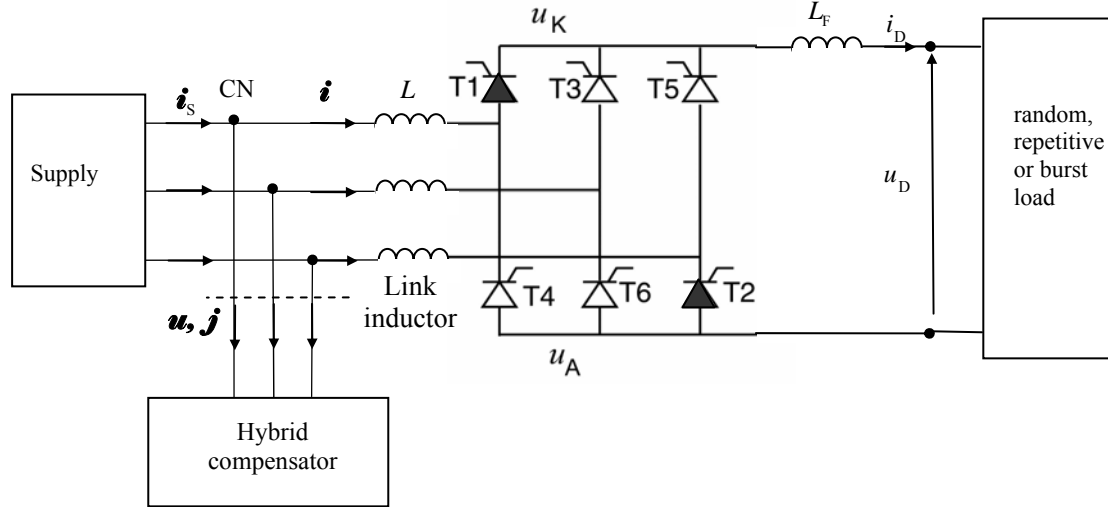


Figure 5.4. Structure of the AC/DC converter of the FVL

Thyristors in Figure 5.4 are enumerated in the sequence of their natural forward bias. These thyristors start to conduct by current pulses applied to the gates in the same sequence. The converter has two distinct states to model: after and during commutation.

After commutation, at any instant of time only two thyristors are conducting. Depending on the highest line-to-line voltage applied to the converter a pair of thyristors will be forward bias. This same pair will conduct after the gate signals are applied. The equivalent circuit after commutation is presented in Figure 5.5.

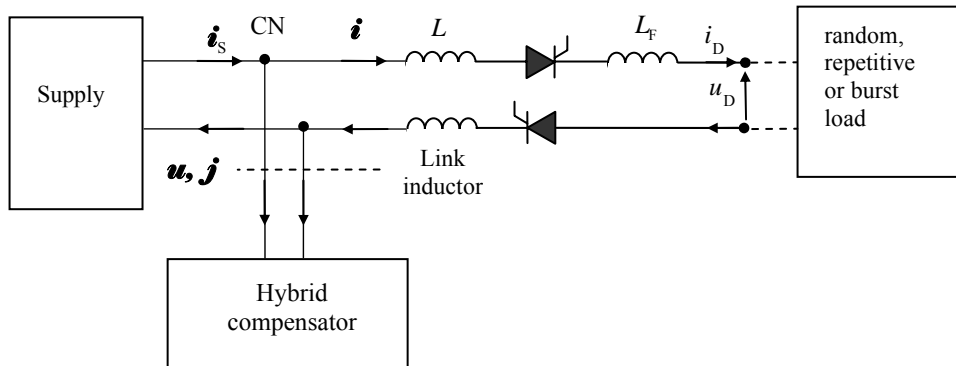


Figure 5.5. Equivalent circuit of the FVL after commutation

The terminal voltage and the equivalent supply voltage depending of the highest line-to-line supply voltage for each mode is presented in table 5.1.

Table 5.1 Converter Modes and Equivalent Voltages.

Mode	Available conducting period (in degrees)	Thyristors	Load terminal voltage	Equivalent supply voltage, $e_m$
1	0° to 60°	T6 and T1	$u_{RS}$	$e_R - e_S$
2	60° to 120°	T1 and T2	$-u_{TR}$	$-(e_T - e_R)$
3	120° to 180°	T2 and T3	$u_{ST}$	$e_S - e_T$
4	180° to 240°	T3 and T4	$-u_{RS}$	$-(e_R - e_S)$
5	240° to 300°	T4 and T5	$u_{TR}$	$e_T - e_R$
6	300° to 360°	T5 and T6	$-u_{ST}$	$-(e_S - e_T)$

Using the equivalent circuit in Figure 5.5 and generalizing for the values presented in Table 5.1, the equation for the voltages at the terminal of the load is

$$u_m = e_m - R_s i_D - L_s \frac{di_D}{dt} \quad (5.6)$$

The unknown terms in (5.6) represent the following:

$u_m$  -load terminal voltage depending on the mode

$e_m$  -supply equivalent voltage depending on the mode from Table 5.1

$i_D$  -load current

To calculate the voltage  $u_D$  after the converter filter, the voltage drop across the converter filter impedance needs to be subtracted from (5.6)

$$u_D = u_m - R_F i_D - L_F \frac{di_D}{dt} \quad (5.7)$$

The load current is then calculated rearranging (5.7) and (5.6) as follows

$$\frac{di_D}{dt} = \frac{1}{(2L_s + L_F)} (e_m - (R_s + R_F) i_D - u_D) \quad (5.8)$$

The unknown voltage  $u_D$  in (5.8) is calculated depending of the type of FVL connected as follows:

For resistive-inductive loads:

$$u_D = R_\ell i_D + L_\ell \frac{di_D}{dt} \quad (5.9)$$

Substituting (5.9) in (5.8) and rearranging to solve for  $i_D$

$$\frac{di_D}{dt} = \frac{1}{(2L_s + L_F + L_\ell)} (e_m - (R_s + R_F + R_\ell)i_D) \quad (5.10)$$

For DC motor loads:

$$u_D = R_\ell i_D + L_\ell \frac{di_D}{dt} + E_a \quad (5.11)$$

Substituting (5.11) in (5.8) and rearranging to solve for  $i_D$

$$\frac{di_D}{dt} = \frac{1}{(2L_s + L_F + L_\ell)} (e_m - (R_s + R_F + R_\ell)i_D - E_a) \quad (5.12)$$

In order to model a FVL characteristic using (5.12); the load torque is changed either repetitive, random or in the form of bursts to affect the value of  $E_a$ .

For inductive-capacitive (pulsing) loads:

$$u_D = R_C i_D + L_\ell \frac{di_D}{dt} + V_C \quad (5.13)$$

Substituting (5.13) in (5.8) and rearranging to solve for  $i_D$ , the first equation of the system of equations is obtained

$$\frac{di_D}{dt} = \frac{1}{(2L_s + L_F + L_\ell)} (e_m - (R_s + R_F + R_\ell)i_D - V_C) \quad (5.14)$$

The voltage across the capacitor is the second equation to solve. This voltage can be calculated using the following expression

$$\frac{dV_C}{dt} = \frac{i_D}{C_t} \quad (5.15)$$

Thyristor are not turned on or off instantaneously. Due to the firing sequence, the supply current commutes from one phase to the other. During commutation three thyristors are conducting at the same as shown in Figure 5.6.

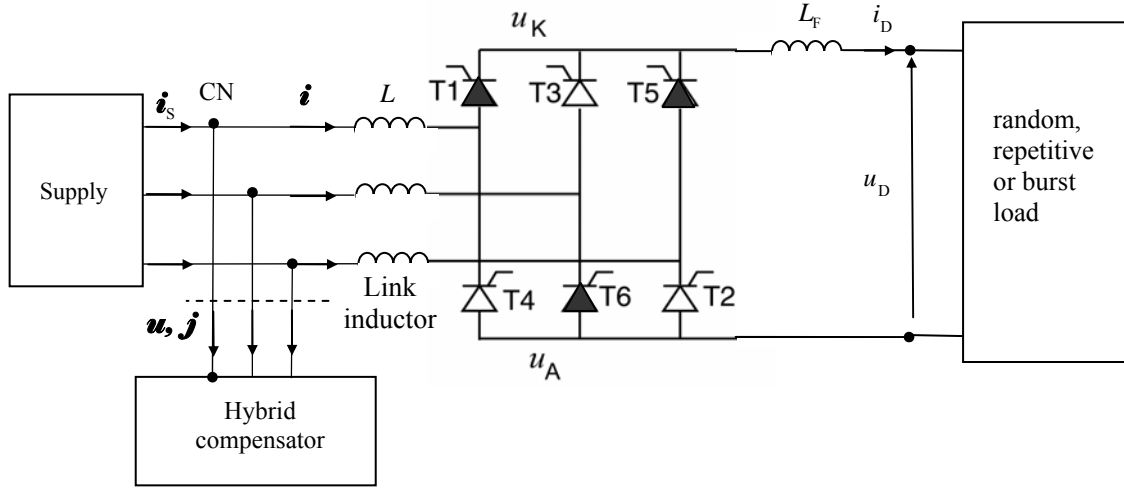


Figure 5.6. Structure of the AC/DC converter of the FVL showing commutation

Commutation takes place six times during a cycle. As the firing sequence and modes are established, the thyristor turning off is the thyristor from the previous mode. The thyristor turning on is the thyristor from the following mode. The equivalent circuit during commutation is presented in Figure 5.7.

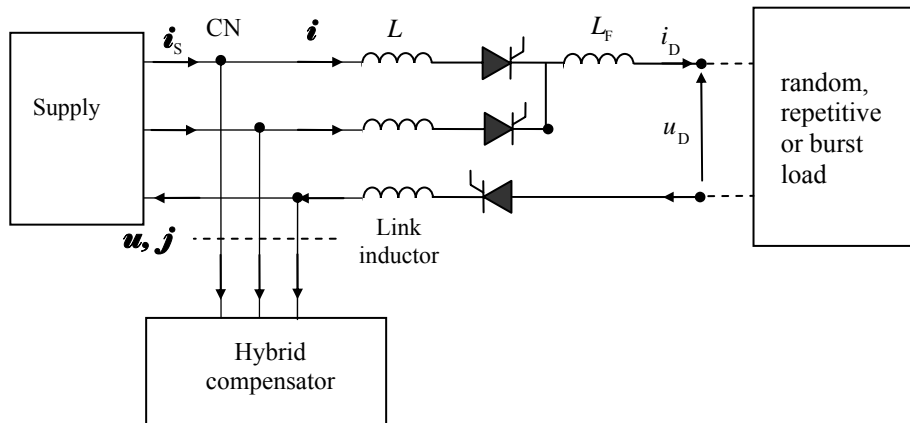


Figure 5.7. Equivalent circuit of the AC/DC converter of the FVL showing commutation

The commutation number and the thyristors turned on and off as well as important voltages associated during commutation are presented in Table 5.2.

Table 5.2 Converter Commutation.

Commutation	Previous mode	Thyristor: turning OFF $\Rightarrow$ turning ON	Next mode	Thyristor remaining ON	Equivalent supply voltage
C1	6	T5 $\Rightarrow$ T1	1	T6	$-\frac{3e_s}{2}$
C2	1	T6 $\Rightarrow$ T2	2	T1	$\frac{3e_R}{2}$
C3	2	T1 $\Rightarrow$ T3	3	T2	$-\frac{3e_T}{2}$
C4	3	T2 $\Rightarrow$ T4	4	T3	$\frac{3e_s}{2}$
C5	4	T3 $\Rightarrow$ T5	5	T4	$-\frac{3e_R}{2}$
C6	5	T4 $\Rightarrow$ T6	6	T5	$\frac{3e_T}{2}$

During commutation, the rate of current decrement of the thyristor turning off is equal to the rate of current increment of the thyristor turning on. Conduction along the three thyristors that are turned on at the same time takes place until the current passing through the thyristor turning off is zero and the current passing through the thyristor turning on is equal to the load current. The system of equation presented in Eq. (5.6)-(5.8) is modified accordingly to the circuit presented in Figure 5.7 and the voltages presented in Table 5.2. The equation for the voltages at the terminal of the load is

$$u_{cn} = e_{cn} - \frac{3R_s}{2} i_D - \frac{3L_s}{2} \frac{di_D}{dt} \quad (5.16)$$

The unknown terms in (5.16) represent the following:

$u_{cn}$  -load terminal voltage depending on the commutation number

$e_{cn}$  -supply equivalent voltage depending on the commutation number from Table 5.2

To calculate the voltage  $u_D$  after the converter filter, the voltage drop across the converter filter impedance needs to be subtracted from (5.16)

$$u_D = u_{cn} - R_F i_D - L_F \frac{di_D}{dt} \quad (5.17)$$

The load current is then calculated rearranging (5.17) and (5.16) as follows

$$\frac{di_D}{dt} = \frac{1}{(\frac{3L_s}{2} + L_F)} (e_m - (\frac{3R_s}{2} + R_F) i_D - u_D) \quad (5.18)$$

The unknown voltage  $u_D$  in (5.18) is calculated depending of the type of FVL as presented in Eq. (5.9) to (5.15).

#### 5.4 Modeling of the Power Variation Compensator

The energy storage for PVC is provided by the Flywheel Energy Storage System , FESS. The amount of energy stored is proportional to the moment of inertia,  $J$  , and the square of the speed,  $E = \frac{1}{2} J \omega^2$ . The flywheel works in conjunction with a Permanent-Magnet Synchronous Motor, PMSM, to provide the required acceleration to the rotor and the flywheel disc. The FESS current supplies the portion of the current necessary to compensate the power variation of the FVL.

The structure of the PVC is shown in Figure 5.8.

The DC link capacitor is used to keep a constant supply voltage for the inverters. Therefore in energy storing mode the energy is transferred from the supply through inverter A into the DC link capacitor. The energy stored in the DC link capacitor is transferred to the PMSM through inverter B and then stored in the flywheel. In energy releasing mode the energy is transferred in the opposite direction as described before. The energy stored in the flywheel is transfer by the PMSM to the DC link capacitor through inverter B.

Energy is transferred from the DC link capacitor to the supply through inverter A.

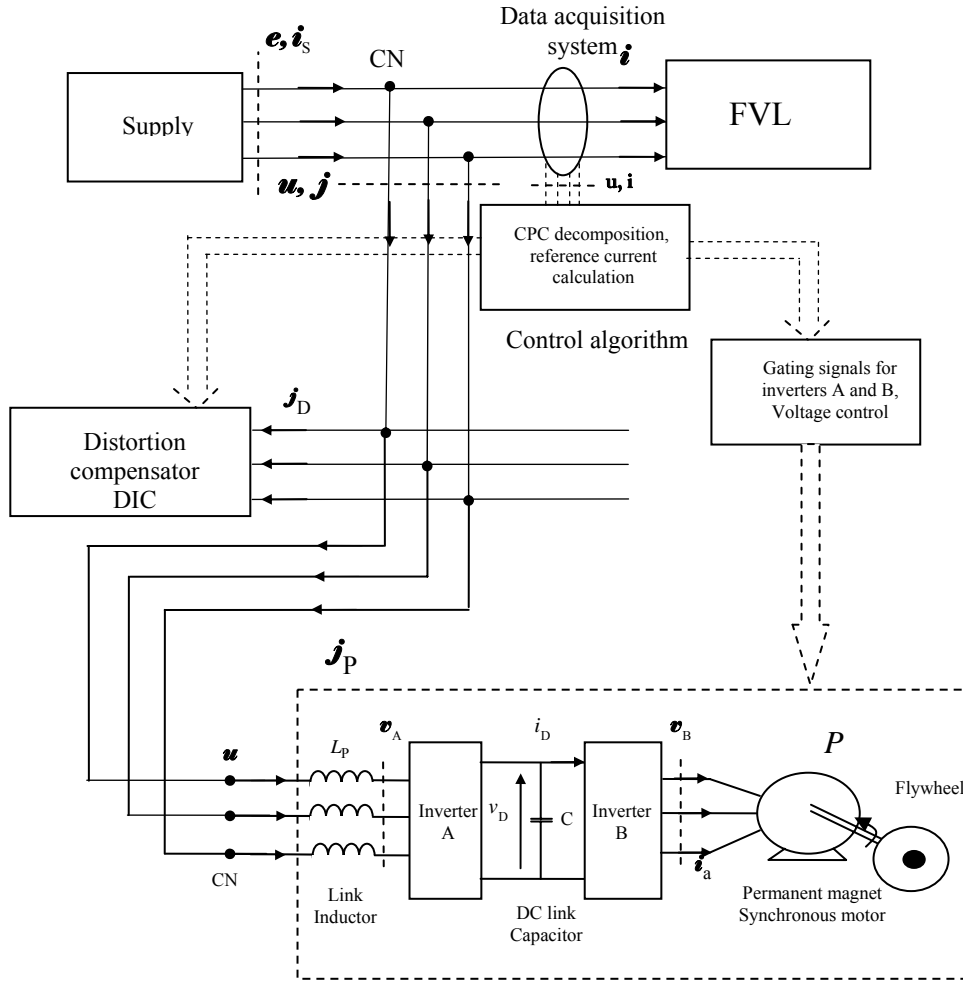


Figure 5.8. Structure of the power variation compensator

Assuming ideal inverters, no power losses, the power balance of the PV compensator is

$$p_p = p_D = p_M \quad (5.19)$$

Where:

$p_p$  -active power of the PVC

$p_D$  -active power of the DC link capacitor

$p_M$  -active power of the PMSM

The power balance expressed in (5.19) and currents and voltages shown in Figure 5.8 are used to develop the system of equations that represent the PVC model. The system of equations to be solved is going to be developed from common node CN to the FESS.

Voltage  $\mathbf{u}$  at the common node CN from Figure 5.8 can be estimated as

$$\mathbf{u} = R_p \mathbf{j}_p + L_p \frac{d\mathbf{j}_p}{dt} + \mathbf{v}_A \quad (5.20)$$

The unknown terms in (5.20) represent the following:

$\mathbf{v}_A$  -voltage at inverter A terminals

$R_p \mathbf{j}_p$  -voltage drop across the resistance of the PVC linking inductor

$L_p \frac{d\mathbf{j}_p}{dt}$  - voltage drop across the inductance of the PVC linking inductor

Voltage  $\mathbf{v}_A$  in (5.20) represents the reference voltage needed at the terminals of Inverter A for power variation compensation.  $\mathbf{v}_A$  is calculated from (5.20) as follows

$$\mathbf{v}_A = \mathbf{u} - R_p \mathbf{j}_p - L_p \frac{d\mathbf{j}_p}{dt} \quad (5.21)$$

All the terms in (5.21) are known. PVC reference current  $\mathbf{j}_p$  is calculated by the control algorithm as in (4.11). Once the reference value of  $\mathbf{v}_A$  is estimated by the control algorithm, a sinusoidal wave pulse width modulated (SW-PWM) based technique establish the switching sequence for inverter A. A description of SW-PWM technique is presented in [47- 49].

Considering the power balance in (5.19), the output power of inverter A is calculated as:

$$p_D = v_D i_D = p_M \quad (5.22)$$

The unknown terms in (5.22) represent the following:

$v_D$  -voltage at DC link capacitor

$i_D$  -current supplied by the DC link Capacitor

Power balance in (5.22) is satisfied by the appropriate reference voltage at the terminals of inverter B ,  $\mathbf{v}_B$  , in Figure 5.8. Once the reference value of  $\mathbf{v}_B$  is estimated by the control algorithm, a SW-PWM based technique establishes the switching sequence for inverter B, as

presented in [47- 49].

The output voltage of inverter B,  $\mathbf{v}_B$ , is the input voltage across terminals of the three-phase PMSM as shown in Figure 5.9.

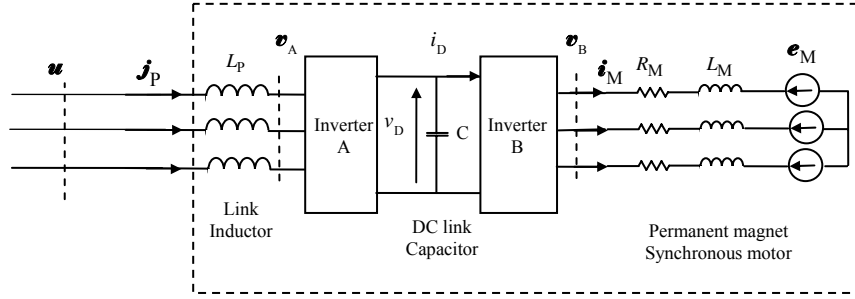


Figure 5.9. PV compensator with equivalent circuit of PMSM

The voltage  $\mathbf{v}_B$  expressed in terms of the PMSM parameters is equal to

$$\mathbf{v}_B = R_M \mathbf{i}_M + L_M \frac{d\mathbf{i}_M}{dt} + \mathbf{e}_M \quad (5.23)$$

Expressing (5.23) in terms of the flux linkage,  $\mathbf{v}_B$  takes the form

$$\mathbf{v}_B = R_M \mathbf{i}_M + \frac{d\boldsymbol{\lambda}}{dt} + \omega \boldsymbol{\lambda} \quad (5.24)$$

The FESS is modeled for a dynamic control of the PMSM. To make the analysis easier, the PMSM is modeled in rotating dq reference frame instead of the stationary three-phase abc frame<sup>1</sup>. Both frames with the stator winding are shown in Figure 5.9.

The dq frame is displaced with respect to the abc representation by angle  $\theta_m$ , which varies in time as shown in Figure 5.10.

The rotor magnetic axis is aligned with the d-axis. The q-axis is in quadrature to d-axis. This makes the PMSM analogous to a DC motor. The magnetic field of the field winding is perpendicular to the armature winding. To control the speed in DC motors, the magnetic field is kept constant while the armature current varies. Applying this analogy to PMSM, to change the

<sup>1</sup> abc is going to be used instead of RST to distinguish the three-phases of the PMSM from the three-phase supply

motor speed the current  $i_{sq}$  is controlled while the magnetic field in d-axis is kept constant.

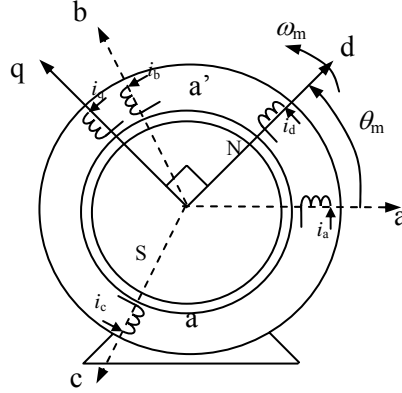


Figure 5.10. abc and dq axis representation of PMSM

The reference voltage at the terminals of inverter B,  $\mathbf{v}_B$ , is transformed in the dq frame by multiplying it by the transformation matrix presented bellow. For simplicity in the model  $\mathbf{v}_B = \mathbf{v}$ .

$$\begin{bmatrix} v_d \\ v_q \end{bmatrix} = \sqrt{\frac{2}{3}} \begin{bmatrix} \cos(\theta_m) & \cos\left(\theta_m - \frac{2\pi}{3}\right) & \cos\left(\theta_m - \frac{4\pi}{3}\right) \\ -\sin(\theta_m) & -\sin\left(\theta_m - \frac{2\pi}{3}\right) & -\sin\left(\theta_m - \frac{4\pi}{3}\right) \end{bmatrix} \begin{bmatrix} v_a \\ v_b \\ v_c \end{bmatrix} \quad (5.25)$$

The equivalent circuit for the stator winding in dq model is illustrated in Figure 5.11.

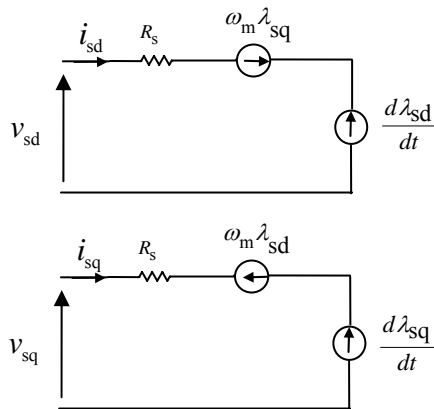


Figure 5.11. Equivalent circuit of the stator winding of the PMSM in dq model

The voltage equations for the stator winding, for both axes, written in dq are expressed as follows

$$\begin{aligned} v_{sd} &= R_s i_{sd} + \frac{d}{dt} \lambda_{sd} - \omega_m \lambda_{sq} \\ v_{sq} &= R_s i_{sq} + \frac{d}{dt} \lambda_{sq} + \omega_m \lambda_{sd} \end{aligned} \quad (5.26)$$

where:

$R_s$  -equivalent resistance of the stator winding

$\lambda_{sd}$  -stator d-axis flux linkage

$\lambda_{sq}$  -stator q-axis flux linkage

$i_{sd}$  -stator d-axis current

$i_{sq}$  -stator q-axis current

$\omega_m$  -speed of the dq system

The flux linkages ,  $\lambda_{sd}$  and  $\lambda_{sq}$  , are expressed as

$$\begin{aligned} \lambda_{sd} &= L_s i_{sd} + \lambda_{fd} \\ \lambda_{sq} &= L_s i_{sq} \end{aligned} \quad (5.27)$$

where:

$L_s$  -inductance of the stator winding, sum of the leakage inductance and magnetic inductance  $L_s = L_{ls} + L_m$  .

Substituting (5.27) into (5.26)

$$\begin{aligned} v_{sd} &= R_s i_{sd} + \frac{d}{dt} (L_s i_{sd} + \lambda_{fd}) - \omega_m L_s i_{sq} \\ v_{sq} &= R_s i_{sq} + \frac{d}{dt} (L_s i_{sq}) + \omega_m (L_s i_{sd} + \lambda_{fd}) \end{aligned} \quad (5.28)$$

The space vector equation for the PMSM with the d-axis as a reference is the result of adding the voltages in (5.28) and this result is multiplied by a constant. The space vector is calculated as follows [50]

$$\vec{v}_s = \sqrt{\frac{3}{2}}(\vec{v}_{sd} + j\vec{v}_{sq}) \quad (5.29)$$

Substituting (5.28) in (5.29)

$$\vec{v}_s = R_s \vec{i}_s + j\omega_m L_s \vec{i}_s + j\vec{e}_{fs} \quad (5.30)$$

where  $\vec{e}_{fs} = j\sqrt{\frac{3}{2}}\omega_m \lambda_{fd}$  is the voltage induced in the stator winding by the magnetic flux of PM.

The speed of the dq system,  $\omega_m$ , in (5.30) is related to the number of poles,  $p$ , of the machine and its mechanical speed,  $\omega_{mech}$ , as follows  $\omega_m = \frac{p}{2}\omega_{mech} = \frac{p}{2}n_{mech}\frac{2\pi}{60}$ . Parameters  $\omega_m$  and  $\lambda_{fd}$  are unknown in (5.28) - (5.30). Other relations for the PMSM are needed to calculate these parameters.

The electromagnetic torque developed by the PMSM is calculated adding the torques acting on the d-axis and on the q-axis. As a result [50]

$$T_{em} = \frac{p}{2}(\lambda_{sd}i_{sq} - \lambda_{sq}i_{sd}) \quad (5.31)$$

Substituting (5.27) into (5.31)

$$T_{em} = \frac{p}{2}((L_s i_{sd} + \lambda_{fd})i_{sq} - L_s i_{sq}i_{sd}) \quad (5.32)$$

Therefore

$$T_{em} = \frac{p}{2}\lambda_{fd}i_{sq} \quad (5.33)$$

In (5.33) the flux linkage  $\lambda_{fd}$  is constant because of the permanent magnets, and torque  $T_{em}$  depends only on current  $i_{sq}$ .

The mechanical system for the FESS can be represented as shown in Figure 5.12.

The motion equation of the mechanical system for the FESS presented in Figure 5.12 is

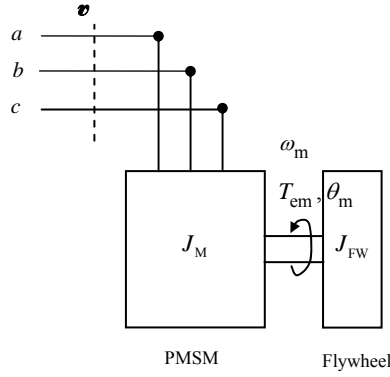


Figure 5.12. Mechanical system representation for the FESS

$$T_{em} = (J_M + J_{FW}) \frac{d\omega_{mech}}{dt} + T_{losses} \quad (5.34)$$

Where:

$J_M$  -equivalent inertia of the PMSM

$J_{FW}$  -equivalent inertia of the flywheel

$T_{losses}$  -total mechanical losses in the system

Calculating  $\omega_{mech}$  from (5.34)

$$\frac{d\omega_{mech}}{dt} = \frac{T_{em} - T_{losses}}{(J_M + J_{FW})} \quad (5.35)$$

In the FESS presented in Figure 5.12 there is no mechanical load connected to the PMSM. The flywheel disc represents an additional inertia,  $J_{FW}$ , combined with the inertia of the motor,  $J_M$ .

The last step to consider is the power balance of the system, as expressed in (5.22). The total power supplied by the DC link capacitor is equal to FESS input power.

$$v_D i_D = \frac{3}{2} i_{sq} v_{sq} \quad (5.46)$$

Energy transfer between inverters A and B is done through the linking capacitor. The voltage

across the bus capacitor is the final equation that completes the system of equations necessary to model PVC. The DC voltage across the capacitor is calculated using the basic equation of energy stored in a capacitor, as follows:

$$p = \frac{dW_C}{dt} = \frac{1}{2} C \frac{dV_C^2}{dt} \quad (5.47)$$

Since the power of the PMSM is

$$p = (e_R + e_S + e_T)i_s - 3R_s i_s^2 - \frac{3}{2} \omega_{\text{mech}} \sqrt{\frac{3}{2}} k_e i_{sq} \quad (5.48)$$

The voltage across the capacitor is then

$$\frac{dV_C^2}{dt} = (2/C)((e_R + e_S + e_T)i_s - 3R_s i_s^2 - \frac{3}{2} \omega_{\text{mech}} \sqrt{\frac{3}{2}} k_e i_{sq}) \quad (5.49)$$

For compensation of power variation, the value of current  $i_{sd}$  is constant and  $i_{sq}$  varies each sample. Variation of  $i_{sq}$  is directly related to the difference between the running active power and its median as follows

$$i_{sq} = \frac{(\tilde{P} - \tilde{P}_m)}{\lambda_{fd} \omega_{\text{sync}}} \quad (5.50)$$

$$i_{sd} = 0 \quad (5.51)$$

## 5.5 Modeling of the Distortion Compensator

The structure of the distortion compensator is shown in Figure 5.12.

The direction of current of the compensator for reducing distortion current is always opposite to the direction of the load current. The distorted component of the load current is cancelled by the current injected from the compensator. And as a result the supply current is sinusoidal. Therefore the supply current at node CN is

$$\mathbf{i}_s = \mathbf{i}_l + \mathbf{j}_p - \mathbf{j}_D \quad (5.52)$$

The voltage  $\mathbf{v}_{\text{ref}}$  Figure 5.10, represents the reference voltage needed at the terminals of the inverter to generate the required DC reference current. Observing the parameters plotted in Figure 5.10, this voltage is calculated as follows

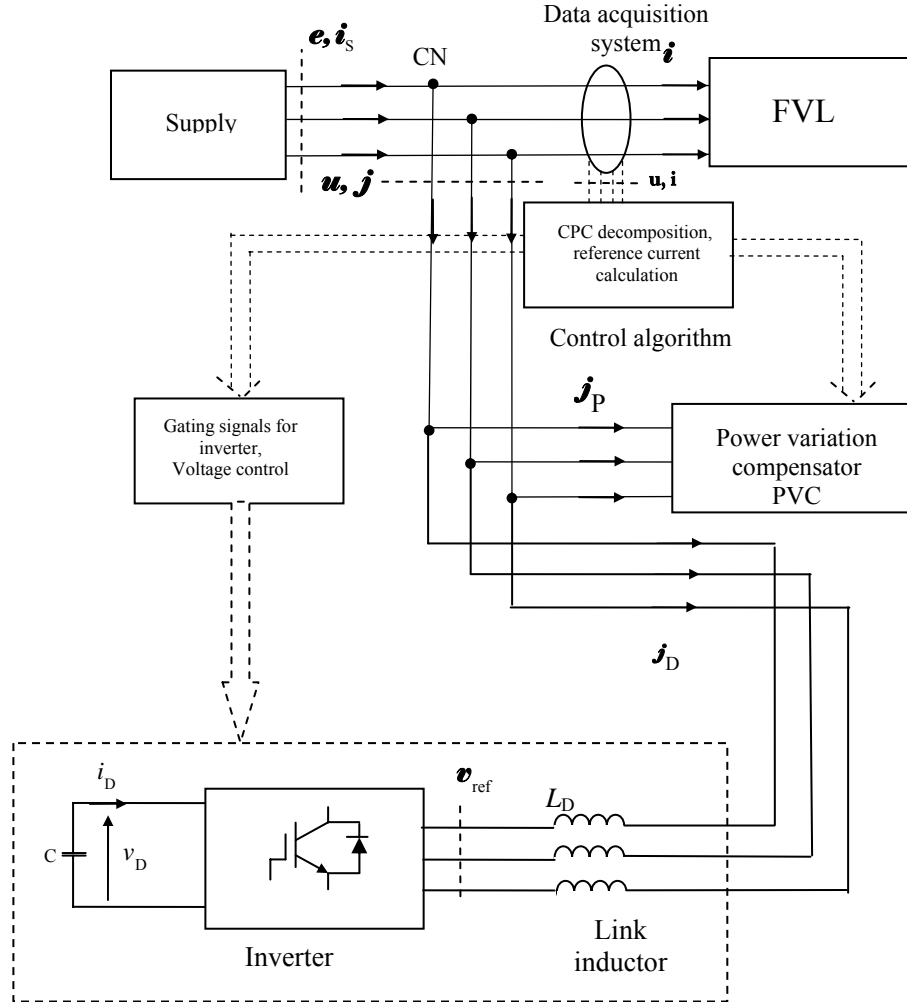


Figure 5.13. Structure of the distortion compensator

$$\mathbf{v}_{\text{ref}} = \mathbf{u} + \underbrace{R_D \mathbf{j}_D + L_D \frac{d\mathbf{j}_D}{dt}}_{\Delta \mathbf{u}} \quad (5.53)$$

The DIC reference current,  $\mathbf{j}_D$  is calculated as in (4.16). The switching compensator in Figure 5.13 is able to: shape the fast varying distorted component of the supply load current, generate of the gating signals for the switches and keep the DC voltage within the required

levels. The space vector pulse width modulated (SV-PWM) technique used to generate the terminal voltage is described in [47- 49].

## **Chapter 6**

### **Computer Simulation of the Hybrid Compensator of Fast Varying Loads**

#### **6.1 Introduction**

Computer modeling of the hybrid compensator of FVL is done in MFC Visual C++ compiler version 6.0. The model user interface is based on dialog boxes and drop down menus. The software is written for research purposes. It allows total configuration of all parameters of the supply system, the FVL load and the hybrid compensator. Most of the signals and variables calculated are saved in pointer arrays for plotting accessibility if desired. Results of the simulation are presented in the form of plots of current and voltage signals and parameters calculated to analyze the results of the compensation.

A flow diagram of the computer model is presented in Figure 6.1.

The model is built of sequential subroutines to generate all the values of the necessary current and voltages. Each calculation of interest is programmed in a single subroutine. Each subroutine performs the calculation for all the integration points or sampling points available, depending on the block. Therefore, no time constraints are set for the execution of the calculations. The main subroutines and block of instructions for all the calculation are programmed in the `flywheelDoc.cpp` file of the program. Variables, structures and subroutines are defined in the `flywheelDoc.h` file of the program. Plots are programmed in the `flywheelView.doc` file of the program. Variables and subroutine definitions for plots are defined in the `flywheelView.h` file of the program.

The flow diagram of the program is composed of ten principal process blocks. Each process block is identified by a number as illustrated in Figure 6.1.

Each block is described also by the main calculation performed by the set of subroutines in the program within this particular block. These subroutines are going to be explained in this

Chapter. The user interface generated by the program is presented in the appendix.

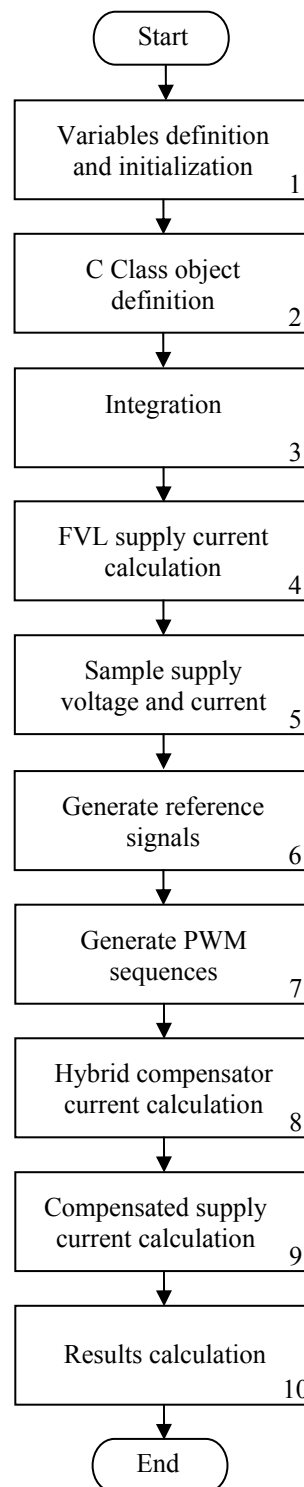


Figure 6.1. Flow diagram of the model

## 6.2 Block 1: Variables Definition and Initialization

Block 1 process represents the first step in building up the computer model for the hybrid

compensator. All values and variables to be used along the program need to be defined and initialized first. There are variables to be used by the subroutines and there are member variables of the C Class defined for the user interface. The latest are going to be developed in the following section.

The variables used for calculations or to store results along the program are specified in flywheelDoc.h. These variables are initialized in the first subroutine in flywheelDoc.cpp.

Global variables, fixed value variables and libraries needed are defined in flywheelDoc.h.

An example of the values defined in flywheelDoc.h extracted from the original code is presented in Figure 6.2.

```
#define maxN      10           // handles up to ten first order differential equations
#define tol      0.000005
#define MaxCount  10
#define tINIT     0.0          // initial time
#define maxCycles 15           // max. number of cycles to be computed
#define maxSamples 256         // max. number of samples to be computed
#define maxPointsC 768         // max. number of points per cycle
#define maxPointsSim 11520     // max. number of points simulated
#define IntPoints  3           // max. integrating points between samples
#define pi        3.141592650  // pi
#define RAD       3.14159265 / 180 // from degrees to radians
#define freq      60.0
//define step     2 * 3.141592650 / 768 // 2 * pi / maxPointsC
#define N1        12000        // max num of elements in points array
#define N2        3900         // max num. of elements in sampled array
#define N3        128          // max num harmonics
```

Figure 6.2. Example of the definition of values in FlywheelDoc.h

Variables related to the same equipment or calculations are grouped in structures. The structures defined in flywheelDoc.h are: Supply, Filter, Motor, Load, Graph, Solution, Switchcomp, Flywheelsys, Cfilter, Solution\_fw, Capload, Type and Results. Each structure holds all the variables for the particular equipment or calculation. An example of the variables defined as structures to represent parameters of the supply system and the FVL in the program are extracted from the original code is presented in Figure 6.3.

The dynamic memory allocation of the pointer variables and variables within the structures are defined first in flywheelDoc.h.

```

typedef struct supply
{
    double Vrms;
    double Rs; //Supply Resistance
    double Ls; //Supply Inductance
} SUPPLY;

typedef struct filter
{
    double Rf; //Converter Load Filter Resistance
    double Lf; //Converter Load Filter Inductance
} FILTER;

typedef struct motor
{
    double Rarm; //Motor armature Resistance
    double Larm; //Motor armature Inductance
    double Earm; //Motor induced Voltage
    double Earm_min; //Motor induced Voltage
    bool Flag;
} MOTOR;

typedef struct load
{
    double Cycledur; //Duration of the disturbance
    bool Constant; //Constant Voltage profile
    bool Exponential; //Exponential Voltage profile
    bool Pulse; //Pulse Voltage profile
    bool Sawtooth; //Sawtooth Voltage profile
    bool Randomcycle; //Random repetition of profile
    bool Fix; //Periodic repetition of
profile
} LOAD;

typedef struct capload
{
    double R; //Cap load R
    double L; //Cap Load L
    double C; //Cap Load C
} CAPLOAD;

typedef struct type
{
    bool DcLoad; //DC Load
    bool CapLoad; //Cap Load
} TYPE;

```

Figure 6.3. Example of the structures related to the FVL specification in FlywheelDoc.h

An example of the dynamic memory allocation for the pointer of a two dimensional array and the initialization of the supply system structure variables is presented in Figure 6.4.

All variables and pointers used in the model are defined and initialized as presented in Figure 6.2 – Figure 6.4. These pointer arrays store the results of calculation for intermediate variables as well as results from compensation.

### 6.3 Block 2: C Class Object Definition

There are three C class type objects in the program: CParameter, CPlot and CResults.

```

/* dynamic memory allocation for two dimensional array k_table*/
Switchcomp.k_table = (int **)malloc(6 * sizeof(int *));
for (i=0; i < 6; i++)
    Switchcomp.k_table[i] = (int *)malloc(2 * sizeof(int));}

// Initial values for the variables

//Supply
Supply.Vrms      = 220;
Supply.Rs        = 0.01;
Supply.Ls        = 0.001;

```

Figure 6.4. Example dynamic memory allocation for the pointer of a two dimensional array and initialization of the supply system structure variables FlywheelDoc.h

CParameters class is dedicated to the definition of the parameters of the whole system. CPlots is dedicated to the selection of the plots to display in the main view screen of the program. CResults is a class that allocates both resultant plots and calculations of interest for analysis of the results of the compensation. The user interface of the program has generated drop down menus from the “main view” screen that prompt to the screens for each class as shown in Figure 6.5.

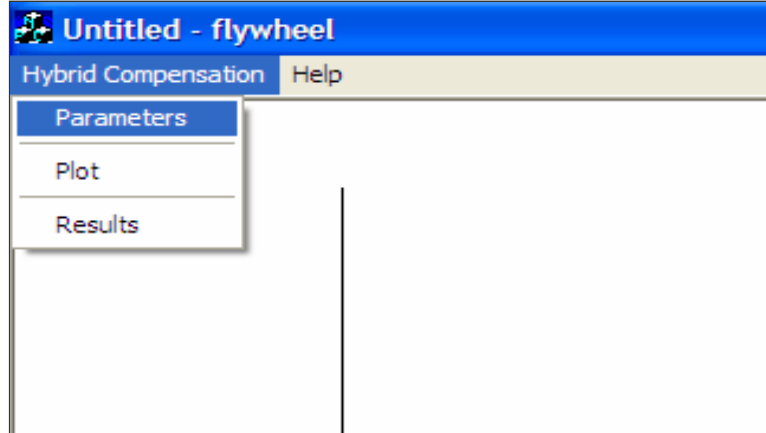


Figure 6.5. Main view screen selections from the menu

All variables within a particular class shown in a user screen are added and defined using the MFC ClassWizard available in Visual C++. A snapshot on some of the Member Variables for CParameter class is shown in Figure 6.6.

Interchangeability between values in the variables defined through structures and the member variables of the dialog boxes of each C class needs to be programmed in the subroutine of the

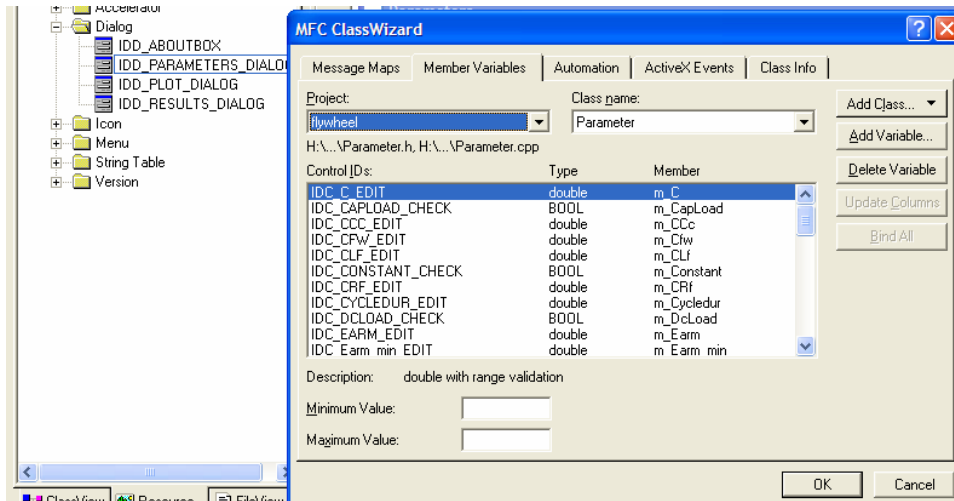


Figure 6.6. MFC ClassWizard for CParameter class

function generated by the MFC ClassWizard. In this function the equivalence between structure variables and member class variables for the supply system is defined as shown in Figure 6.7.

Figure 6.7 shows the part of the code corresponding to the supply only.

```
void CFlywheelDoc::OnSettingParameters()
{
    Parameter SettingParametersDlg; //Defining Object of CParameters Class

    SettingParametersDlg.m_Vrms          = Supply.Vrms;
    SettingParametersDlg.m_Rs            = Supply.Rs;
    SettingParametersDlg.m_Ls            = Supply.Ls;

    if (SettingParametersDlg.DoModal () == IDOK)
    {
        Supply.Vrms          = SettingParametersDlg.m_Vrms;
        Supply.Rs            = SettingParametersDlg.m_Rs;
        Supply.Ls            = SettingParametersDlg.m_Ls;

        UpdateAllViews (NULL);
    }
}
```

Figure 6.7. CParameter class definition as structure variables

A similar procedure is programmed for all the member variables defined in the dialog box for all the classes.

### 6.4 Block 3: Integration

Block 3 corresponds to the function designed to define the integration points and simulation duration. The model is designed to run the simulation for up to 15 cycles, to allocate up to 768 integration points per cycle for calculation of signals, and to allocate up to 256 samples per

cycle. Integration points are calculated from the user's entry on: number of cycles to simulate; number of samples per cycle; and number of integration points within each sample. The function doing the integration is presented in Figure 6.8.

```
// This procedure sets the total integration points from the user interface

void CFlywheelDoc::integration()
{
    Graph.PointsC = Graph.Points * Graph.Samples;
    Graph.PointsSim = Graph.Cycles * Graph.Points * Graph.Samples;
    Graph.SamplesSim = Graph.Cycles * Graph.Samples;
}
```

Figure 6.8. Integration subroutine

By default the model is simulated with the maximum values presented before.

#### 6.5 Block 4: FVL Supply Current Calculation

Block 4 calculates the supply current for the FVL in consideration. The result of this calculation is stored in a pointer array in memory for use when implementing the algorithm for hybrid compensation. It is build up from several sub-processes as presented in Figure 6.9.

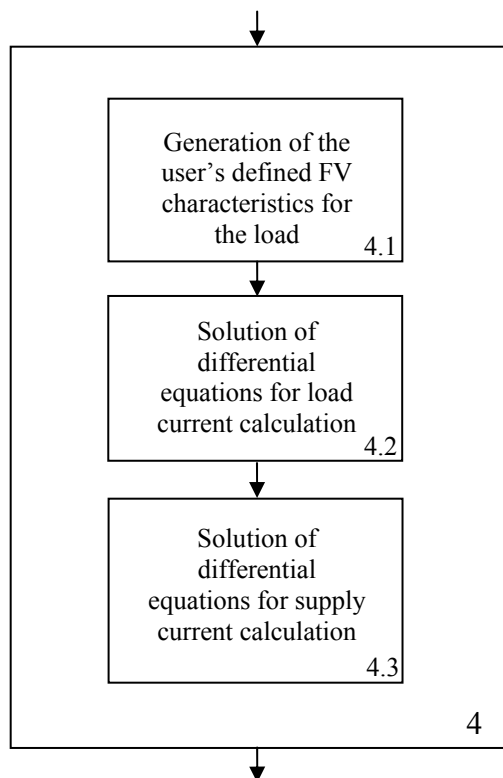


Figure 6.9. Processes within block 4

The user defines what type of FVL is going to be compensated. The user's interface provides the options of a converter fed DC motor or a pulsing load. The load torque characteristic of the DC motor load can be varied so that a single power pulse, repetitive or random power pulses can be obtained. A view of this user screen in the Parameters dialog box is shown in Figure 6.10.

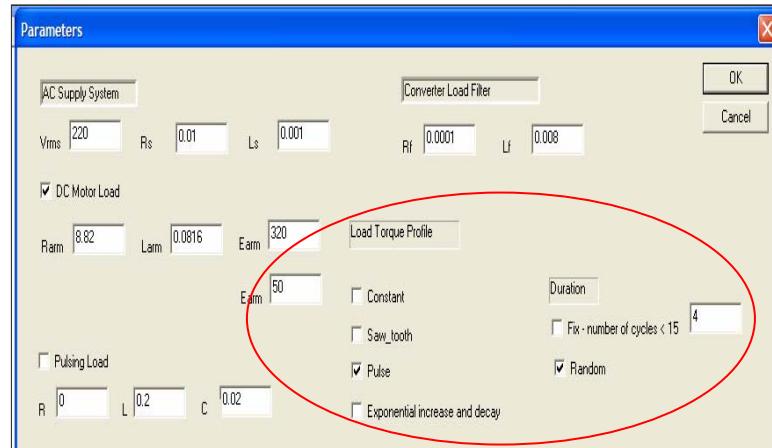


Figure 6.10. FVL setting in parameters dialog box

Once the type of variation in the power pulses is selected, then the function that calculates the load current is called. The load current and the supply current are calculated for all the simulation points defined in the integration. The differential equations presented in Chapter 5 are solved using a Runge-Kutta Fehlberg 4<sup>th</sup>/5<sup>th</sup> order subroutine. This subroutine is called every time a numerical solution for a differential equation in the program is needed. It distinguished between the set of differential equations to solve is done by assigning a value to the variable “cases”. The first approximations of Runge-Kutta Fehlberg 4<sup>th</sup>/5<sup>th</sup> order subroutine are illustrated in Figure 6.11. If cases=0 calls out the differential equations to be solved for the load current and the supply current after commutation. If cases=2 then the differential equations to be solved for the PV compensator current are called. If cases = 3 the differential equations to be solved for the DC current are called.

## 6.6 Block 5: Sample Supply Voltage and Current

Block 5 process simulates sampling of the supply current and voltages calculated previously

```

void CFlywheelDoc::rkf(double t0, double h, double x0[], double xend[], int mode, int com_mode, int sample, int cases)
{
    tEND = t0 + hSTART;
    count_rkf = 0;
    // Here begins a very long while loop
    while ((t0 < tEND) && (count_rkf < MaxCount))
    {
        count_rkf = count_rkf + 1;
        /* Get derivatives and the increments to t to use in the next step.(xend holds the k1's.)*
        if (cases == 0)
            getcom_DERIVS(x0, f, t0, mode, com_mode, sample);
        if (cases == 2)
            getcom_DERIVS_fw(x0, f, t0, mode, com_mode, sample);
        if (cases == 3)
            getcomp_DERIVS(x0, f, t0, mode, com_mode, sample);
        for (i_rkf = 0; i_rkf < numberOfEquations; ++i_rkf)
        {
            workarray[0][i_rkf] = h*f[i_rkf];
            xend[i_rkf] = x0[i_rkf] + workarray[0][i_rkf] / 4.0;
        }
        /* end of first estimate */
    }
}

```

Figure 6.11. First two approximations of the Runge-Kutta Fehlberg 4<sup>th</sup>/5<sup>th</sup> order subroutine at a fixed rate. By default, 256 samples are taken each cycle. Therefore the size of the array of the sampled signals is reduced by 3 from the size of the array of the total integrated points in the program by default. These values can be modified as explained in Block 2. The sampled values are stored in a new array.

## 6.7 Block 6: Generate Reference Signals

Block 6 uses the data stored in the arrays obtained by block 5 to generate the reference signals for the hybrid compensator. Block 6 is build up from several sub-processes as presented in Figure 6.12.

The first step needed to generate the reference signals for the hybrid compensator is: application of the CPC principles and formulas to perform the supply current decomposition into: running fundamental active, reactive and distorted component as it was presented in Chapter 3. Block 6.1 contains the subroutine that performs this decomposition for the supply current in phase R as shown in Figure 6.13. CPC decomposition for supply current in phase S is done similarly.

The reference currents for hybrid compensation are calculated using the predicted values of the current components, as described in Chapter 4. Prediction subroutine for the current

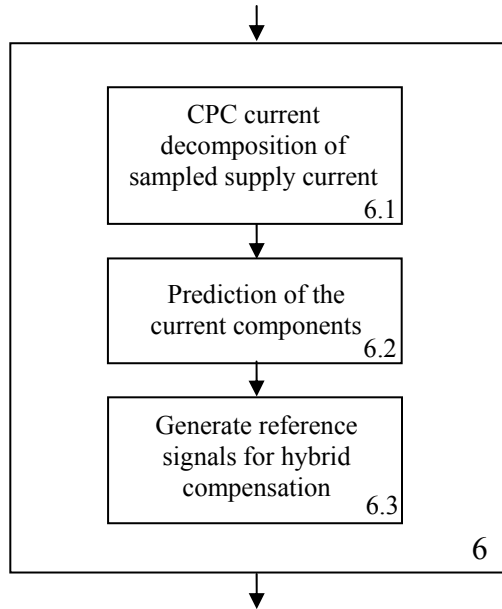


Figure 6.12. Processes within block 6

components is presented in Figure 6.14.

```

void CFlywheelDoc::Decomposition()
{
    int N;
    double Y, Theta, YS, ThetaS, Ang_Volt, Ang_VoltS;
    double twopi_N;

    sample = 0;
    N = Graph.Samples;
    twopi_N = 2 * pi / N;

    Y = abs(Solution.CRMSI1[sample]) / abs(Solution.CRMSU1[sample]);
    Theta = arg(Solution.CRMSU1[sample]) - arg(Solution.CRMSI1[sample]);
    Solution.Ge1[sample] = Y * cos(Theta);
    Solution.Be1[sample] = Y * sin(Theta);

    for (sample = 0; sample < Graph.SamplesSim; sample++)
    {
        Solution.U1[sample] = 0;
        Solution.Iact1[sample] = 0;
        Solution.Ireact1[sample] = 0;
        Solution.Idist[sample] = 0;
    }

    for (sample = 0; sample < Graph.SamplesSim; sample++)
    {
        Ang_Volt = sample * twopi_N + arg(Solution.CRMSU1[sample]);
        Solution.U1[sample] = sqrt(2) * abs(Solution.CRMSU1[sample]) * cos(Ang_Volt);
        Solution.Iact1[sample] = Solution.Ge1[sample] * sqrt(2) * abs(Solution.CRMSU1[sample]) * cos(Ang_Volt);
        Solution.Ireact1[sample] = Solution.Be1[sample] * sqrt(2) * abs(Solution.CRMSU1[sample]) * sin(Ang_Volt);
        Solution.Idist[sample] = Solution.SupplyCurr[sample * Graph.Points] - Solution.Iact1[sample] -
        Solution.Ireact1[sample];
    } // end for
} // end Decomposition procedure

```

Figure 6.13. CPC current decomposition subroutine

The reference signals for hybrid compensation are generated implementing the formulas presented in Chapter 4. The results of the prediction are manipulated mathematically to obtain

the reference current for power variation compensation.

```

void CFlywheelDoc::Prediction()
{
    int N;
    double Mag_Volt, Ang_Volt, Mag_VoltS, Ang_VoltS;
    double twopi_N;

    N = Graph.Samples;
    twopi_N = 2 * pi / N;

    for (sample = 0; sample < Graph.SamplesSim; sample++)
    {
        Solution.Pred_SupplyCurr[sample] = 0;
        Solution.Pred_Iact1[sample] = 0;
        Solution.Pred_Ireact1[sample] = 0;
        Solution.Pred_Idist[sample] = 0;
    }

    for (sample = 1; sample < Graph.SamplesSim; sample++)
    {
        Mag_Volt = sqrt(2.0) * (2 * abs(Solution.CRMSU1[sample]) - abs(Solution.CRMSU1[sample-1]));
        Ang_Volt = (sample + 1) * twopi_N + arg(Solution.CRMSU1[sample + 1]);
        Solution.Pred_SupplyCurr[sample + 1] = 2 * Solution.SupplyCurr[sample * Graph.Points] -
        Solution.Pred_Iact1[sample + 1] = (2 * Solution.Geq1[sample] - Solution.Geq1[sample - 1]) * Mag_Volt *
        cos(Ang_Volt);
        Solution.Pred_Ireact1[sample + 1] = (2 * Solution.Beq1[sample] - Solution.Beq1[sample - 1]) * Mag_Volt *
        sin(Ang_Volt);
        Solution.Pred_Idist[sample + 1] = Solution.Pred_SupplyCurr[sample + 1] - Solution.Pred_Iact1[sample + 1] -
        Solution.Pred_Ireact1[sample + 1];
    }
}

```

Figure 6.14. Prediction of current components subroutine

The reference current for distortion compensation is given by the predicted current component of the supply current, as presented in Figure 6.14.

```

/Subroutine to get the reference active current to be compensated
void CFlywheelDoc::Ref_act_curr()
{
    int N, N_ave;
    double Ang_Volt, Ang_VoltS;
    double twopi_N;

    N = Graph.Samples;
    twopi_N = 2 * pi / N;
    N_ave = Solution_fw.AveCoef * N;
    Solution.Geq1_ave = 0.0;

    for (sample = 0; sample < Graph.SamplesSim; sample++)
    {
        Solution.Geq1_ave = Solution.Geq1_ave + Solution.Geq1[sample];
    }
    Solution.Geq1_ave = Solution.Geq1_ave / N_ave;

    for (sample = 0; sample < Graph.SamplesSim; sample++)
    {
        Ang_Volt = sample * twopi_N + arg(Solution.CRMSU1[sample]);
        Solution.Iact1_Ref[sample] = Solution.Geq1_ave * sqrt(2) * abs(Solution.CRMSU1[sample]) * cos(Ang_Volt);
        Solution_fw.Iact1_Ref[sample] = Solution.Pred_Iact1[sample] - Solution.Iact1_Ref[sample];
    }
}

```

Figure 6.15. Reference PV current subroutine

The reference current for PVC has two components. The first component is given by the difference between the predicted running fundamental active current and the median. The

calculation of this component is presented in Figure 6.15 for phase R. The second component is the predicted running fundamental reactive current calculated as in Figure 6.14. The sum of these two components results in the reference current for power variation.

### 6.8 Block 7: Generate PWM Switching Sequences

Processes in block 7 use the data stored for the reference current as a basis to determine the switching sequence of the inverters. The decision is done by implementing vector control of the PMSM with SW-PWM for inverters of the PV compensator and SV-PWM for the inverter of the DC compensator as presented in Chapter 5. Block 7 is built up from several sub-processes. The blocks to implement switching sequence for the PV compensator are presented in Figure 6.16.

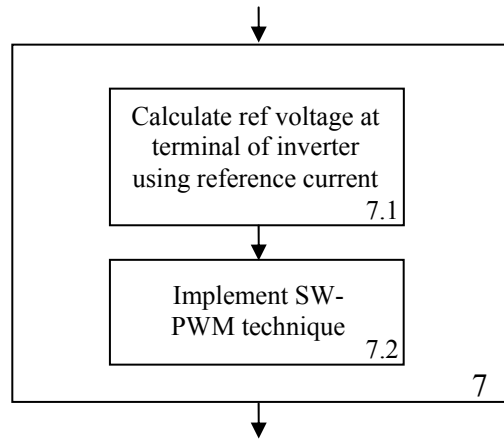


Figure 6.16. Processes within block 7 for PV compensator.

There are two subprocesses within block 7. The two blocks to implement the switching sequence are presented in Figure 6.17.

### 6.9 Block 8: Hybrid Compensator Current Calculation

The set of differential equations for the Power variation compensator developed in Chapter 5 are solved using the runge-Kutta Fehlberg 4<sup>th</sup>/5<sup>th</sup> order subroutine.

Runge-Kutta Fehlberg 4<sup>th</sup>/5<sup>th</sup> order is a numerical method widely used and suitable to solve the first order differential equations with accuracy.

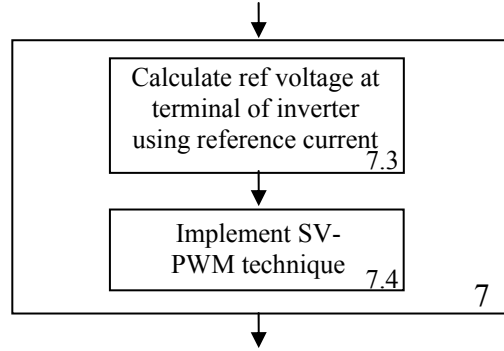


Figure 6.17. Processes within block 7 for DC compensator.

The subroutine containing the set of differential equations related to inverter A and the supply side of the PV compensator are shown in Figure 6.18.

```

void CFlywheelDoc::solutioncalc_fw()
{
    complexd Va, Va1;
    double Va1_s;
    initialize_fw();
    sample = 0;
    finalTime = tFINAL - hSTART / 2.0;

    while ((t0 < finalTime) && (count < MaxCount))
    {
        Va1_s = Ref_voltage1(sample);
        pwmseq1_fw(Va1_s, t0, sample);
        Va1 = Ref_voltage2(sample);
        rkf(t0, h, x0, xend, mode, 0, sample, 2); // cases = 2, flywheel system, Charging mode
        Solution_fw.SupplyCurr_fw[sample] = xend[0];
        Solution_fw.SupplyCurrS_fw[sample] = xend[1];
        Solution_fw.SupplyCurrT_fw[sample] = xend[2];
        Solution_fw.Isd[sample] = xend[3];
        Solution_fw.Isq[sample] = xend[4];
        dq0_to_abc(xend, sample);
        Solution_fw.Flywheelmechspeed_fw[sample] = xend[5];
        Solution_fw.Flywheeltheta_fw[sample] = xend[6];
        Solution_fw.CapVolt_fw[sample] = sqrt(xend[7]);
        Solution_fw.LoadCurr_fw[sample] = (1 / Solution_fw.CapVolt_fw[sample]) * (ea * xend[0] + eb * xend[1] + ec *
xend[2]);
        t0 += hSTART;
        sample++;
    } // end of while
}
  
```

Figure 6.18. Set of differential equations for inverter A and supply side of the PV compensator subroutine

The subroutine containing the set of differential equations related to inverter B and the FESS of the PV compensator are shown in Figure 6.19.

The subroutine containing the set of differential equations related to DIC compensator is shown in Figure 6.20.

## 6.10 Block 9: Compensated Supply Current Calculation

Block 9 adds the two currents resulting from solving the differential equations of the PV and

DIC compensator to the supply current of the FVL load as presented in Figure 6.21.

```
void CFlywheelDoc::getcom_DERIVS_fw(double x0[], double f[], double t0, int mode, int com_mode, int sample)
{
    f[0] = (1.0 / (Flywheelsys.Lffw)) * (Solution.RectVolt[sample] - (Flywheelsys.Rffw * x0[0]) - Solution_fw.VpwmA1[sample]);
    f[1] = (1.0 / (Flywheelsys.Lffw)) * (Solution.RectVoltS[sample] - (Flywheelsys.Rffw * x0[1]) - Solution_fw.VpwmB1[sample]);
    f[2] = (1.0 / (Flywheelsys.Lffw)) * (-(Solution.RectVolt[sample] + Solution.RectVoltS[sample]) - (Flywheelsys.Rffw * x0[2]) -
    Solution_fw.VpwmC1[sample]);
    f[3] = (1.0 / Flywheelsys.Lsfw) * (Solution_fw.Vsd[sample] - Flywheelsys.Rsfw * x0[3] + (Flywheelsys.Pfw / 2.0) * x0[5] *
    Flywheelsys.Lsfw * x0[4]);
    f[4] = (1.0 / Flywheelsys.Lsfw) * (Solution_fw.Vsq[sample] - Flywheelsys.Rsfw * x0[4] - (Flywheelsys.Pfw / 2.0) * x0[5] *
    (Flywheelsys.Lsfw * x0[3] + sqrt(3.0 / 2.0) * Flywheelsys.KEfw));
    f[5] = (1.0 / (Flywheelsys.Jeqfw + Flywheelsys.Jdfw)) * ((Flywheelsys.Pfw / 2.0) * sqrt(3.0 / 2.0) * Flywheelsys.KEfw * x0[4] -
    0.001 * 3.2);
    f[6] = (Flywheelsys.Pfw / 2.0) * x0[5];
    f[7] = (2.0 / (Flywheelsys.Cfw)) * (ea * x0[0] + eb * x0[1] + ec * x0[2] - (Supply.Rs * pow(x0[0],2) + Supply.Rs * pow(x0[1],2) +
    Supply.Rs * pow(x0[2],2)) - (3.0 / 2.0) * x0[5] * sqrt(3.0 / 2.0) * Flywheelsys.KEfw * x0[4]);
}
```

Figure 6.19. Set of differential equations for inverter B and FESS of the PV compensator subroutine

```
void CFlywheelDoc::getcomp_DERIVS(double x0[], double f[], double t0, int mode, int com_mode, int sample)
{
    f[0] = (1.0 / Cfilter.Lc) * (Solution.LoadCompVolt[sample] - (Cfilter.Rc * x0[0]) - Solution.RectVolt[sample]);
}
```

Figure 6.20. Differential equation for the DC compensator subroutine

```
void CFlywheelDoc::solutionsyscurr()
{
    for (sample = 0; sample < Graph.PointsSim; sample++)
        Switchcomp.SysCurr[sample] = Solution.SysCurr[sample] + Solution.LoadCompCurr[sample];
}
```

Figure 6.21. Compensated supply current subroutine

## 6.11 Block 10: Results

Block 10 compiles the subroutines for analysis of the results of compensation. Some of the subroutines included in this block are the subroutine for calculation of the running active power of the compensated load, harmonic spectrum analysis of the compensated supply current, and calculation of deviations of the resultant currents from the reference currents.

The use of the screens of the user interface is explained in appendix A.

## Chapter 7

### Verification of the Performance of the Model of the Hybrid Compensator

#### 7.1 Introduction

Verification of the results of simulation is done for three distinct fast varying loads at the following constraints: the three-phase supply voltage is considered symmetrical with 60 Hz frequency; the FVL is a balanced three-phase load supplied from a three-phase AC/DC converter with an inductive filter. Parameters of the system are presented in Appendix B.

Three test loads has been considered to evaluate the hybrid compensator model, each test load characterizes a particular type of FVL:

- Test load 1 is a FVL characterized by a single random power pulse of 5 cycle duration and  $\Delta P$  of 2.3 p.u. It is referred to as FVL1, Fig, 7.1.

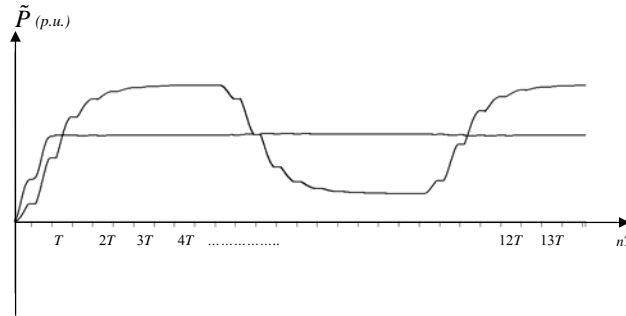


Figure 7.1. Running active and median power of FVL1

- Test load 2 is a FVL characterized by repetitive power pulses of 3 cycle duration and  $\Delta P$  of 2.3 p.u. It is referred to as FVL2, Figure 7.2

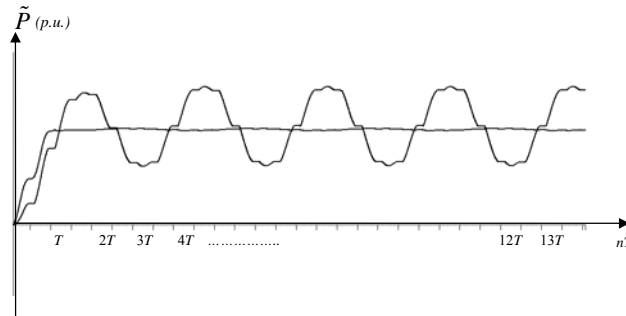


Figure 7.2. Running active and median power of FVL2

- Test load 3 is a FVL characterized by random power pulses of 4 cycles duration and  $\Delta P$  of 2.3 p.u. It is referred to as FVL3, Figure 7.3.

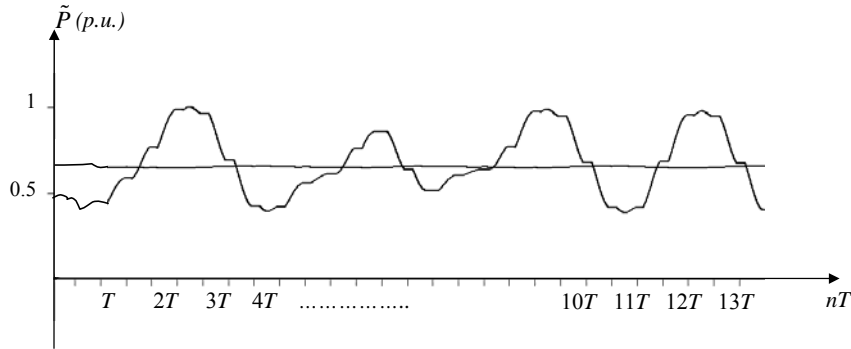


Figure 7.3. Running active and median power of FVL3

These three FVLs result in three different variations in the running active and median power as presented in Figure 7.1 – Figure 7.3.

The variation in the amplitude and duration of the power pulses for each test load presented is simulated accordingly to the constraints presented above. All the parameters specified by the constraints are user inputs in the computer model.

## 7.2 Simulation of Test Loads Supply Current

The supply currents of FVL1, FVL2 and FVL3 that results from the variation of the active power presented previously is illustrated in Figure 7.4.

Supply currents in Figure 7.4 are strongly distorted and fast varying. These waveforms are characteristic of the FVL characterized in Chapter 2 and used as test loads. There are 768 integration points per cycle in the calculation of the supply currents presented in Figure 6.17. These data are stored in memory.

## 7.3 Simulation of CPC Decomposition of the Supply Current

Current decomposition of the sampled supply current of the test loads is performed accordingly to Chapter 3. Results of the decomposition implemented in the program are shown in the following plots.

The running rms value of the fundamental active current component of the supply current of the test loads is presented in Figure 7.5.

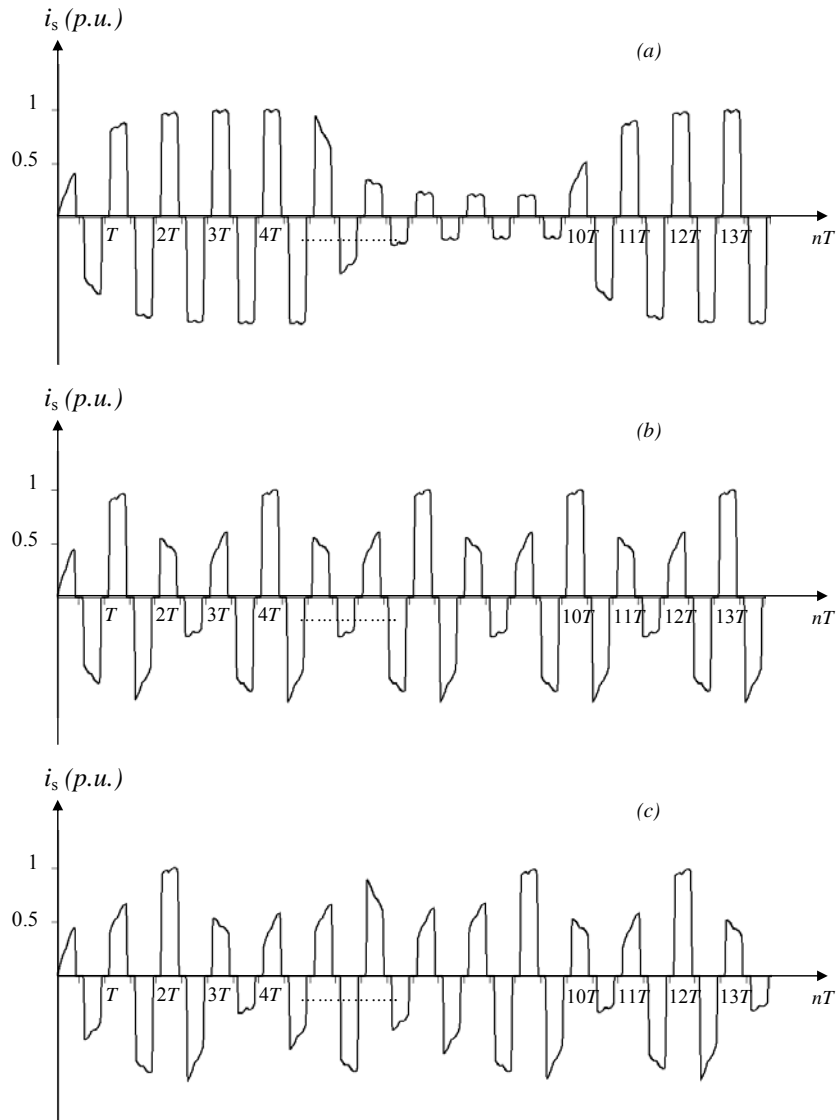


Figure 7.4. Supply current of test loads. (a) FVL1, (b) FVL2, (c) FVL3

There is a variation in the magnitude of the running rms value of the fundamental active current in accordance to expectations in all cases shown in Figure 7.5.

The running rms value of the fundamental reactive current component of the supply current of the test loads is presented in Figure 7.6.

A similar variation in the magnitude of the running rms value of the fundamental reactive

current as the one presented in Figure 5.5 is obtain in accordance to expectations in all the cases shown in Figure 7.6.

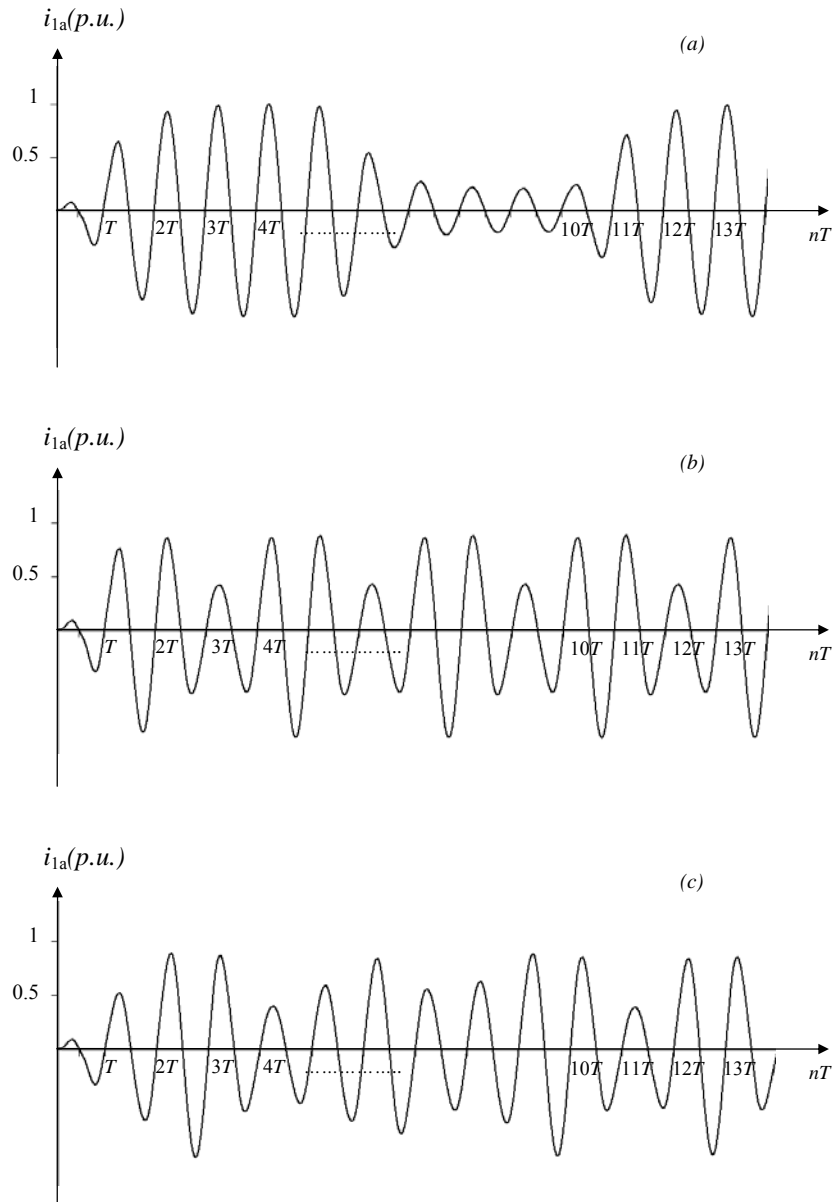


Figure 7.5. Running rms value of the fundamental active current. (a) FVL1, (b) FVL2, (c) FVL3

The Running rms value of the distorted component of the supply current of the test loads is presented in Figure 7.7.

There is a significant variation in the profile of the running rms value of the distorted component of the supply current in each test load as shown in Figure 7.7. It is a rapidly varying

quantity. The current decomposition performed to the supply current of the test loads has been done using the algorithm for semi-periodic currents presented in Chapter 3 and implemented as in Chapter 6. All the results are in accordance to the expectations.

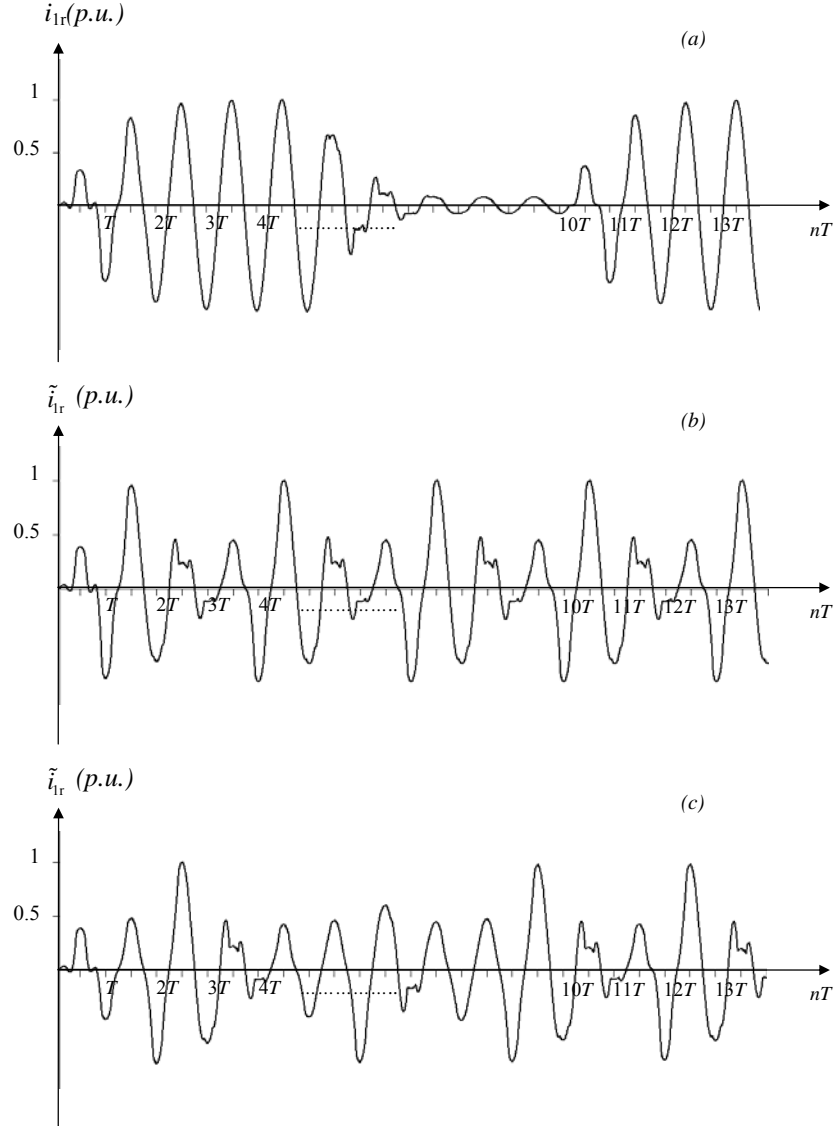


Figure 7.6. Running rms value of the fundamental reactive current. (a) FVL1, (b) FVL2, (c) FVL3

#### 7.4 Simulation of the Reference Signals for the Hybrid Compensator

Generation of reference signals for hybrid compensation requires that the physical components are predicted. This predicted component is next used to generate the reference signals for the compensators as presented in Chapter 4. The computer model demonstrated that

the difference between the running rms value of the fundamental active and reactive current component and its predicted value can not be visually distinguished. Parameters used to calculate these quantities are slowly varying. This property is fundamental to facilitate an accurate prediction of these current components. On the other hand, as expected there are differences between the predicted and the current running rms value of the distorted component of the supply current. The difference between the actual and the predicted running rms value of the distorted component of the supply current for the test loads is presented in Figure 7.8.

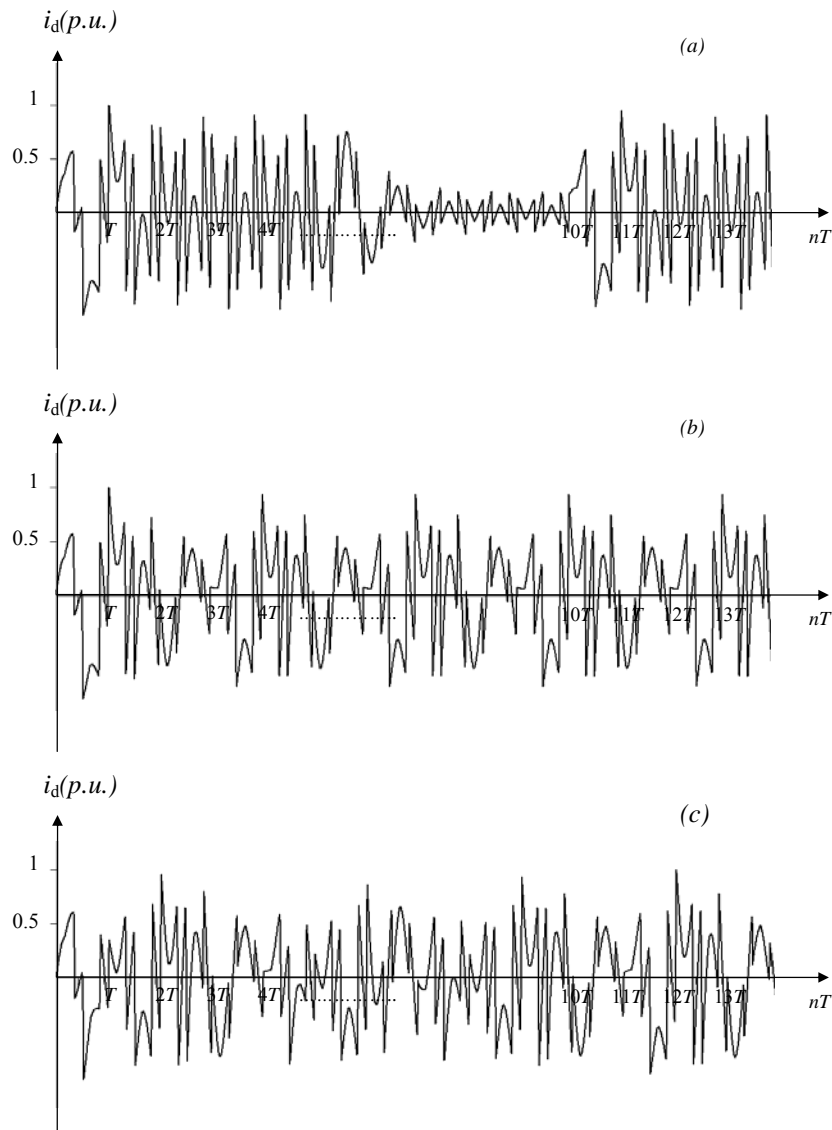


Figure 7.7. Distorted component of the supply current. (a) FVL1, (b) FVL2, (c) FVL3

The major differences between the actual and the predicted running rms value of the distorted component of the supply current in Figure 7.8 take place during commutation. This variation is difficult to predict as explained in Chapter 4. This difference can be reduced only by an increase of the sampling rate. The difference varies in magnitude depending on the type of FVL. The difference is smaller when the power pulses take place and the running rms value of the supply current is smaller.

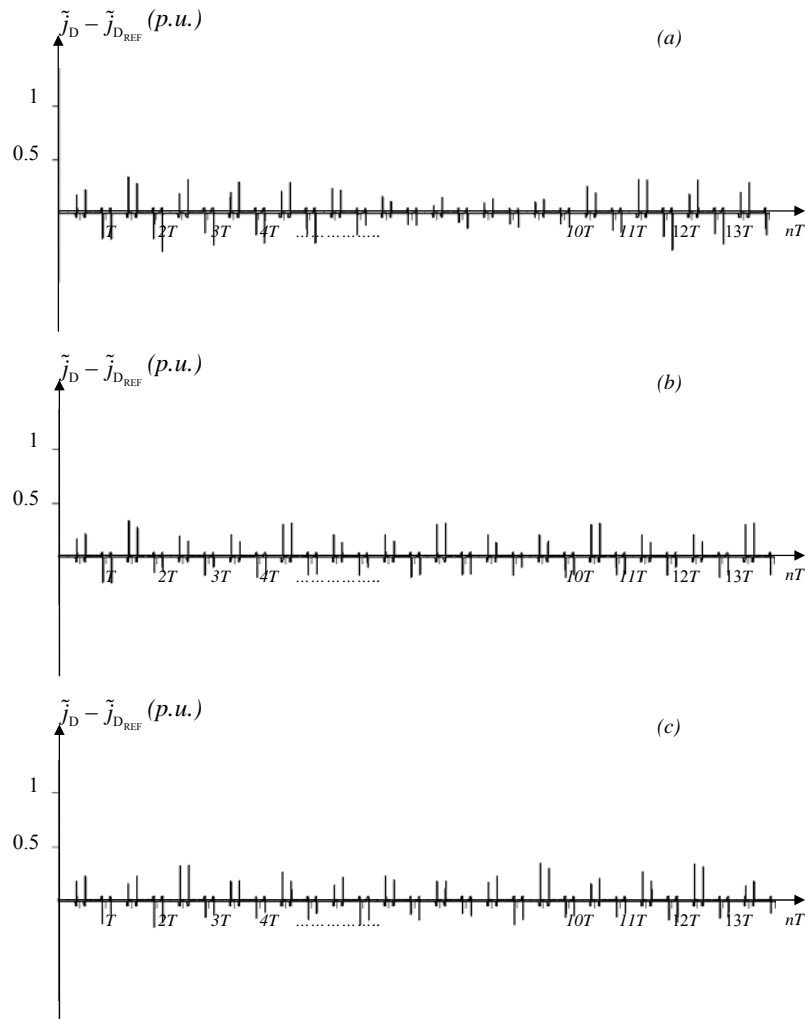


Figure 7.8. Difference between the actual and the predicted running rms value of the distorted component of the supply current. (a) FVL1, (b) FVL2, (c) FVL3

The PV compensator reference currents to reduce the power variation of the test loads are plotted in Figure 7.9. These currents are calculated with the formulas presented in Chapter 4.

The PV reference current waveform is particular to each type of FVL. The waveforms presented in Figure 7.9 comply with the characterization done of the requirements for reduction of the power variation during FVLs operation. The PV reference current results in a slowly varying signal as expected.

The DC compensator reference currents for the test loads are plotted in Figure 7.10. These currents are calculated with the formulas presented in Chapter 4. They represent the amount of current that the control algorithm needs to generate to compensate the distortion of the supply current.

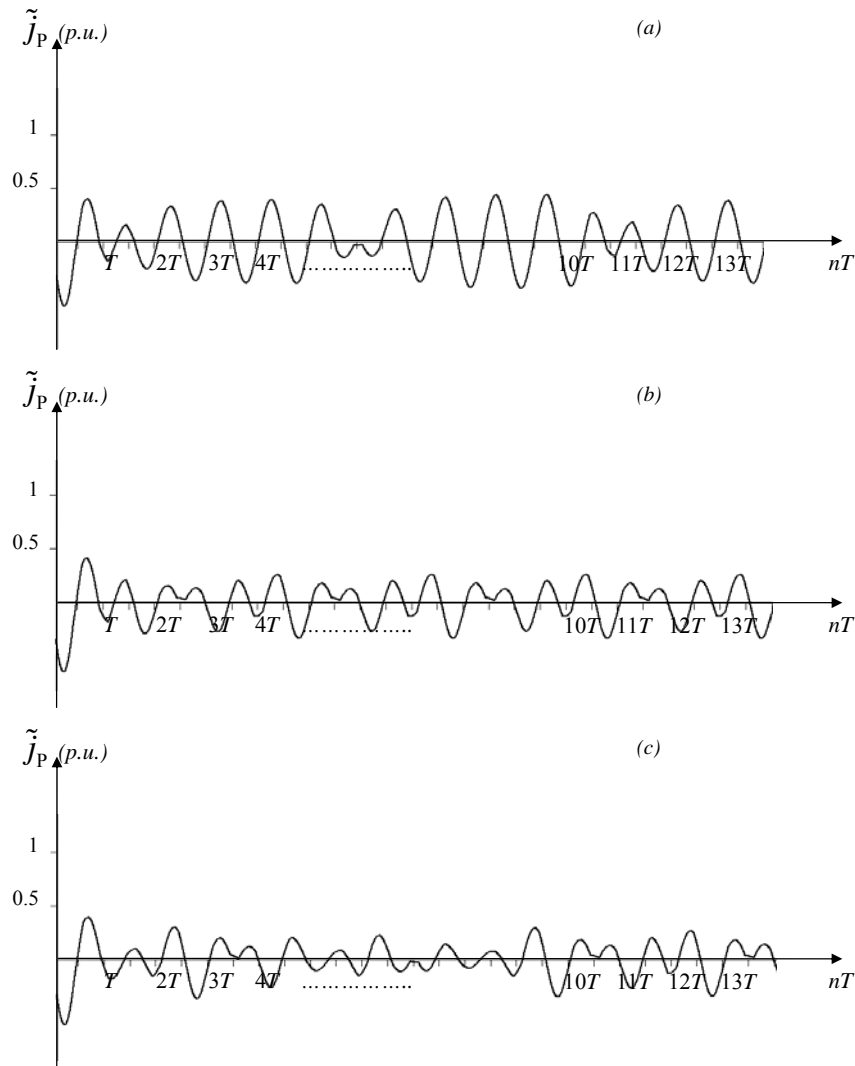


Figure 7.9. Power variation compensator reference current,  $\tilde{j}_{P_{REF}}$ . (a) FVL1, (b) FVL2, (c) FVL3

The DC compensator reference currents to reduce distortion of the test loads are plotted in Figure 7.10. These currents are calculated with the formulas presented in Chapter 4.

The DC reference current waveform is particular to each type of FVL. The waveforms presented in Figure 7.10 comply with the characterization done of the requirements for reduction of burst of waveform distortion during FVLs operation. The DC reference current results in a fast varying signal.

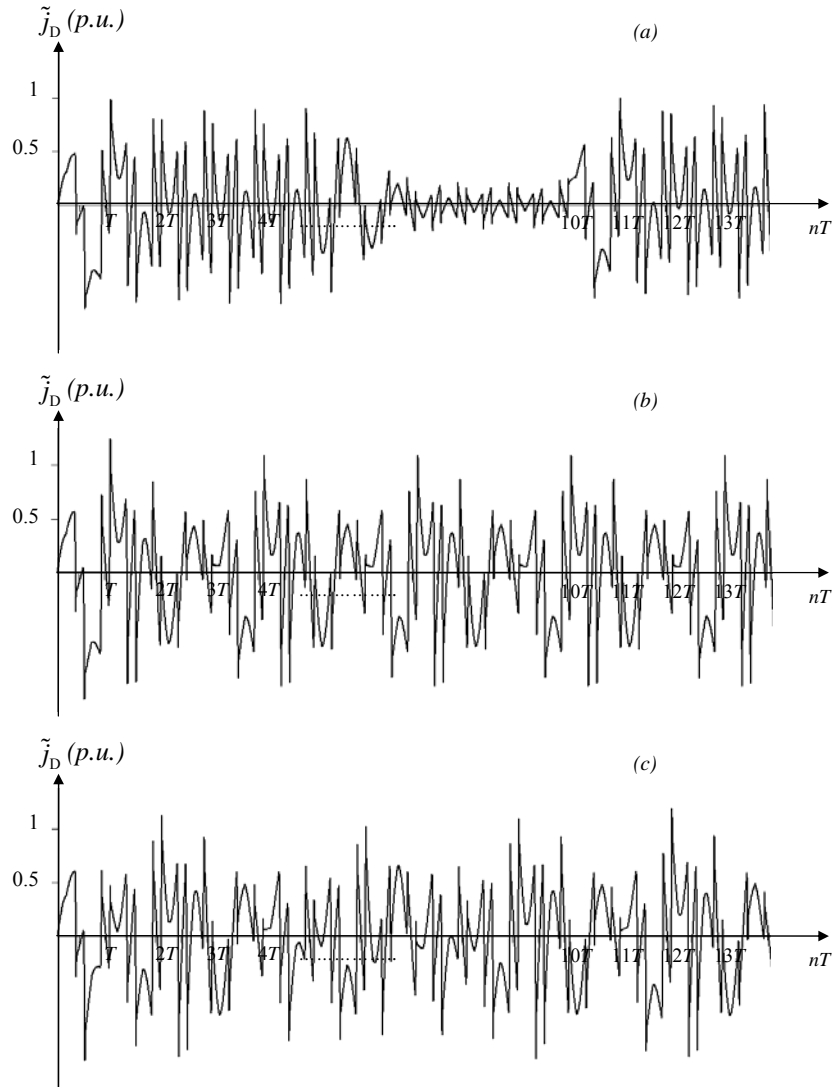


Figure 7.10. Distortion compensator reference current,  $\tilde{j}_{D_{REF}}$ . (a) FVL1, (b) FVL2, (c) FVL3

### 7.5 Simulation of the Compensator Current

The computer model of the equations developed in Chapter 5 along with the two reference

signals presented in the previous section are needed for computer modeling of the hybrid compensation of the test loads.

The compensator current is generated by the addition of two currents: the PV compensator current,  $j_p$ , and the DC compensator current,  $j_D$ . These currents are calculated during simulation of the compensator operation.

The PV compensator current for each test load is presented in Figure 7.11.

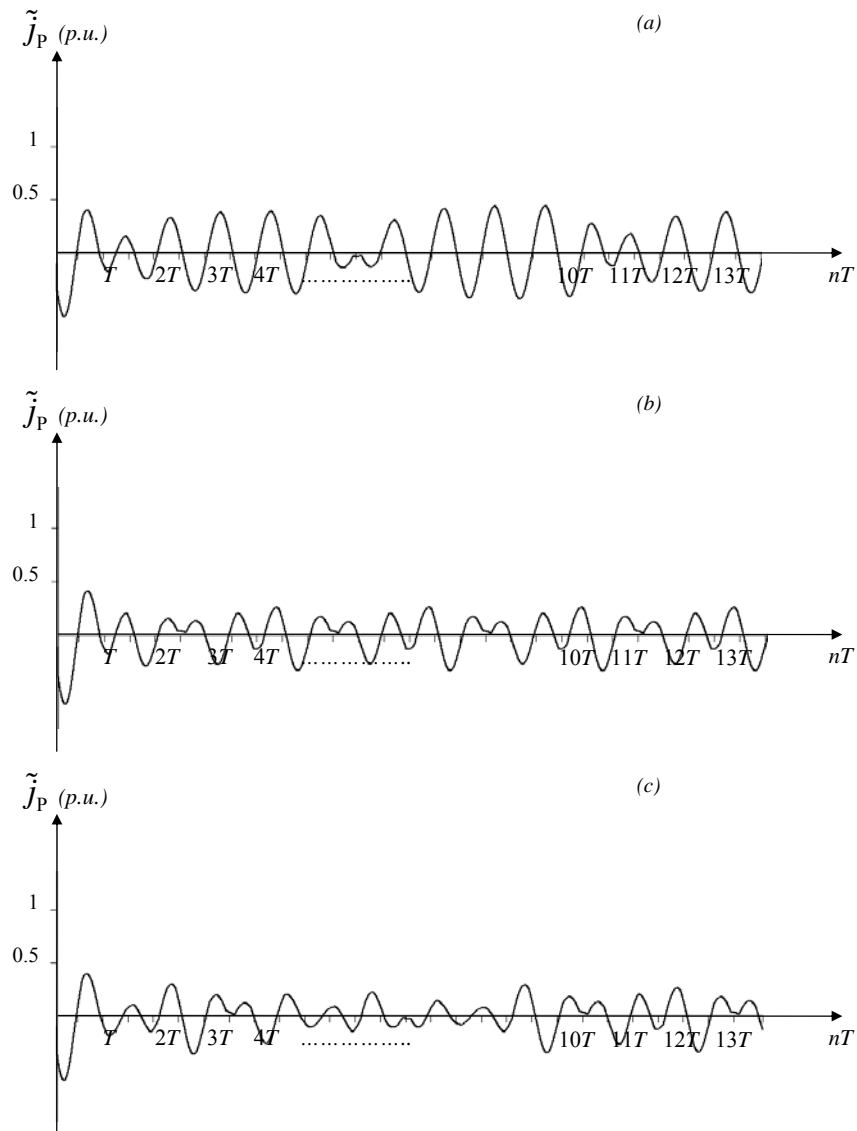


Figure 7.11. Power variation compensator current,  $\tilde{j}_p$ . (a) FVL1, (b) FVL2, (c) FVL3

These currents in Figure 7.11 are compared to the reference signals presented in Figure 4.3.

Results of comparison show that there is no visible difference between them. These results are expected, the algorithm has an accurate result when predicting a slowly varying parameter as the running rms value of the fundamental active current used to calculate this reference current.

The DIC compensator current for each test load is plotted in Figure 7.12.

The non-compensated supply current and the compensated supply current,  $i'_s = i_s + j = i_s + (j_p + j_D)$  for the test loads are illustrated in Figure 7.13 – Figure 7.15. Results of the computer model of the hybrid compensator demonstrated that most of the power variation, phase shift and the strong distortion are reduced.

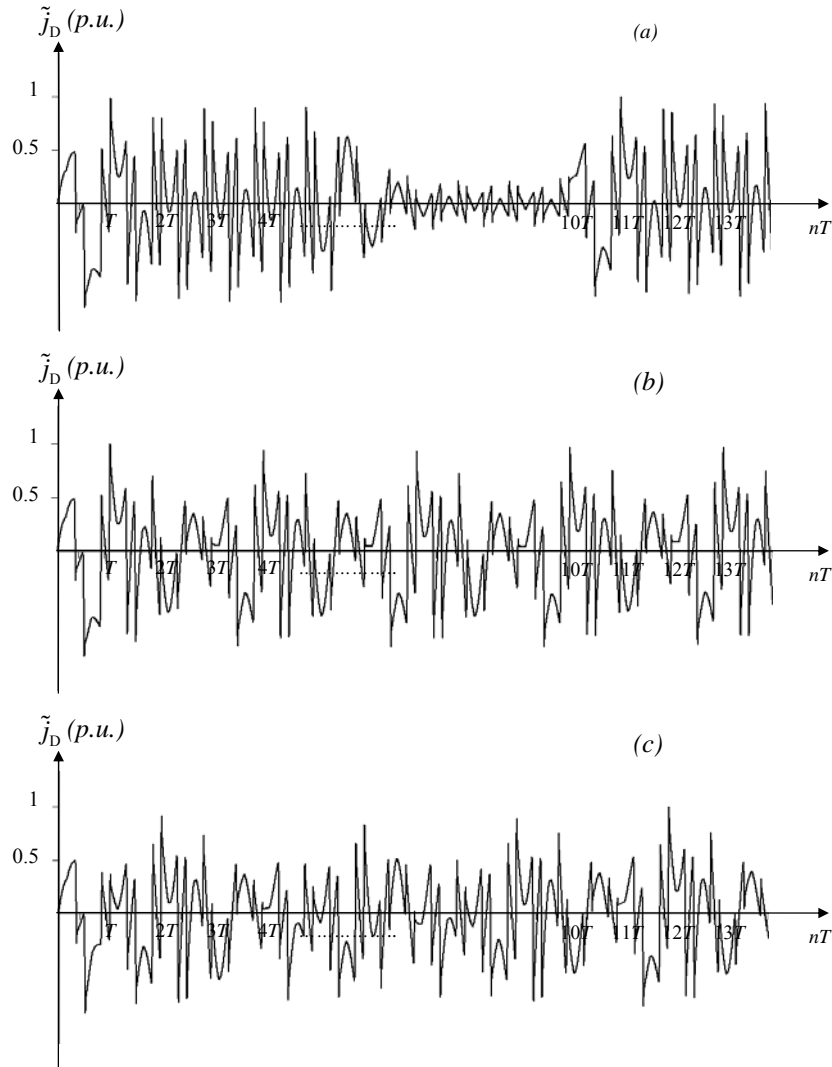


Figure 7.12. Distortion compensator current,  $\tilde{j}_D$ . (a) FVL1, (b) FVL2, (c) FVL3

The running active power of the compensated FVL is shown in Figure 7.16. Results presented in Figure 7.16 can be compared with the waveforms of the running active power of the test FVL presented in Figure 7.1 to 7.3. Results of the computer model of the hybrid compensator demonstrated that the power variation has been reduced.

Compensation results in a reduction of the variation of the active power in the operation of the three test loads FVLs. The average difference between the reference active power and the active power of the compensated FVL can be calculated using the data stored in memory. The difference calculated is approximately 0.2% for FVL1 and 0.68% for FVL2 and FVL3.

Analysis of the harmonic spectrum plotted in Figure 7.17 shows how the distortion has been reduced by the compensator for all test loads. After compensation, the contribution of harmonics to the compensated supply current distortion is minimal.

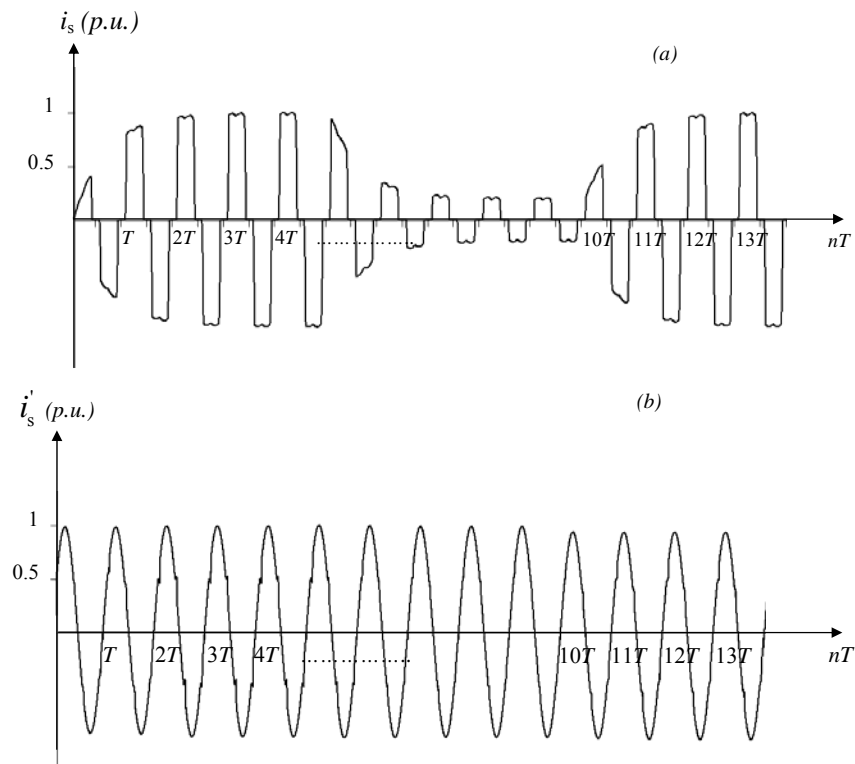


Figure 7.13. Supply current of FVL1. (a) non-compensated, (b) compensated

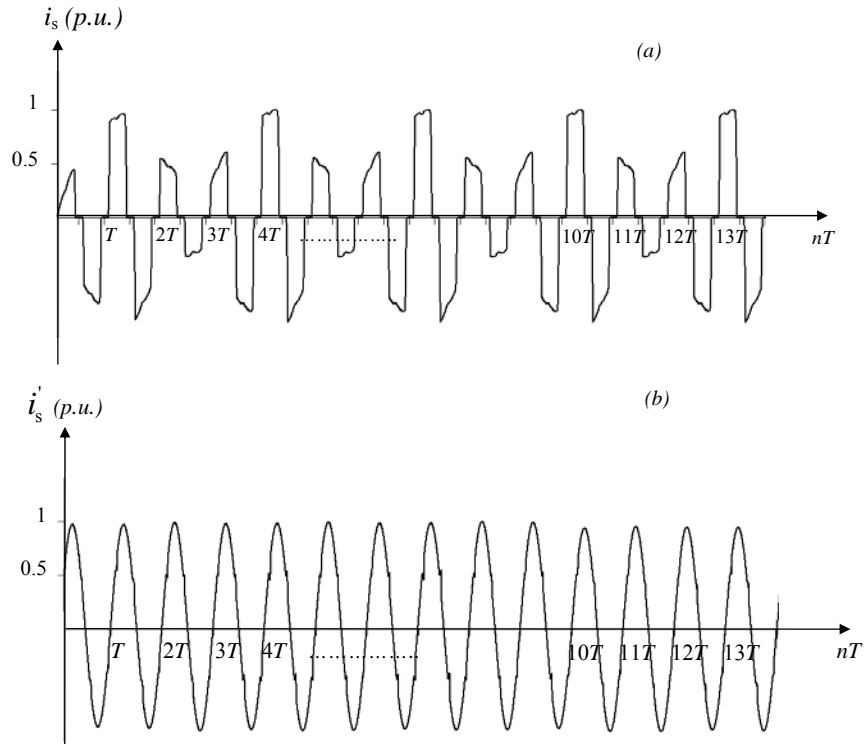


Figure 7.14. Supply current of FVL2. (a) non-compensated, (b) compensated

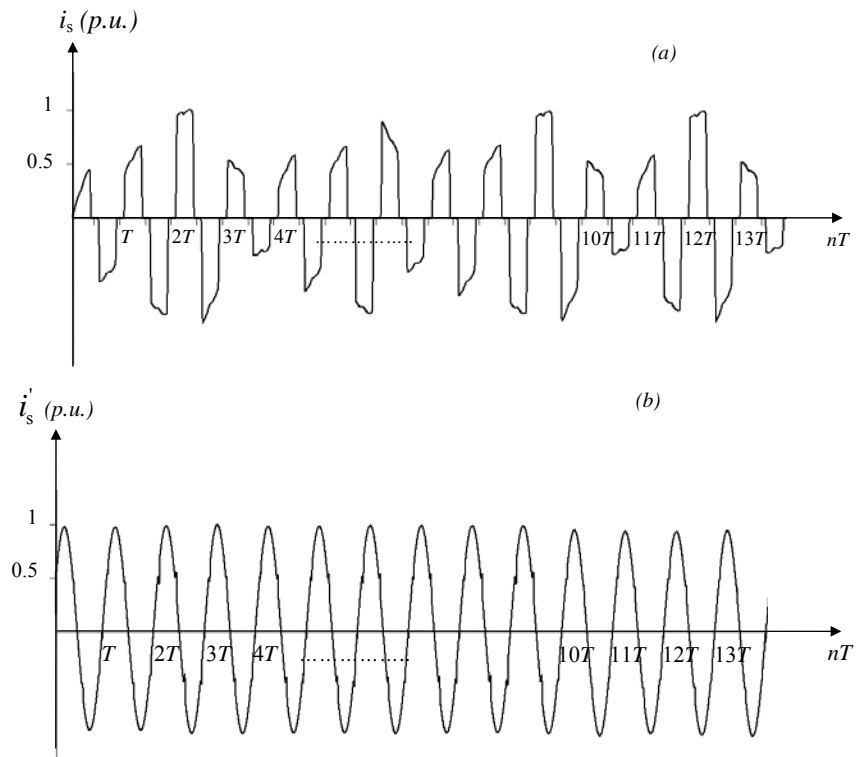


Figure 7.15. Supply current of FVL3. (a) non-compensated, (b) compensated

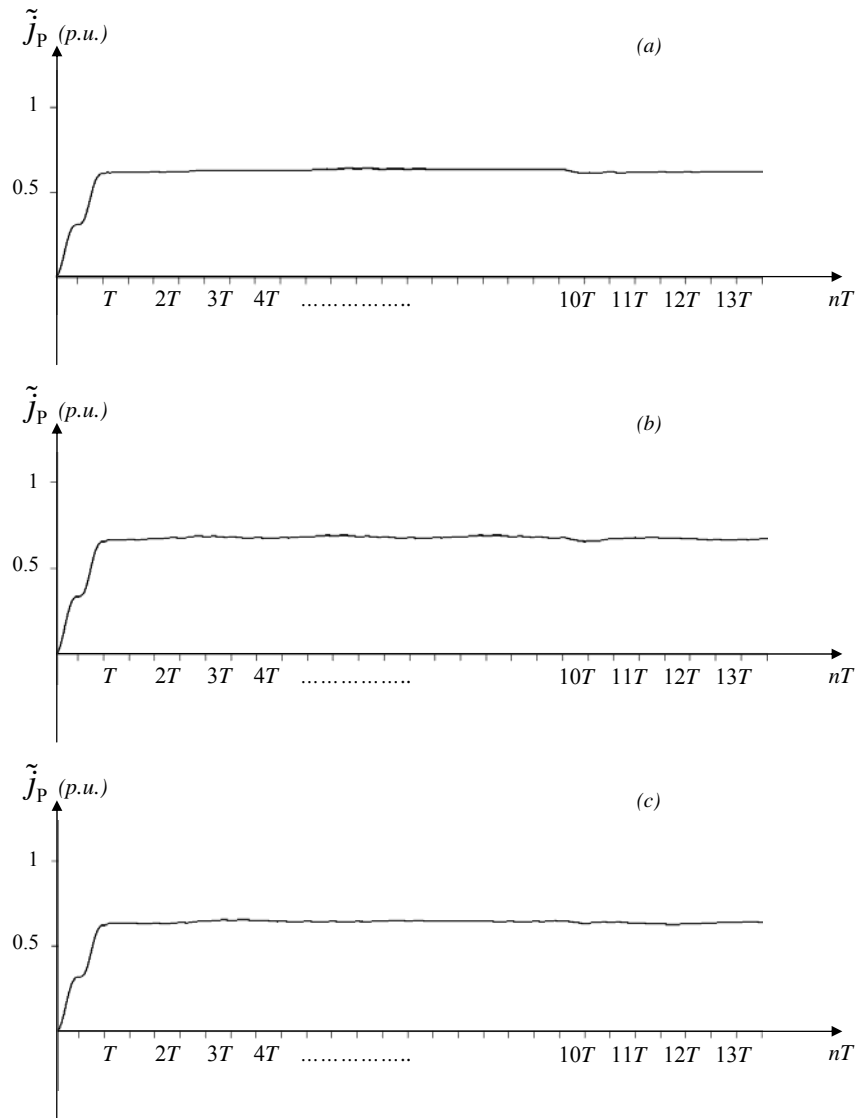


Figure 7.16. Running active power of compensated load. (a) FVL1, (b) FVL2, (c) FVL3

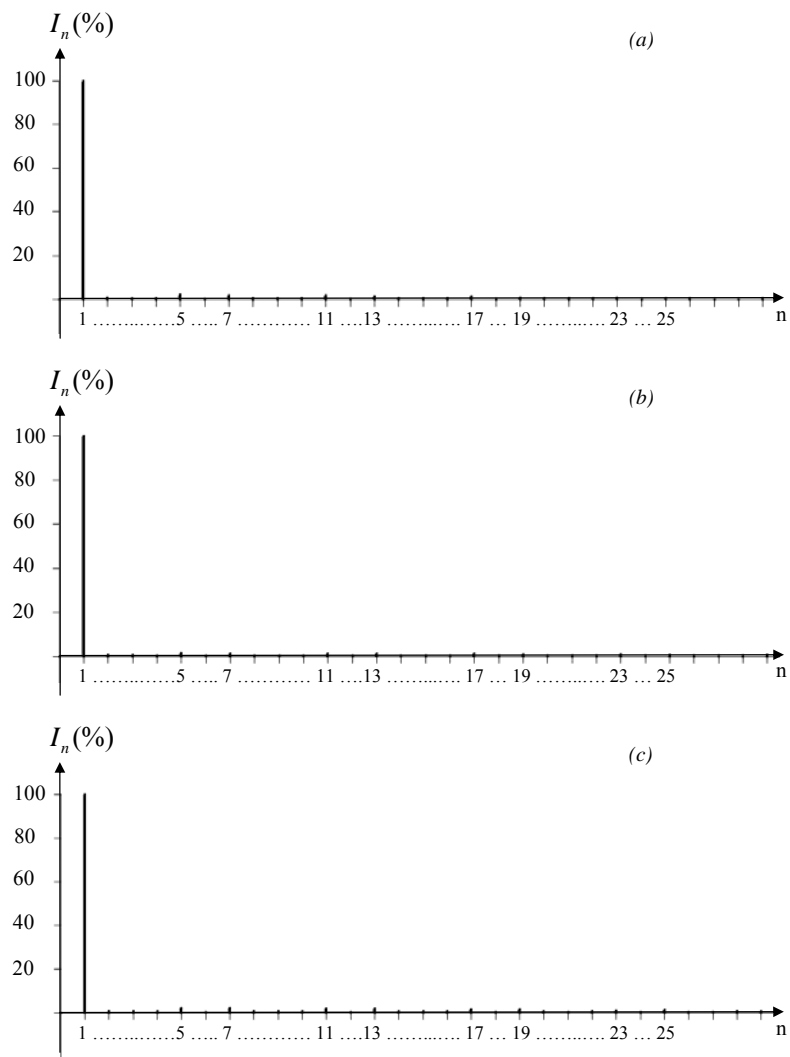


Figure 7.17. Harmonic spectrum of compensated supply current. (a) FVL1, (b) FVL2, (c) FVL3

## **Chapter 8**

### **Conclusions**

A characterization of FVL is developed in this dissertation. FVL are characterized by differentiating the power pulses that result from their operation. FVL has been classified as Repetitive, Random and Burst. Burst-FVL can be also repetitive or random; it depends on the operational nature of the load.

The operation of FVL in distribution systems causes the harmful effects associated with voltage sags, levels of distortion and variation in the active power. If these values exceed the standards they need to be compensated.

Even though FVLs currents are non-periodic, CPC theory allows the calculation of the running active, reactive and distorted components of the supply current. These components are used in the algorithm for generation of the reference signals for the compensator.

A model for hybrid compensation of power variation and distortion is presented in an open loop scheme for the first time. The model provided compensation for the active and reactive power variation. In addition, compensation for the distorted component by the switching compensator is performed too. The integration of both compensators in the model results in an almost sinusoidal current of constant rms value, independently of the load power variation. The compensator can be implemented to compensate only active power variation, reactive power or distortion if desired. The use of the power variation compensator for both active and reactive power contributes to the reduction of the size of the switching compensator. As a consequence the range of application of such compensator is increased.

For future research a prototype of the compensator needs to be built. This will allow the evaluation of the effectiveness of the algorithm in compensation of power variation and distortion for a test system. The evaluation of optimized techniques for prediction of the supply

current and a close loop scheme for the compensation algorithm is another proposed area of future research.

## References

- [1] Gerbec, D.; Gasperic, S.; Smon, I.; Gubina, F., "Allocation of the load profiles to consumers using probabilistic neural networks", IEEE Transactions on Power Systems, Volume 20, Issue 2, May 2005 Page(s):548 - 555
- [2] Gerbec, D.; Gasperic, S.; Gubina, F., "Determination and allocation of typical load profiles to the eligible consumers", 2003 IEEE Bologna Power Tech Conference Proceedings, Volume 1, 23-26 June 2003 Page(s):5 pp. Vol.1
- [3] Youman Deng; Xiaojuan Ren; Changcheng Zhao; Dapu Zhao, "A heuristic and algorithmic combined approach for reactive power optimization with time-varying load demand in distribution systems", IEEE Transactions on Power Systems, Volume 17, Issue 4, Nov. 2002 Page(s):1068 - 1072
- [4] Dilek, M.; Broadwater, R.P.; Thompson, J.C.; Sequin, R., "Simultaneous phase balancing at substations and switches with time-varying load patterns", IEEE Power Engineering Society Winter Meeting, 2002, Volume 2, 27-31 Jan. 2002 Page(s):1325 vol.2
- [5] Fang Xing; Zhizhong Guo; Zhongqin Cai, "Improved moment method for network reconfiguration with time-varying load in distribution systems", 2004 International Conference on Power System Technology, 2004. PowerCon 2004, Volume 1, 21-24 Nov. 2004 Page(s):139 - 144 Vol.1
- [6] Henry, R.E., "Cable sizing for fast transient loads" 2003 IEEE Technical Conference Industrial and Commercial Power Systems, 2003, 4-8 May 2003, Page(s): 18 - 32.
- [7] Henry, R.E., "Response of power cables to fast transient loads", Conference Record of the 2004 IEEE Industry Applications Conference, 2004. 39th IAS Annual Meeting., Volume: 2, 3-7 Oct. 2004, Page(s):750 - 757.
- [8] Freiherr von Karnten, R.E., "Starting of drives in the cement industry requirements, methods and solutions", IEEE-IAS/PCA 2003 Cement Industry Technical Conference, 2003. Conference Record, 4-9 May 2003, Pages: 75 - 94.
- [9] Kotz, G.R.; Regan, M.P., "Motor applications for hydraulic roll crushers," 36th IEEE Cement Industry Technical Conference, 1994. XXXVI Conference Record, 29 May-2 June 1994 Page(s):99 - 116.
- [10] R. Errath, R.A., "Roll crusher with variable speed DC drive," 36th IEEE Cement Industry Technical Conference, 1994. XXXVI Conference Record, 29 May-2 June 1994 Page(s):67 - 83.
- [11] Elsmam, R.; Errath, R.A., "Replacing hydraulic kiln drives-key messages and recommendations to cement plant operators from a case study," IEEE/PCA Cement Industry Technical Conference, 1996. XXXVIII Conference Record, 14-18 April 1996 Pages:53 - 68.

- [12] Rosario, P.P; Hall R.A.; Maijer, D.M., “Liner wear and performance investigation of primary gyratory crushers” *Minerals Engineering*, v 17, n 11-12, November/ December, 2004, Page(s):1241-1254
- [13] Arseneau, R., “The performance of demand meters under varying load conditions”, *IEEE Transactions on Power Delivery*, Volume 8, Issue 4, Oct. 1993 Page(s):1708 – 1711
- [14] Jun-Keun Ji; Seung-Ki Sul, “DSP-based self-tuning IP speed controller with load torque compensation for rolling mill DC drive”, *IEEE Transactions on Industrial Electronics*, Volume: 42,, Issue: 4 , Aug. 1995, Page(s):382 - 386.
- [15] Godfrey, N. R. (BHP ENGINEERING); Parkes, L.S.; Wilkie, R.J., “High Performance Speed Regulation of Rolling Mill DC Drives Connected to a Common Voltage Bus”, *The Fourth Conference on Control Engineering*, The Institution of Engineers Australia, August 1990, Page(s):70 – 75
- [16] Wodrich, R.T., “High speed reactive compensation systems for industrial applications”, *Cement Industry Technical Conference, IEEE-IAS/PCA 2001.* , 29 April-3 May 2001 Page(s):41 – 50.
- [17] Mutluer, B.; Cadirci, I.; Ermis, M.; Cetin, A.; Ozay, N.; Gultekin, B.; Kose, N.; Ermis, C.; Terciyanli, A.; Unver, O.; Unal, V.; ”A unified relocatable SVC for open-cast lignite mining in Turkey”, *IEEE Transactions on Industry Applications*, Volume: 40, Issue: 2, March-April 2004, Page(s): 650 – 663
- [18] Rodriguez, J., B.; Moran, L.; Pontt, J.; Espinoza, J.; Diaz, R.; ”Operating experience of shovel drives for mining applications”, *IEEE Transactions on Industry Applications*, Volume: 40, No 2, March-April 2004, Page(s): 664 – 671
- [19] Boulet, B.; Lalli, G.; Ajersch, M., “Modeling and Control of an Electric Arc Furnace”. *Proceedings of the 2003 American Control Conference*, 2003. Volume 4, 4-6 June 2003 Pages: 3060 - 3064 vol.4
- [20] Tongxin Zheng; Makram, E.B., “An Adaptive Arc Furnace Model”. *IEEE Transactions on Power Delivery*, Volume 15, Issue 3, July 2000 Page(s):931 - 939
- [21] Manchur, G.; Erven, C.C., “Development of a model for predicting flicker from electric arc furnaces”. *IEEE Transactions on Power Delivery*, Volume 7, Issue 1, Jan. 1992, Page(s): 416 – 426
- [22] Banerjee, B., ”Resistive Welders and Flickers: An Analysis of Solutions Using Ultracapacitors and Active VAR Compensation”, EPRI, Palo Alto, CA: 2001. 1006485
- [23] Soo Woong Park; Suck Joo Na; “A new current measurement method in resistance spot welding”, *IEEE Transactions on Instrumentation and Measurement*, Volume 39, Issue 5, Oct. 1990 Page(s):767 – 772

- [24] Ashmole, P.; Amante, P., "System flicker disturbances from industrial loads and their compensation". Power Engineering Journal Volume 11, Issue 5, Oct. 1997 Page(s):213 – 218
- [25] Osher, J.E.; Barnes, G.; Chau, H.H.; Lee, R.S.; Lee, C.; Speer, R.; Weingart, R.C., "Operating characteristics and modeling of the LLNL 100-kV electric gun", IEEE Transactions on Plasma Science, Volume 17, Issue 3, June 1989 Page(s):392 – 402.
- [26] Gully, J.H., "Power supply technology for electric guns", IEEE Transactions on Magnetics, Volume 27, Issue 1, Jan 1991 Page(s):329 – 334.
- [27] Summerfield, M., "Development of a linear piston-type pulse power electric generator for powering electric guns", IEEE Transactions on Magnetics, Volume 29, Issue 1, Part 2, Jan 1993 Page(s):1066 – 1069.
- [28] Podlesak, T.F.; Burke, T.; Singh, H.; Ayres, G.; Schneider, S., "Solid state switches for electric gun applications", IEEE Transactions on Magnetics, Volume 33, Issue 1, Part 1, Jan 1997 Page(s):490 – 494.
- [29] Pastore, R.; Braun, C.; Schneider, S.; Carter, J.; Fox, R., "Preliminary Evaluation of High Power Solid-State Switches for Electric Guns Applications", Conference Record of the 1992 Twentieth Power Modulator Symposium, 23-25 Jun 1992, Page(s): 281.
- [30] Akagi, H.; Kanazawa, Y.; Nabae, A., "Instantaneous reactive power compensators comprising switching devices without energy storage components". IEEE Transactions on Industry Applications May/June 1984, Vol. IA-20, Page(s):625–630.
- [31] Akagi, H.; Nabae, A., "The p-q theory in three-phase systems under nonsinusoidal conditions". European Transaction on Electrical Power, ETEP, Jan./Feb. 1993, Vol. 3, No. 1, Page(s):27–31.
- [32] Czarnecki, L.S., "An orthogonal decomposition of the current of nonsinusoidal voltage source applied to non-linear loads". International Journal on Circuit Theory and Applications, Vol. II 1983, Page(s):235 – 239.
- [33] ---, "Orthogonal decomposition of the currents in a 3-phase nonlinear asymmetrical circuit with a nonsinusoidal voltage source". IEEE Transactions on Instrumentation and Measurement, Volume 37, Issue 1, March 1988, Page(s):30 – 34. [7] ---, "On some misinterpretations of the instantaneous reactive power p-q theory". IEEE Transactions on Power Electronics, Volume 19, Issue 3, May 2004, Page(s):828 – 836.
- [34] ---, "On some misinterpretations of the instantaneous reactive power p-q theory". IEEE Transactions on Power Electronics, Volume 19, Issue 3, May 2004, Page(s):828 – 836.
- [35] Czarnecki, L.S., Swietlicki, T., "Powers in Nonsinusoidal Networks, Their Analysis, Interpretation and Measurement", IEEE Transactions on Instrumentation and Measurement, Volume IM-39, No. 2, April 1990, Page(s):340 – 344.

- [36] ---, "New power theory of the 3-phase non-linear asymmetrical circuits supplied from nonsinusoidal voltage sources", IEEE International Symposium on Circuits and Systems, 7-9 June 1988, vol.2, 1988, Page(s):1627 – 1630.
- [37] Czarnecki; H.L.Ginn III; E. A. Mendrela; "Decomposition of Pulsed Loads Current for Hybrid Compensation", Int. Workshop on Power Definitions and Measurements under Nonsinusoidal Conditions, (Milano, Italy, 2003)
- [38] Czarnecki, L.S., "Circuits with semi-periodic Currents: Main Features and Power Properties". European Transaction on Electrical Power, ETEP, January/February 2002, Vol. 12, No. 1, Page(s):41 – 46.
- [39] Czarnecki, L.S.; Chen, G.; Staroszczyk, "Application of Running Quantities for Control of an Adaptive Hybrid Compensator", European Transactions on Electric Power, ETEP, Volume 6, No. 5, Sept/Oct. 1996, Page(s):337 – 344.
- [40] Brown, Daryl R.; Chyala, William D., "Flywheel energy storage: An alternative to batteries for UPS systems". Energy Engineering: Journal of the Association of Energy Engineering, Vol. 102, No 5, 2005, Page(s):7 – 26.
- [41] Ribeiro, Paulo F.; Johnson, Brian K.; Crow, Mariesa L.; Arsoy, Aisen; Yilu, Liu, "Energy Storage Systems for advanced power applications", Proceedings of the IEEE, Vol. 89, No. 12, December 2001, Page(s):1744 – 1756.
- [42] Zhang, J., Huang L., Chen, Z., Wu, S., "Research on flywheel energy storage system for power quality", International Conference on Power System Technology, PowerCon 2002 Proceedings. Volume 1, 13-17 Oct. 2002 Page(s):496 – 499
- [43] Darrelmann, H., "Comparison of high power short time flywheel storage systems", The 21<sup>st</sup> International Telecommunications Energy Conference, 1999, INTELECT '99.6-9 June 1999 Page(s):
- [44] Richardson, M.B., "Flywheel energy storage system for traction applications", International Conference on power Electronics, machines and Drives, 2002 (Conf. Publ. No 487), 4-7 June 2002 Page(s):275 – 279
- [45] Reiner, G., Wehlau, N., "Concept of a 50 MW/650 MJ power source based on industry-established MDS flywheel units", Digest of Technical Papers Pulsed Power Plasma Science, 2001, PPPS-2001, Volume 1, 17-22 June 2001 Page(s):187 - 190 vol.1
- [46] Weissbach, R.S., Karady, G.G., Farmer, R.G., "A combined uninterruptible power supply and dynamic voltage compensator using a flywheel energy storage system", IEEE Transactions on Power Delivery, Volume 16, Issue 2, April 2001 Page(s):265 – 270
- [47] Espinoza, J.R., "Inverters", Power Electronics Handbook, Rashid, Muhammad H., Editor in Chief, Academic Press, San Diego, California, 2001, Chapter 14, Page(s): 227 – 229, 265 – 237.

- [48] Silva, J., “Control methods for Power Converters”, Power Electronics Handbook, Rashid, Muhammad H., Editor in Chief, Academic Press, San Diego, California, 2001, Chapter 19, Page(s): 448 – 449.
- [49] Bose, B.K., Power Electronics and AC Drives, Prentice-Hall, Englewood Cliffs, New Jersey 07632, 1987.
- [50] Mohan, N., Advanced Electric Drives, MNPERE, Minneapolis, MN, 2001

## Appendix A

### User Interface Screens of the Computer Model

#### 1 Main View Screen

The main view screen of the program is presented in Figure A.1.

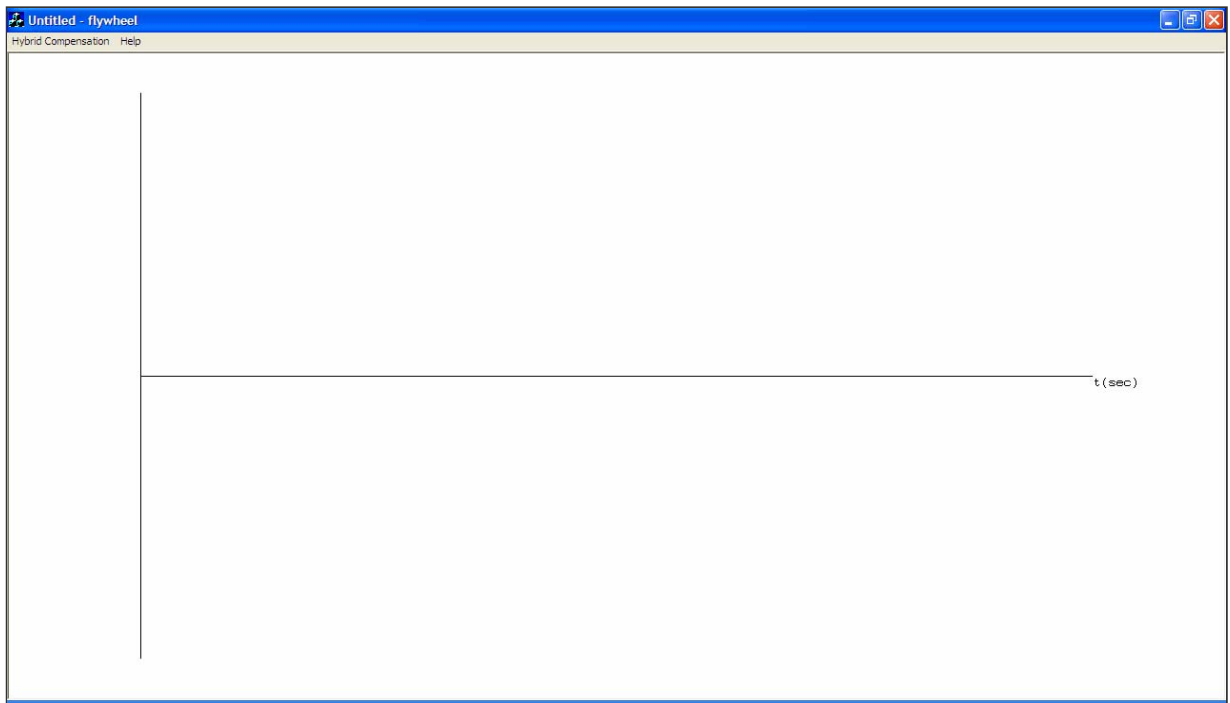


Figure A.1. Main view screen

The main view screen displays when first run, the gridline of the plots. However, initially no signal is selected to be plot. Dialog boxes are opened form the main view to entering parameter settings as well the selection of the plots to be drawn. This dialog boxes are selected using the pull-down menu *Hybrid Compensation* in the top left corner of the window. The other pull-down menu is the help menu that contains information on the name of the program and version.

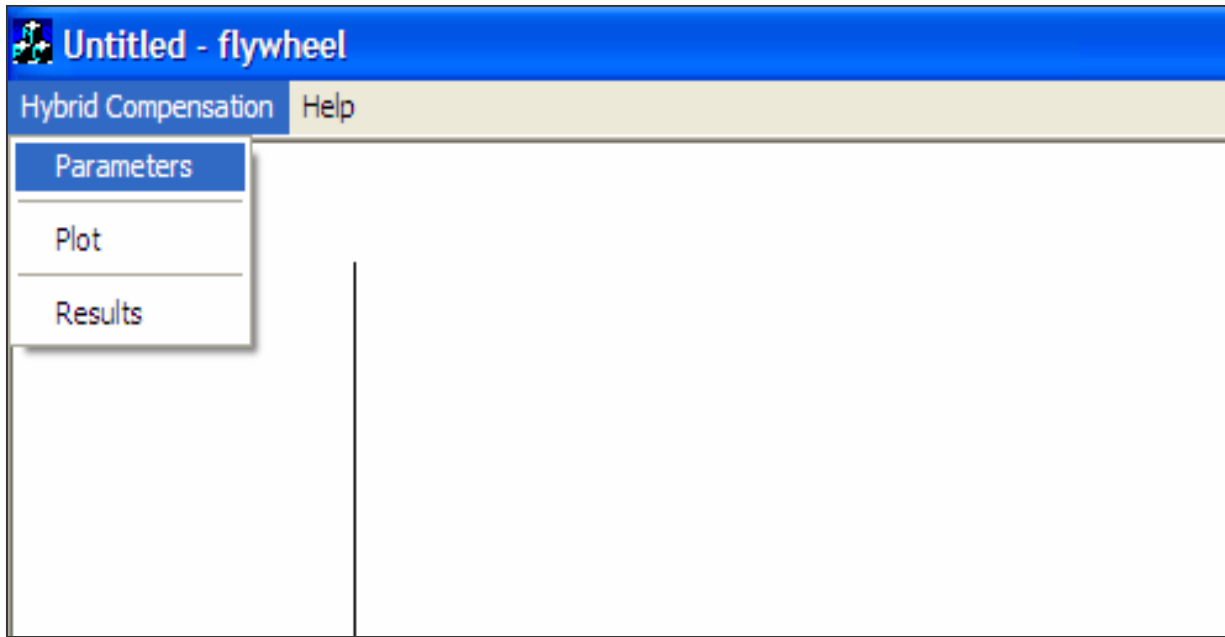


Figure A.2. Main view screen selections from the menu

## 2 Parameters Setting Screen

All the parameters for the simulation are entered by selecting the *Parameters* under *Hybrid Compensation*. The dialog box for entering parameters is shown in Figure A.3.

The Parameters dialog box is organized into several sections with tabs and input fields:

- AC Supply System:**
  - $V_{rms}$ : 220
  - $R_s$ : 0.01
  - $L_s$ : 0.001
- Converter Load Filter:**
  - $R_f$ : 0.0001
  - $L_f$ : 0.008
- DC Motor Load:**
  - ☒ DC Motor Load
  - $R_{arm}$ : 8.82
  - $L_{arm}$ : 0.0816
  - $E_{arm}$ : 320
  - $E_{arm}$ : 50
  - ☐ Pulsing Load
    - $R$ : 0
    - $L$ : 0.2
    - $C$ : 0.02
- Load Torque Profile:**
  - ☐ Constant
  - ☐ Saw\_tooth
  - ☒ Pulse
  - ☐ Exponential increase and decay
  - Duration: 
    - ☐ Fix - number of cycles < 15: 4
    - ☒ Random
- Flywheel System:**
  - Inductor Link:**
    - $R_{l\_fw}$ : 15
    - $L_{l\_fw}$ : 0.001
  - Capacitor Link:**
    - $C_{fw}$ : 0.2
    - Ref Vdc: 500
  - Active Power Compensation:**
    - Average length: 12
  - PWM (1) parameters:**
    - $m \leq 1$ : 0.8
    - $p=ft/fs$ : 81 (multiple of 3)
  - PWM (2) parameters:**
    - $m \leq 1$ : 0.8
    - $p=ft/fs$ : 81 (multiple of 3)
  - Brushless DC Motor/Generator:**
    - $R_{s\_fw}$ : 0.416
    - $L_{s\_fw}$ : 0.001365
    - $J_{eq\_fw}$ : 0.00034
    - $P_{fw}$ : 4
  - Flywheel Disc:**
    - $J_{d\_fw}$ : 327.63
- Switching Compensator:**
  - Comp Rc: 0
  - Comp Lc: 0.0019
  - Comp Cc: 1e-008
  - Comp Ref Vdc: 500

Figure A.3. Parameters dialog box screen

*Parameters* dialog box screen allows entering all the setting for the parameters of the mathematical model.

- Supply: the supply setting screen is shown in Figure A.4

The screenshot shows a 'Parameters' dialog box with a blue title bar and a red 'X' button in the top right corner. The dialog is divided into two main sections: 'AC Supply System' and 'Converter Load Filter'. The 'AC Supply System' section contains fields for 'Vrms' (220), 'Rs' (0.01), and 'Ls' (0.001), which are circled in red. Below these are checkboxes for 'DC Motor Load' (checked) and 'Pulsing Load' (unchecked). The 'DC Motor Load' section includes fields for 'Rarm' (8.82), 'Larm' (0.0816), and 'Earm' (320). The 'Pulsing Load' section includes fields for 'R' (0), 'L' (0.2), and 'C' (0.02). The 'Converter Load Filter' section contains fields for 'Rf' (0.0001) and 'Lf' (0.008). The 'Load Torque Profile' section includes checkboxes for 'Constant', 'Saw\_tooth', 'Pulse' (checked), and 'Exponential increase and decay'. The 'Duration' section includes a checkbox for 'Fix - number of cycles < 15' (unchecked) and a field for '4'. 'OK' and 'Cancel' buttons are located in the top right corner.

Figure A.4. Supply setting screen of parameters dialog box

The rms value of the supply voltage and equivalent resistance and inductance of the supply can be specified in *Parameters* as shown in Figure A.4. An example of the supply voltage plot for the default parameters is shown in Figure 2.5(a).

- Fast varying load: the FVL type and parameters setting screen is shown in Figure A.5

The screenshot shows a 'Parameters' dialog box with a blue title bar and a red close button. The dialog is divided into several sections. The 'AC Supply System' section includes input fields for Vrms (220), Rs (0.01), and Ls (0.001). The 'Converter Load Filter' section, which is circled in red, includes input fields for Rf (0.0001) and Lf (0.008). Below this, the 'DC Motor Load' section has a checked checkbox and input fields for Rarm (8.82), Larm (0.0816), Earm (320), and Earm (50). The 'Load Torque Profile' section includes a 'Duration' input field (4) and several checkboxes: 'Constant', 'Saw\_tooth', 'Pulse' (checked), 'Random' (checked), and 'Exponential increase and decay'. The 'Pulsing Load' section has a checkbox and input fields for R (0), L (0.2), and C (0.02). 'OK' and 'Cancel' buttons are located in the top right corner.

Figure A.5. FVL setting in parameters screen dialog box

The check boxes give the user a choice between modeling the different types of loads in Figure 5.2 and Figure 5.3. As described in Chapter five all loads are energized by an AC/DC converter. The filter parameters of the converter filter are configurable as shown in Figure A.5. The selection between a DC motor or a capacitive load is shown in Figure A.6.

Figure A.6. FVL power pulses setting in parameters screen dialog box

If a DC motor load is selected as shown in Figure A.6, the parameters of the armature winding can be set. The variation in the range of the induced electromotive force of the DC motor is equivalent to the range of change of the load torque. The profile of the load torque can be selected by check boxes too. Four choices are given to the user, constant load torque; saw-tooth load torque variation; pulse load torque variation; exponential increase and decay load torque variation. The user can adjust the load torque variation for a fixed number of cycles. It can also be adjusted for a random profile within the max number of cycles specified by the user.

If a capacitive load is selected then a pulsing load with inductive-capacitive parameters is simulated. Parameters of the pulsing load can be configured by the user.

All the edit boxes in parameters screen have a default value that can be altered on user's preference or design specifications. Also a DC motor load has been selected by default in the program. The default variation in the torque profile for the FVL DC motor load is chosen to be random pulses.

Hybrid compensator:

- Power variation compensator: the PVC setting screen is shown in Figure A.7

The screenshot shows the 'Hybrid compensator' settings dialog box. It contains the following sections and parameters:

- Flywheel System** (header)
- Inductor Link**:  $R_{l\_fw}$  (15),  $L_{l\_fw}$  (0.001)
- Capacitor Link**:  $C_{fw}$  (0.2),  $RefV_{dc}$  (500)
- Active Power Compensation**: Average length (12)
- PWM (1) parameters**:  $m \leq 1$  (0.8),  $p=f_t/f_s$  (81) (multiple of 3)
- PWM (2) parameters**:  $m \leq 1$  (0.8),  $p=f_t/f_s$  (81) (multiple of 3)
- Brushless DC Motor/Generator**:  $R_{s\_fw}$  (0.416),  $L_{s\_fw}$  (0.001365),  $J_{eq\_fw}$  (0.00034),  $P_{fw}$  (4)
- Flywheel Disc**:  $J_{d\_fw}$  (327.63)
- Switching Compensator**:  $Comp R_c$  (0),  $Comp L_c$  (0.0019),  $Comp C_c$  (1e-008),  $Comp RefV_{dc}$  (500)

Figure A.7. Hybrid compensator setting screen in parameters dialog box

Both the linking inductor and DC link capacitor and reference DC voltage are configurable by the user as shown in Figure A.7. All parameters for SW-PWM control of inverters A and B are configurable. The modulation index,  $m$  is recommended to be equal or less than 1. The default value is 0.8. The ratio between the frequency of the triangular carrier and the switching frequency,  $p$ , is recommended to be a multiple of 3.

The length of the period for calculation of the median active power can be set by the user. The default length for  $T_a$  is equal to 12 cycles as shown in Figure A.7.

Parameters of the equivalent circuit of the PMSM are user defined. The equivalent inertia of the motor, number of poles and the flywheel inertia can be set by the user as illustrated in Figure A.7

Distortion compensator: the DC setting screen is shown in Figure A.7. Parameters for the switching compensator capacitor and DC reference voltage are configurable by the user as shown in Figure A.7.

### 3 Plot Setting Screen

All the plots generated after the simulation is performed can be selected using check boxes. This dialog box is selected in *Plots* under *Hybrid Compensation* as illustrated in Figure A.8.

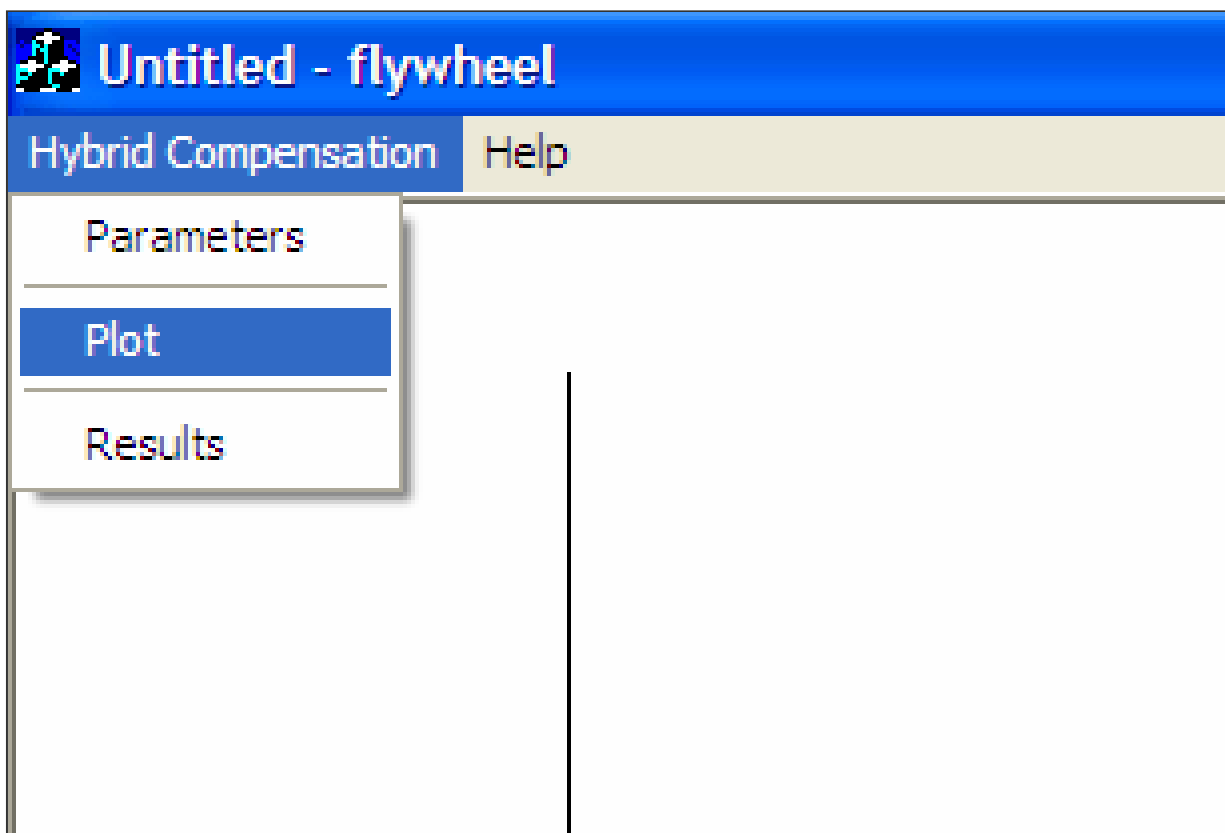


Figure A.8. Main view screen plot selection from the menu

The dialog box screen to select the plots is shown in Figure A.9.

*Plot* dialog box screen allows the user to select plot for current and voltages of the supply system, the FVL, the hybrid compensator, pre, reference and post compensation signals.

The **Plot** dialog box contains the following sections and options:

- Plot Set**
  - Number of Cycles  $\leq 15$ :  ☐ Recalculation of signals
  - Number of Samples  $\leq 256$ :
  - Int. Points per Sample:
- NON COMPENSATED SYSTEM SIGNALS**
  - Drawing Load Signals**
    - ☐ Supply Voltage
    - ☐ Supply Current Phase R
    - ☐ Supply Current Phase S
    - ☐ Load Current
    - ☐ Load Torque profile
  - Drawing Current Components**
    - ☐ RMS Current
    - ☐ Active Current
    - ☐ Reactive Current
    - ☐ Distorted Current
  - Drawing Load Components**
    - ☐ Equivalent Conductance
    - ☐ Equivalent Susceptance
  - Drawing Predicted Current Components**
    - ☐ Predicted Active Current
    - ☐ Predicted Reactive Current
    - ☐ Predicted Distorted Current
- Drawing PV Compensator Reference Signals**
  - ☐ Reference Active Current
  - ☐ Reference PV Current
  - ☐ Reference Active Power
- Drawing Flywheel System Signals**
  - AC/DC Converter (1)**
    - ☐ Capacitor Voltage
    - ☐ Supply Current Flywheel Phase R
    - ☐ Supply Current Flywheel Phase S
    - ☐ Load Current Flywheel
  - PWM**
    - ☐ PWM (1) signals
    - ☐ PWM (2) signals
  - Inverter (2)**
    - ☐ Flywheel Current Phase R
    - ☐ Flywheel Current Phase S
    - ☐ Flywheel mechanical speed
  - Drawing Supply System Signals**
    - ☐ Supply System Current
    - ☐ Compensated Active Current
    - ☐ Comp load only Supply System Current (not in use)
    - ☐ Comp total supply current
- Drawing DC Compensator Signals**
  - ☐ Compensator Current
  - ☐ Compensator Voltage
- Drawing Compensator Solution Signals**
  - ☐ Compensator Solution Voltage
  - ☐ Compensator Solution Current
- Drawing Compensator Solution Signals**
  - ☐ Solution System Current

Figure A.9. Plot dialog box screen

The user can customize the plot and some simulation parameters by changing the plot set as shown in Figure A.10.

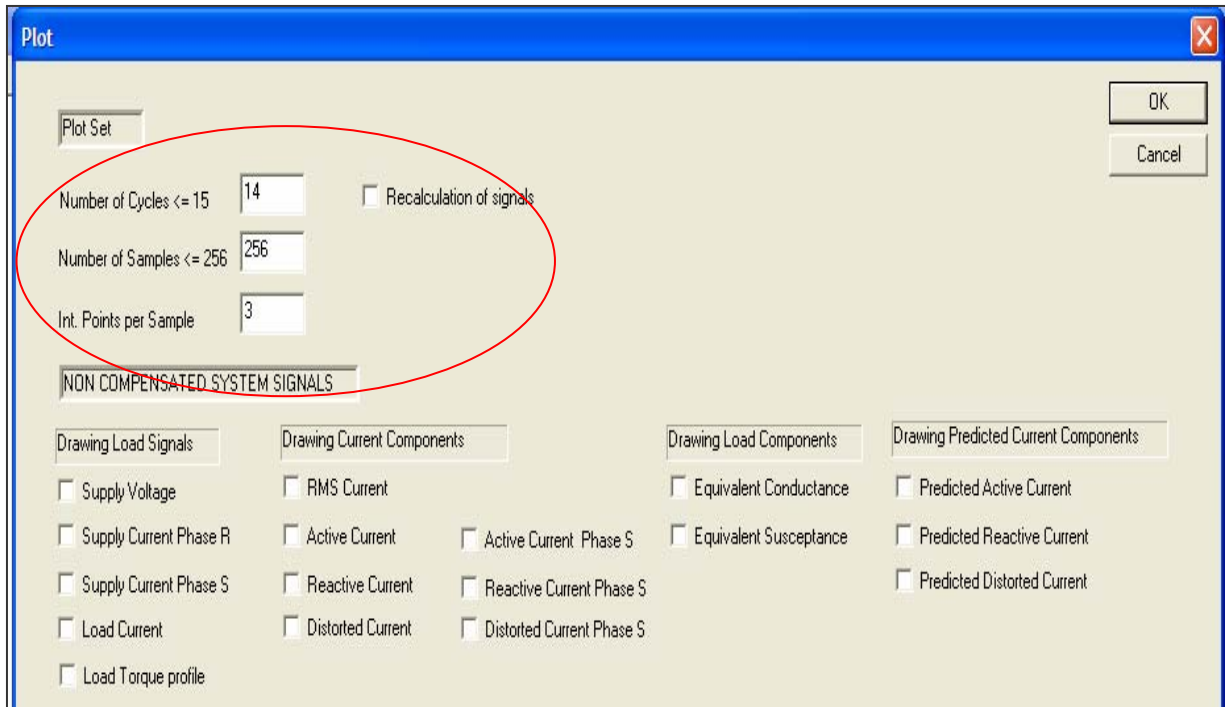


Figure A.10. Plot set and selection of signals before compensation

Changing any of the parameters in the plot set changes both the numerical solution of the system as well as the plot size and scale. If the number of cycles is reduced, the calculation is performed up to the new specified cycle. The same principle applies to the maximum number of samples per cycle and the number of integration points per sample. This observation implies the fact that if the user changes the number of cycles to a smaller number than the default value of 14 cycles, let us say to 10 cycles. Then the calculations and plots are done up to 10 cycles. If the calculations have been done at least for the first time with the default number of cycles, this value can be reduced without the need of performing a recalculation; doing the opposite will bring erroneous results

Current and voltages of the FVL, CPC decomposition of the supply current and reference signals for the distortion compensator can be plot through this dialog box as shown in Figure A.10.

The available plots for the reference signals of the power variation compensator, FESS, distortion compensator and compensated currents can be appreciated in Figure A.11.

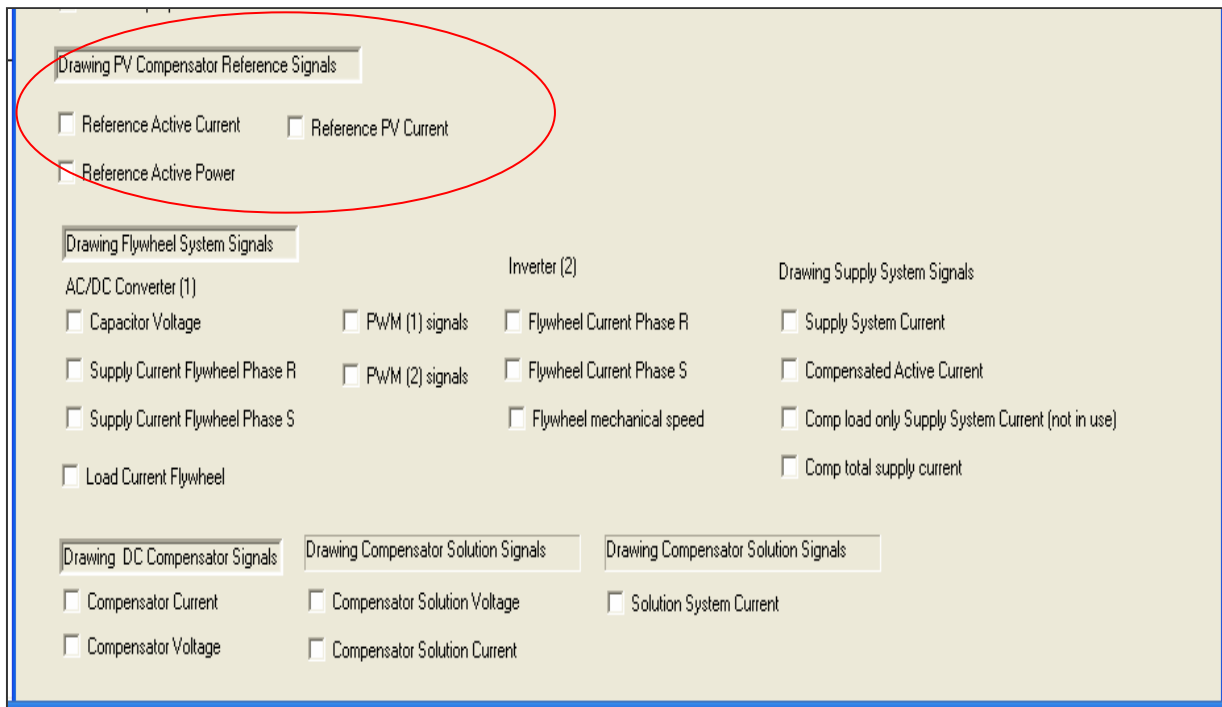


Figure A.11. Plots available for the reference signals of the PVC, FESS, DC and compensated signals

All the plots of signals for the default case presented in previous Chapters of the dissertation has been generated by the program and selected to be plot in *Plot* dialog box screen.

#### 4 Results Setting Screen

The analysis of results after compensation can be selected using check boxes. This dialog box is selected in *Results* under *Hybrid Compensation* screen as illustrated in Figure A.12.

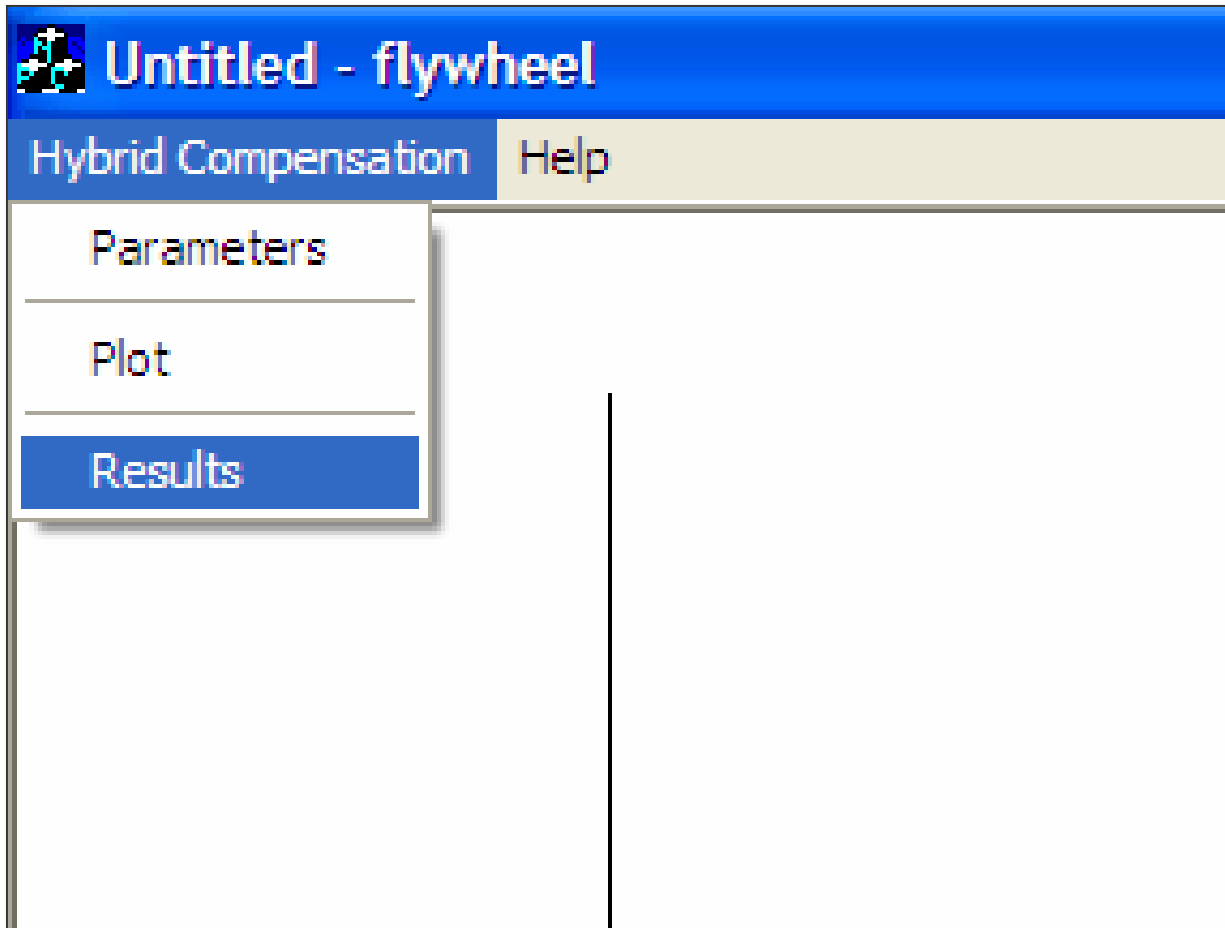


Figure A.12. Main view results screen selection from the menu

The dialog box for analysis of compensation results is shown in Figure A.13.

**Results**

**Power Variation**

☐ Active power variation of compensated load

☐ Comparison of non-compensated and compensated power variation

☐ Difference between reference and current active power Ave. dif 9.6525803 %

Ave. dif between Ref PV current and actual 4.28116652E %

Ave. dif between Ref DC current and actual 28.7080711E %

**Distortion**

No of Harm 30 < No Samples per period/2

Harm to Plot 1

☐ Quasi-harmonic component of non-compensated supply current QHD 0

☐ Harmonic component of compensated supply current THD 0

☐ Harmonic spectrum (median) of compensated supply current

☐ Reconstructed compensated supply current

OK

Cancel

Figure A.13. Results dialog box screen

Calculations related to the compensated supply signal are performed in *Results*. The main plots available or calculations available are related to variation of the reference value with respect to the compensated ones; difference in percent of the reference values and the resultant ones and distortion of the compensated signal as shown in Figure A.14.

Results

Power Variation

☐ Active power variation of compensated load
 ☐ Comparison of non-compensated and compensated power variation
 ☐ Difference between reference and current active power
 Ave. dif 9.6525803 %

Ave. dif between Ref PV current and actual 4.28116652E %
 Ave. dif between Ref DC current and actual 28.7080711E %

Distortion

No of Harm 30 < No Samples per period/2
 Harm to Plot 1

☐ Quasi-harmonic component of non-compensated supply current QHD 0
 ☐ Harmonic component of compensated supply current THD 0
 ☐ Harmonic spectrum (median) of compensated supply current
 ☐ Reconstructed compensated supply current

OK

Cancel

Figure A.14. Results and plots available for the compensated signal

**Appendix B**  
**Parameters for verification of the Computer Model**

	<b>Parameter</b>	<b>Value</b>
<b>Distribution System</b>	$V_{\text{rms}}$	220 V
	$R_s$	0.01 $\Omega$
	$L_s$	0.001 H
<b>Fast varying load</b>	$R_f$	0.0001 $\Omega$
	$L_f$	0.008 H
<b>Power variation compensator</b>	$R_p$	15 $\Omega$
	$L_p$	0.001 H
	$V_{\text{REF}}$	500 V
	$R_M$	0.416 $\Omega$
	$L_M$	0.001365 H
	$p$	4
	$J_M$	0.00034 Kg.m <sup>2</sup>
	$J_{\text{FW}}$	327.4 Kg.m <sup>2</sup>
	$R_D$	0 $\Omega$
	$L_D$	0.0019 H
<b>Distortion Compensator</b>	$V_{\text{REF}}$	500 V

## **VITA**

Veronica Bohorquez was born in 1969, in Maracaibo, Venezuela. She received her Bachelor of Science in Electrical Engineering from Universidad del Zulia in Venezuela, 1993. She received her master's in electrical engineering from Universidad Nacional Experimental Politecnica "Antonio Jose de Sucre" in Venezuela, 2000. Between 1994 and 2004 she held faculty duties at the Power Department, Electrical Engineering School of Universidad del Zulia where she was last ranked as an Associated Professor. The research areas of her interest are: power electronics, harmonics, and non periodic signals compensation. She is currently a doctorate candidate at the Electrical and Computer Engineering Department at Louisiana State University. Veronica Bohorquez is currently employed by the Rig Solutions Department of National Oilwell Varco in Houston, Texas.